AETHER

DSE Group 04 - 2022

TUDelft

AETHER
Final Report - Draft

by

Group 04

Antonio García Bulder	4872592	Nanami Hashimoto	4779495
Jonathan Tegischer	4782925	Vasileios Zygouris	4562801
Keiya Iwamida	4773047	Yaren Curgul	4563026
Laura Domenech Garrido	1543997		

As part of the course "Design Synthesis Exercise" (AE3200)
at the Delft University of Technology.

TUDelft

Preface

This report is created by 7 students and it is the fourth and final deliverable in a series of reports, as part of the Design Synthesis Exercise of the faculty of Aerospace Engineering, conducted in the fall of the 2021-2022 academic year. For the past 10 weeks, the team members have dedicated themselves to the design of an electric Vertical Take Off and Landing aircraft for the transportation of passengers with reduced mobility.

This project took place during the COVID-19 pandemic, leading to a large part of the project, including communication between group members, coaches and staff, to be conducted online.

The team would like to thank Dr. Marilena Pavel for her support and guidance during the project. Furthermore, the team would like to thank MSc Nils Barfknecht, MSc Shichen Liu and Ir. Johan Leijtens for their participation, assistance and advice. Lastly, the team thanks Marko Rehbein and the DSE committee for their assistance and for making this project possible.

<div align="right">

Group 04
Delft, January 26, 2022

</div>

<div align="center">

Antonio García Bulder
Jonathan Tegischer
Keiya Iwamida
Laura Domenech Garrido
Nanami Hashimoto
Vasileios Zygouris
Yaren Curgul

</div>

Nomenclature

Symbol	Definition
$\bar{a}$	Average acceleration
A	Rotor area
A_{eq}	Equivalent flat plate area
AR	Aspect ratio
b	Wingspan
c	Chord length
C	Rate of climb
C_D	Drag coefficient
C_{D0}	Zero lift drag coefficient
C_{Dp}	Profile drag coefficient
C_L	Lift coefficient
C_T	Thrust coefficient
D	Drag
D_{clm}	Drag of climb
e	Oswald efficiency factor
E_{clm}	Climb energy
E_{criose}	Cruise energy
E_{des}	Descent energy
E_{IGE}	IGE hover energy
E_{OGE}	OGE hover energy
$E_{reserve}$	Reserve energy
$E_{transition}$	Transition energy
$E_{vertical-clm}$	Vertical climb energy
$E_{vertical-des}$	Vertical descent energy
g	Gravitational acceleration
k	Figure of merit
k_i	Induced power factor
L	Lift
L_{Amax}	Maximum sound pressure level
L_T	Lift of tail
$M_{battery}$	Mass of battery
$M_{inverter}$	Mass of an inverter
M_{motor}	Mass of a motor
$M_{payload}$	Mass of payload
$M_{propeller}$	Mass a propeller
$M_{proprotor}$	Mass of a proprotor
$M_{propulsion}$	Mass of propulsion subsystem

Symbol	Definition
M_t	Mach tip speed
$M_{rotation}$	Rotational tip mach number
$MF_{avionics}$	Avionics mass fraction
$MF_{structure}$	Structural mass fraction
$MF_{subsystems}$	Subsystem mass fraction
N_b	Number of blades
N_{rotor}	Number of rotors
P	Power
P_{climb}	Power required for climb
P_{cruise}	Power required for cruise
P_d	Drag power
$P_{descent}$	Power required for descent
P_{hover}	Power required for hover
P_i	Induced power
$P_{i,hover}$	Induced drag power for hover
P_{par}	Parasite power for vertical climb
P_{prof}	Profile power
P_{req}	Power required
P_{vc}	Power required for vertical climb
P_{vd}	Power required for vertical descent
R	Rotor radius
Re	Reynolds number
S	Wing area
t	Time
T	Thrust
T_{clm}	Thrust for climb
T_F	Thrust of front rotor
T_h	Hover thrust
T_{IGE}	Thrust for IGE hover
T_R	Thrust of rear rotor
V	Velocity
V_a	Speed of sound
V_c	Vertical climb velocity

Symbol	Definition
v_i	Induced velocity
$V_{initial}$	Initial climb speed / lift off speed
v_h	Induced velocity for hover
$v_{i_{vc}}$	Induced velocity for vertical climb
V_R	Resultant velocity
V_{stall}	Stall speed
V_{tip}	Tip speed
w	Disk loading
W	Weight
$(W/S)_{max}$	Maximum wing loading
W_0	Gross weight
w_{cabin}	Cabin width
Y	Year of battery manufacturing
Z	Height of rotors w.r.t. the ground
α	Angle of attack
α_d	Rotor disk angle of attack
β	Rotor tilt angle
γ	Climb/descent angle
$\theta_{r/R}$	Twist
κ	Induced velocity correction factor
λ	Battery power density
ρ	Density
ρ_V	Cell volume density
μ	Advance ratio
ΩR	Tip speed velocity
σ	Blade solidity

Abbreviation	Definition
AAM	Advanced air mobility
AE	Aerodynamics
ADA	Americans with Disabilities Act
AGL	Above ground level
AKA	Also known as
ASL	Above sea level
ATC	Air traffic control
BEV	Battery electric vehicle
BMI	Body Mass Index
BWB	Blended Wing Body
C	Cost
CA	Cabin
CAD	Canadian Dollars
CAGR	Compound annual growth rate
CDC	Centers for Disease Control and Prevention
CFR	Code of Federal Regulations
CON	Constraint
CRT	Certification
DNL	Day Night Level
DOT	Design option tree
DSE	Design synthesis exercise
EASA	European Union Aviation Safety Agency
eVTOL	Electric vertical take off and landing
ETSI	European Telecommunications Standards Institute
FAA	Federal Aviation Authority
FBD	Functional breakdown diagram
FFD	Functional flow diagram
FOM	Figure of merit
GHG	Greenhouse emissions
ICEV	Internal combustion engine vehicle
IFE	In-flight entertainment

Abbreviation	Definition
IGE	In-ground effect
ISA	International standard atmosphere
HVAC	Heating, ventilation and air conditioning
MAC	Mean aerodynamic chord
MNS	Mission need statement
MOC	Means of compliance
MTOW	Maximum take off weight
NASA	National Aeronautics and Spcae Administration
OEW	Operational empty weight
OGE	Out-of-ground effect
OP	Operation
OSPL	Overall Sound Pressure Level
Pax	Passenger
PER	Performance
PNL	Percieved Noise Level
POS	Project objective statement
PP	Propulsion and power
PRM	Passengers with reduced mobility
RFP	Request for proposal
SC	Special condition
STA	Stability
STOL	Short takeoff and landing
STR	Structure
SUS	Sustainability
SWOT	Strength, weakness, opportunity and threat
TAS	True airspeed
TBD	To be decided
TC	Technical
TL	Top level
TRL	Technology Readiness Level
UAM	Urban air mobility
USD	United States Dollar
VFS	Vertical Flight Society

Executive Summary

Description of the Assignment

This era is undoubtedly a time when conventional aircraft design is challenged and revolutionized by the emergence of Advanced Air Mobility (AAM). AAM is a new concept of air transportation using electric vertical takeoff and landing (eVTOL) aircraft, integrating new, transformational designs and flight technologies into existing and modified airspace operations. In this context, Aether is living up to this vision designing a full eVTOL concept aircraft adapted to the requirements of a unique spectrum of travelers, i.e. passengers with reduced mobility (PRM). An aircraft blend of airplane and rotorcraft, Aether is an optimized solution for urban, suburban and rural travel, transporting passengers between hubs and airports, called vertiports, separated by 100 miles in just under an hour. It is a human piloted hybrid aircraft - a helicopter during take-off, climb and descent and an airplane during cruise, which can transport 2 PRMs, including one helper, or 4 passengers with full mobility.

The writers wish to note that Aether is the Delft University of Technology's Design Synthesis Exercise (DSE) project answering to the 39th Vertical Flight Society (VFS) Annual Student Design Competition request for proposal.

Passenger Experience

For the design of the cabin of Aether, safety and comfort were key. By taking into account the passenger needs based on all types of disabilities and specific requirements, the preliminary sizing of the cabin was performed. The most restrictive passenger types for the sizing and design of the cabin were those traveling in a wheelchair since it was crucial for these passengers to have the choice of staying on their own wheelchairs throughout the whole experience and be as independent as possible. This way, most of the cabin parameters were based on wheelchair certifications, such as aisle width, door width and seat width and length, providing total passenger security during flight. A chair was then designed that is able to accommodate passengers without a wheelchair and passengers with a wheelchair together with the medical equipment they might carry. The cabin was also designed for the passengers travelling on stretchers are For the entrance and exit of the cabin, Aether is equipped with a ramp as well as tactile paving. The height of the cabin was also designed to allow for vertical standing in all points necessary. Additionally, different luggage compartments were designed to place checked luggage as well as carry-on luggage.

Propulsion and Performance

The sizing for the propulsion system and the general performance is based on the power requirements for each phase of flight. The sizing of the wing was done for every iteration using the latest estimation of MTOW (maximum take off weight). The sizing of the propeller was determined based on geometrical factors, namely requirement on maximum width, fuselage width and clearance between proprotors and the fuselage, and it was determined that the radius of the propeller is 1.384 [m]. As a result of the power analysis, the transition phase from OGE (out-of-ground effect) hover to climb had the largest power requirement. The class I and class II mass estimation, determined as a result of the propulsion system sizing, yielded a maximum take off weight value of 2667 [kg] and 2799 [kg], respectively. Finally, the sizing for propeller blades selected the Clark X airfoil with a twist of -1.56 [deg], a solidity of 0.180, and 5 blades per propeller. As for the material of the blade, the Toray BT250E-6 cure epoxy prepreg was chosen. The final analysis has shown that the system will be able to perform its prescribed mission, with the proviso that the battery meets the power density requirements.

Aerodynamics

A lift and drag tool based on Lifting line theory and Vortex Ring method was realized for the determination of the forces on the wing and optimization of the basic geometric features. Using inputs from Propulsion, a wing planform of 27.5 $[m^2]$ with a span of 15 $[m]$ was determined and the NACA 63(2)-615 airfoil was selected based on maximum lift and lift-to-drag ratio at low angles of attack.

The tail sizing methodology followed is similar to the one used in wing design and was later optimized for minimized span of both the horizontal and vertical tail. A T-tail configuration was chosen for accommodating further clearance between the horizontal tail and the rear rotors.

The fuselage drag was analyzed to be further used by the Stability group and was found to be approximately 4 $[kN]$.

Noise calculations were performed for the rotorcraft phases of the flight. It was determined that maximum sound pressure level (SPL) occurs during vertical climb and is 86$[dBA]$. The peak frequency emitted by the aircraft is $4 \cdot 10^3 [Hz]$.

Structures & Materials

The material selection of the structures as well as the sizing for the main structure of Aether was performed. These being the wing box and the structure for the support of the proprotors. The wing box is the structure in charge of carrying the loads acting in the wing during all flight phases. It is compound of two spars located in 0.2 and 0.7 of the chord connected by the skin of the wing. An analysis of the internal loads acting in this structure during cruise and hover was performed for a later detailed wing box design and sizing. For the structure supporting the proprotors, two different structures were designed. For the rear rotors, a hollow shaft was designed. Analysing the structure in bending during hover, it was found that the minimum thickness needed is of 3.2 $[mm]$. For the wing mounted rotors, a shaft structure which serves as rotating axis for the tilt-rotors was analysed in a three-point bending situation during hover. It was found that a minimum diameter of 3 $[cm]$ is needed.

Stability and Control

The design for stability and control consists of four main parts: Center of Gravity range, static stability, dynamics stability, and controller design. In the beginning of this chapter, the CG range is calculated by using the class II weight estimation method and loading calculation of payload. The outcome says the CG range is 0.22 to 0.34 of the mean aerodynamics chord, and it is also presented as a so-called potato diagram. Then, the longitudinal static stability analysis is conducted, and the minimum required horizontal tail area is concluded as 19% of the main wing. Vertical tail size was decided based on empirical data, which resulted in 4.43 $[m^2]$. Following is dynamics stability analysis in longitudinal direction. A state space model was created for this analysis and the eigenvalue for the short period and phugoid motion were obtained. That is -0.0432 ± 1.5327 i and -0.0049± 0.0119 i respectively. This concludes that both motions are barely stable. Furthermore, controller architecture for hovering condition is considered and shown in a block diagram. Lastly, a section describes consideration on stability and control of the transition phase.

Operations and Logistics

An outline of the operations and logistics are presented to show how the aircraft will be used and interacts with the passengers in real-life application. An insight into the use case shows that sizing the scale of operations within a service area requires an assessment into multiple aspects such as the number and location of vertiports, the possible range of service according to possible risks of operation over certain locations, and expected number of service according to needs and acceptance

of the public on novel vehicles. An outline of the necessary infrastructure is also presented, and this evaluates the necessary functions of every vertiport as well as the central vertiport of a service area. Maintenance and air traffic management are also necessary infrastructures for the operation and the basic operation of these facilities are also elaborated. An evaluation of the operation procedures show the basic flow of service for the passengers, and it outlines the customer interface, the pre-flight operations, the in-flight operations, the post-flight operations and the emergency procedures. Finally, the battery recharging system and the vehicle maintenance is briefly described to conclude this chapter.

Cost

The life cycle cost of Aether has been broken down into four main phases: Research and development, production, operation, and disposal. For each phase the associated costs have been calculated. For the research and development costs, the testing phase amounts to the highest single cost and investment for the whole project due to the high certification costs. It was found that operating in the USA is desirable due to the lower direct energy costs as compared to Europe, and thus the cost analysis is made with the assumption of being located in the USA. For the production costs, a calculation of the 1st and 100th unit produced is done that incorporates the learning curve, and the disposal cost analysis found that recycling carbon fiber is responsible for the majority of the disposal cost. Table 6 summarises the total costs of each life cycle cost phase, considering that operation is located in the USA.

Table 6: *Breakdown of life cycle phase costs, which assumes operation in the USA.*

Life cycle cost phase	Total cost (USD)
Research and development	51,867,062
Operation (1 year)	561,374
Production (1st unit)	4,360,827
Production (100th unit)	990,176
Disposal	5,533

Once all the costs were calculated, the ticket prices could be computed. Including the reduction of production cost due to the learning curve, the maximum ticket price for a break even point of 10 years totaled 146 $ for the 1st unit and 115 $ for the 100th unit. This translates to a cost per mile of 1.46 $ and 1.15 $ for the 1st and 100th unit, respectively. Finally the total revenue has also been calculated for both ticket prices, and assuming that a total of 500 units are sold. Table 7 outlines the total revenue for Aether according to the two ticket prices. A return on investment calculation has also been made, and found that without government subsidies a maximum return on investment possible was 162%.

Table 7: *Total revenue with various amounts of units sold and ticket prices of* 146 $ *and* 115 $.

	Total revenue ($bn)		
Units sold	100	200	500
146 $ ticket price	1.60	3.24	8.18
115 $ ticket price	1.24	2.53	6.40

Sustainable Development Strategy

A major objective of Aether is to be competitive in the eVTOL market while simultaneously staying sustainable to the environment and community. In terms of the environmental sustainability, the noise levels are acceptable for use in the city and in vicinity of animals, and the disposal of the aircraft will be carried in the most sustainable way possible by reusing or recycling as much of the aircraft as possible. For the economic advancements in the community, Aether will provide numerous jobs at the headquarters and at vertiports, and will allow people to improve by providing jobs in the tertiary sector. Furthermore the reduction of road traffic will significantly reduce costs for the road traffic management. Finally, Aether will increase the accessibility and ease of access of social activities and work opportunities for many people, and consequently increase the happiness index of the community. Reduction in traffic will also reduce anxiety and stress level which will also create a happier and safer community.
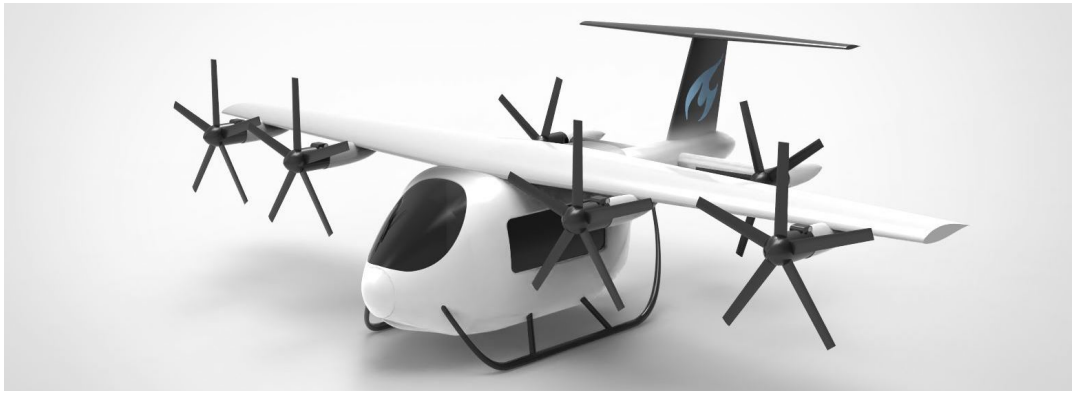
Final Remarks

The Aether aircraft is designed to serve the mission need statement to "Sustainably and securely transport passengers with reduced mobility from point A to point B through air." According to the research conclusions of this report, an aircraft similar in the design of this report would only be feasible with batteries of energy density of 400 [Wh/kg]. In terms of cabin design, considering all passenger needs found from the market analysis, a comforting and accessible cabin has been designed for, so that people with disabilities of all types are able to use the aircraft safely. Control and stability issues have been addressed, as Aether has been designed so that any single failure of the motors or electrical system would have minimal consequences on the mission. Also, analyses show that the aircraft is stable when on ground and in flight, with a controller architecture ensuring easy control of the aircraft for pilot. Finally, affordability wise, the Aether aircraft has been found to be most affordable and convenient when used for intracity rather than intercity travel, providing a faster and cheaper travel when compared to current transportation means. Choosing the right location of operations of maximum demand, (such as inter-island travel, for example) is crucial for the design to succeed and profits to be maximised by filling the market gap, while at the same time providing high class air travel quality to the under served disabled passengers around the globe.

Limitations and Recommendations

An important section of the requirements which was not analysed in the report relates to ditching and emergency procedures of the aircraft. In the initial conceptual design brainstorm, an inflatable raft attached in the inside of the undercarriage was proposed to be incorporated into the design.

However, due to the limited time frame of this DSE project, this design option was not analysed and sized for, and thus it is recommended that an appropriate raft is chosen and that enough space is made in the undercarriage to accommodate the raft. For emergency landings, an extensive analysis would have to be made on the landing stability of the aircraft in the event that the aircraft must land on rocky or uneven terrain.

Contents

1
Introduction

With an ever increasing exandion of urban areas, more than half of the world's population lives in densely populated cities[1].   Together with congestion, cities are becoming really high concentration points of emissions, which already cause many serious health issues. With technology rapidly advancing in the aeronautical industry, urban air transportation is increasingly becoming closer to reality and slowly entering the market to replace land transportation and solve congestion. An example of such vehicles are called Vertical Take Off and Landing (VTOL) aircraft and with the world moving into a sustainable future, electric VTOLs (eVTOLs) are now needed the most to reduce the carbon footprint of cities. Although these vehicles are increasing stakeholders' and consumers' interests, People with Reduced Mobility (PRM) are rarely taken into account in the design process of these vehicles. Due to this, Aether's team of engineers aim to design an eVTOL aircraft specifically designed to accommodate and transport PRMs in between urban, suburban, and rural areas.

The aim of this report is to explain the detailed design of Aether, an eVTOL air taxi for the transportation of People with Reduced Mobility. More specifically, this report explains all the phases and steps taken that lead to the final design of Aether. This includes an analysis of the design space, an analysis of the subsystems, and further operations needed for its production and first flight to later enter the consumers' market. This project follows the request for proposal of the 39th annual student design competition of the Vertical Flight Society.

The structure of the report is divided into three main parts: Part I explains all the steps taken to determine the preferred concept to be studied. Part II describes the analyses performed on the final concept needed for the final design phase and verification and validation of the core properties. Finally, Part III describes the operational and logistics aspects of the final design as well as the cost, certification, and sustainability approach.

---

[1] https://ourworldindata.org/urbanization [cited 21 January 2022]

I

PROJECT DESIGN SPACE

2
Project Overview

This chapter outlines what the project is about by introducing the mission description in Section 2.1. Once the goal and purpose has been described, the project objectives are stated in Section 2.2 through the mission need statement and project objective statement. Finally, Section 2.3 explains how the project is organised in terms of the organisational and technical roles within the team.

2.1. Mission Description

Advanced Air Mobility (AAM) is a recently established concept which envisions a new type of aerial transportation capable of serving a new type of market previously not served by the aviation industry. This new category of transportation is possible with new types of aircraft which are able to move passengers and cargo between urban, suburban, and rural environments. Additionally, electric propulsion is shaping the future of sustainable transportation, and with AAM, a new generation of aircraft called electric vertical take off and landing (eVTOL) aircraft are entering the aerial transportation market. These are aircraft which have the vertical take off and landing capability of a helicopter, with the efficient cruise performance of an airplane. At the moment typical concepts of eVTOL aircraft including tiltrotors, tailsitters, and lift plus cruise concepts suggest that aerial transportation similar to that of "flying cars" is possible in the near future.

While this new method of travel promises sustainable and fast transportation, people with reduced mobility (PRM) are one minority which have not yet been taken into consideration for the designs of these new eVTOL aircraft. According to European regulation n° 1107/2006 EC, a Person with Reduced mobility is "any person whose mobility when using transport is reduced due to any physical disability (sensory or motor, permanent or temporary), any intellectual disability or impairment, or any other cause of disability or age, and whose situation needs appropriate attention and the adaptation to his/her particular needs of the service made available to all passengers." [1] This implies that people with reduced mobility are any individual which has an intellectual or physical disability.

Taking into consideration this emerging technology and its clear gap in the PRM market, the mission of Aether is to provide a service of AAM that is specifically designed to accommodate for PRM using a sustainable eVTOL aircraft. The project has been proposed by the Vertical Flight Society (VFS) through their annual student design competition, with this year marking the 39th competition and being sponsored by Bell[1]. The specific requirement of the VFS is that "...designers must begin to account for a broad spectrum of travellers that includes persons with disabilities of all types. This calls for an electric vertical take-off and landing (eVTOL) concept that factors the unique requirements for such passengers."

---

[1]https://www.strasbourg.aeroport.fr/EN/Passengers/ [cited 18 January 2022]

The profile of the mission is provided by the VFS and can be visualised by Figure 2.1. The idea is that after passengers have boarded the aircraft, a 10 second in ground effect (IGE) hover is performed before vertically climbing to 100 [ft] to perform a 10 second out of ground effect (OGE) hover. Then, the aircraft would enter its transition phase and start a steady climb to 2000 [ft], where transition is completed and the aircraft enters is cruise phase. Finally, the aircraft descends back to 100 [ft] to perform an IGE hover phase for 10 seconds, then vertically descends to perform an IGE hover for another 10 seconds before landing. A more detailed description of each phase with more technical details can be found in Section 5.2.
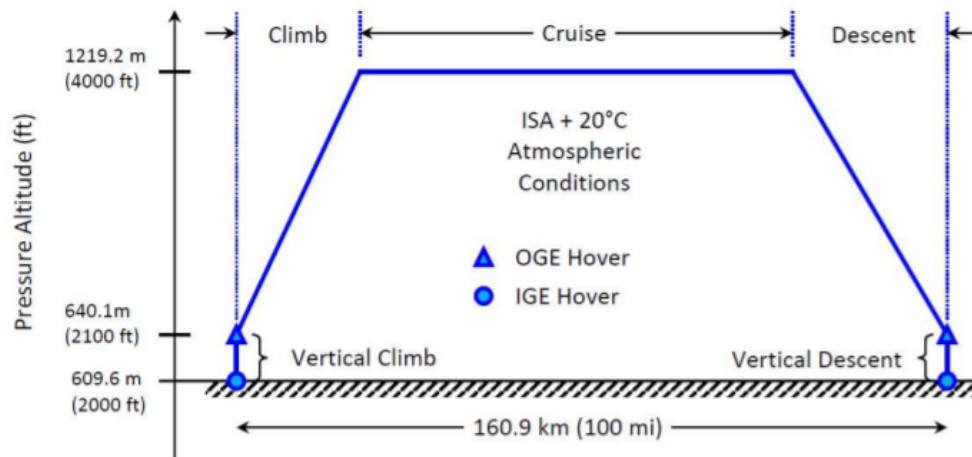
Figure 2.1: *Mission profile of Aether [2]*

2.2. Project Objectives

For Aether, the Mission Need Statement (MNS)is as follows:

> *Transport passengers with reduced mobility from point A to point B through air sustainably.*

and the project objective statement (POS) is the following:

> Design an all-electric Vertical Take-Off and Landing aircraft capable of transporting no less than two passengers with reduced mobility over a range of 100 miles by 7 students in 10 weeks.

2.3. Project Organisation

To organise the project and maintain structure within the group, a distribution of roles was made at the beginning of the project that assigned technical and organisational roles to team members. Figure 2.2 outlines the role distribution and paths of communication. Blue boxes represent organisational roles, whereas yellow boxes describe the technical roles of the project. The paths of communication, represented by the black lines, indicate that organisational managers and officers have a direct path of communication to any other organisational officer or manager, whereas for the technical roles one engineer would have to consult the systems engineer in order to communicate to another engineer from another department.

Figure 2.2: *Organogram*

<div style="text-align: right">

3

</div>

<div style="text-align: right">

Market Analysis

</div>

This chapter describes the outcome of market analysis conducted to know if and where this air taxi service can fit in the market. gives a definition of the market, as well as current and future trends of UAM market. Then the stakeholder 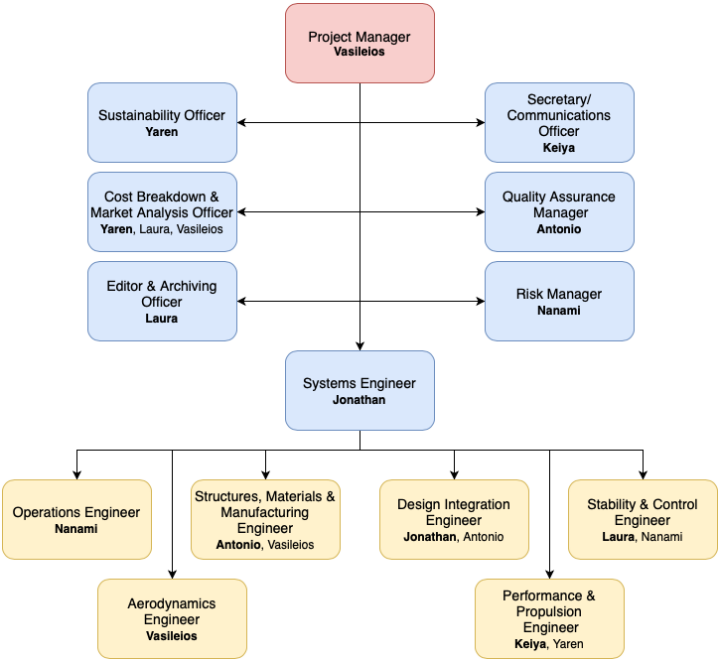is identified in Section 3.2, and Section 3.3 describes market needs and the gap in the market. The competitors in the market are introduced in Section 3.4 with their characteristics and in Section 3.5, SWOT analysis is conducted to know the strengths, weaknesses, opportunities, and threats of this service. Lastly, several locations are selected for the operation as examples Section 3.6.

3.1. Market Overview

The first thing to do in market analysis is to define the market and having the overview of the market. This section describes the definition of the market and the overview UAM market including the current trends and future prospects.

3.1.1. Market definition

In the market definition, the boundaries of this service in the market competition are defined. This includes defining the target case and customers. First of all, the service range is already decided as around 100 miles. This can be a trip from one city to another city, or a trip from a city to a rural area that has bad access by regular trains or busses. Another possibility is being a bridge of other transportation methods, such as between two airports or an airport to a major station. In the early phase business, it is a good idea to pick the route that the flow of people is large so that it can target wider range of customers. Therefore, this service aims to transport passengers between two cities or two other transportation modes.

With the target case defined, the target customers are also determined. The biggest advantages of air taxi compared with other transportation methods are its fast speed, flexibility of route, and no or very low possibility of traffic congestion. In other words, it can travel to wherever with vertiport in a shorter period of time without worrying about delay. From this idea, two types of customers have come up. The first type is people who are so tight on schedule and wants to reduce travel time as much as possible. This type mainly includes business people. Then the second type of customers are people who do not want to be bothered by transferring trains or busses. This would also include business people who want to save time, but it also includes travelers who are not familiar with complicated local traffic or people who have difficulties with changing transportation because of physical or psychological reasons. The target customer can be expanded in the later phase of the business, but in the first stage, these people are defined as target customers.

3.1.2. Current trends and future prospects of UAM market

The UAM market is predicted at USD 2.6 billion in 2020 with a CAGR of 13.5%, which means a market size of USD 2.95 billion in 2021[1]. The global air taxi market is expected to make up 27.7 % of the total UAM market which means USD 817.50 million by 2021. The expected CAGR is 26.2% between 2021 and 2030, with a projected market size of USD 6.63 billion by 2030.

The passenger eVTOL market of the overall UAM market can be segmented into different range, for example: city Taxi with a range of 15 to 50[km] for intracity travel, Airport Shuttle with a range of 15

---

[1] https://www.marketsandmarkets.com/Market-Reports/urban-air-mobility-market-251142860.html
[cited 18 November 2021]

to 50[km] for airport transport, and Intercity Jets which have a range of up to 250[km] Figure 3.1. [3] shows the market share of each segment with respect to the total distance flown by UAM passenger drones. The numbers are expressed in thousands, and the figure also gives a growth projection for the upcoming 30 years.

Also, there is a clear trends in propulsion type: electric propulsion. In 2021, 40.3% of eVTOL for air taxi service is found to have equip an electric propulsion system [2]. This trend is expected to continue due to a high concern for environmental problems.
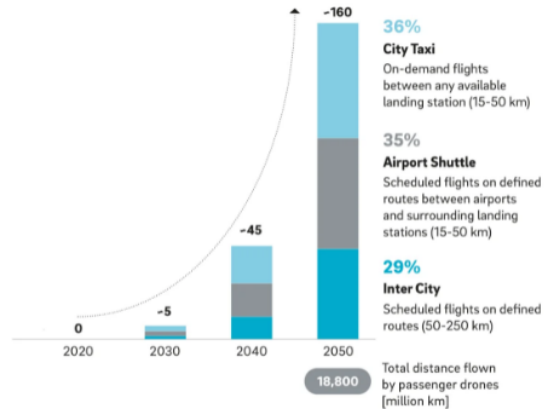

Figure 3.1: *Operating UAM passenger drones ['000] [3]*

3.2. Stakeholder Identification

The next step of market analysis is identifying the stakeholder. Stakeholder is, by definition of the Cambridge dictionary, "a person such as an employee, customer, or citizen who is involved with an organization, society, etc.". This primarily includes producers and users of this service, but it also includes parties related to legal, ethical, economical, and environmental matters etc. The identified stakeholders are classified depending on their interest and influence level. They can be seen in Table 3.1.

Table 3.1: *Stakeholder Identification*

	Interest High	Low
Influence High	Manufacturing companies, Vertiport owner	Local government, EASA, FAA
Low	Passengers, Aircraft's operator, Engineers,	Local residents, Academic institution, NGOs, Investers, Local bank, Insurance company, Media

3.3. Market Needs and Gap

Market needs ranges over various categories, such as functionality, price, reliability, experience, and accessibility. Customers always seek for a safe and comfortable transport with an affordable price.

These needs are considered in most air taxi services or other transportation methods. However, there is one type of need that is often paid much attention - a service for passengers with reduced mobility.

According to the the world report on disability, 14.9 % of the worlds population between the ages of 15-59 are considered moderately to severely disabled. For people aged 60 and over, the percentage of people with a disability increases to 46.1 %. With an estimated world population of 7.9 billion in January of 2022, a total of 1.53 billion people have a moderate to severe disability[3]. As mentioned

---

[2] https://www.alliedmarketresearch.com/air-taxi-market [cited 18 November 2021]
[3] https://www.worldometers.info/world-population/#ref-1 [cited 18 January 2022]

in Section 2.1, intellectual and physical disabilities of any kind are considered as disabilities. This also means that taking transportation is significantly more challenging and often facilities will not be catered to their needs.

While transportation using a car or taxi is a viable option, city traffic and medium distance trips can take longer than what the PRM considers as comfortable. With the introduction of AAM and the implementation of an eVTOL aircraft would satisfy the PRM needs of a comfortable and fast method of transportation that is able to travel in urban, suburban, and rural environments.

3.4. Competitors

An important step in the market analysis is the identification of the competitors which are in the same market. This is an opportunity to learn their strengths and possible trends in the design of eVTOL aircraft, and how ones aircraft can be changed such that it offers a unique service to the customer. From the market research, nine similar eVTOL aircraft are identified and data on some of their features is noted. A summary of the list of competitors with their characteristics is tabulated in Table 3.2.

Table 3.2: *List of competitors of Aether.*

Project Name	Pax	Configuration	Range	Top speed	Start operation	Autonomy level
Lilium Jet[4] [4]	6 pax + 1 pilot	Wing + 36 tilted-ducts	250+ km	280 km/h	2024	Semi-autonomous
Joby[5]	4 pax + 1 pilot	Wing + 6-12 tilted prop-rotors	242 km	241 km/h	2024	Piloted
Airbus A3 Vahana [6]	1 pax	Tandem tilt-wing with prop-rotors	50 km	220 km/h	2018	Autonomous
Wisk[7][8]	2 pax	Fixed wing + 12 independent lift fans	100 km	160 km/h	Unknown Trial in 2020	Autonomous
Heaviside[9]	1 pax	Fixed wing, tilted propellers	161 km	290 km/h	2019	Unknown
Volocity [10]	2 pax	Multirotor with 18 propellers	35 km	110 km/h	2016	Autonomous
Voloconnect [11]	4 pax	Fixed-wing with two propulsion fans + six electrical motors and rotors	100 km	250 km/h	2023	Autonomous
CityAirbus [12]	4 pax	Fixed wing + 8 electric propellers	80 km	120 km/h	2023	Piloted first, Autonomous later
AirisOne [13]	5 pax	Wing + three set of fans	322 km	282 km/h	Unknown	Autonomous

Considering the number of passengers, autonomous level, and the achievable range, Lilium Jet and Joby would be the two biggest competitors to this project. Both have a wing and tilted rotors or ducts. Lilium raised USD 842 million by the time writing this report, and Joby raised USD 656 million by November 2021 [14]. Both aim to start their operation in 2024.

Knowing the competitor's ticket price is also important. Lilium set their base scenario as USD 2.25 per seat mile with a load factor of 4.5 out of 6 [4]. This contains 25% of profit margin. Similarly, Joby

---

[4] https://lilium.com/ [cited 17 November 2021]

[5] https://www.jobyaviation.com/ [cited 17 November 2021]

[6] https://www.airbus.com/en/innovation/zero-emission/urban-air-mobility/vahana [cited 17 November 2021]

[7] https://wisk.aero/ [cited 17 November 2021]

[8] https://evtol.news/kitty-hawk-cora/ [cited 17 November 2021]

[9] https://kittyhawk.aero/heaviside/ [cited 17 November 2021]

[10] https://www.volocopter.com/solutions/volocity/ [cited 17 November 2021]

[11] https://www.volocopter.com/solutions/voloconnect/ [cited 17 November 2021]

[12] https://www.airbus.com/en/innovation/zero-emission/urban-air-mobility/cityairbus-nextgen [cited 17 November 2021]

[13] https://evtol.news/airisone/ [cited 17 November 2021]

[14] https://qz.com/2085078/covid-helped-kickstart-the-age-of-cargo-drones-and-air-taxis/ [cited 25 January 2022]

set their price point of USD 3.00 per seat mile at a load factor of 2.3, or USD 1.73 per seat mile at a full load factor of 4 passengers [5].

In addition, one notable feature which all competitors lack is the ability to accommodate PRM that require a wheelchair or stretcher. This gives Aether a considerable advantage in having a unique selling point and thus a greater probability of penetrating the market successfully.

3.5. SWOT Analysis

With the market and competitors analysed, the strengths, weaknesses, opportunities, and threats (SWOT) of Aether can be analysed. A SWOT analysis is created to summarise all of these properties and is tabulated in Table 3.3. The main strength of Aether is that it will provide a fast transportation service for PRM, but at the same time catering for the PRM is a weakness as it is unfamiliar and limiting. Entering an emerging market is the biggest opportunity which could provide high returns on investment, but consequently is under threat by the multinationals already present in the market.

Table 3.3: *Outcome of SWOT analysis for market analysis.*

Strength	Weakness
The service has a clear target	The price per passenger can be higher due to lower passenger loading rate
PRM have the choice to use air taxi for transport (more inclusive service)	Special equipments for the specific customer needs can lead to larger MTOW
The service offers faster transport for PRM	The turnover rate can be lower due to longer boarding and disembarking time and changing cabin configuration
Fewer emissions compared to the current jet aircrafts	Possibility that cabin design is too focused to certain disabilities
Accessible to wide range of people because the cabin configuration can be changed to target PRM and non-PRM customers	PRM have more limiting requirements for operation since they can be more sensitive to noise, light and turbulence
Opportunities	**Threat**
There is widespread trends for sustainable transportation alternatives	The aircraft design can be too expensive for PRM
Capability to enter into a wider market because PRM are also targeted	The fundraising plan is unsure yet
Urban air transport will become more inclusive and diverse since there will be an option for PRM	Certification for PRM transportation and eVTOLs too unclear
Electrical batteries show rapid improvement	Public acceptance may be lower than normal air taxi due to increased perceived safety threats for PRM
Large investments into UAM, more likely to acquire government grants for a product designed for PRM	Multinational companies such as Airbus are rapidly developing solutions in the UAM market

3.6. Location selection

In this section, different locations are considered for a possible operational launch area. To begin with, criteria to choose operation location are listed in the following:

- **Mobility demands and existing transport modes:** This criterion decides if there is a demand for a new transport system. This depends on how much flow of people there are, and if there is alternative transport modes such as bullet trains or highways. Also, since this service has extra focus on passenger with reduced mobility, the availability of accessible transport for these passengers should also be taken into account.

- **City planning:** Planning of a city is also an indispensable factor for selecting a suitable city to provide the air taxi service. A city showing a trend of urban sprawl could be one of the options, as there would be an issue about congestion in traffic. Another possibility is a city with a doughnut effect, which is that the city centre becomes more hollow or empty mainly

because of the rise in the living cost of the city center. This effect would lead to a demand of expanding the city traffic to wider areas, and eVTOL can be one of the options.

- **Natural/ Geographical environment:** Weather conditions and the surrounding landscape also affect air taxi operation. Aircrafts have a limit of wind gust that can be operated, which is typically around about 90 km/h for start-up or shut-down phase[15]. In addition, the area that is at the edge of the tectonic plate has a higher risk of seismic activity and volcanic eruptions. This should be taken into consideration in a risk analysis. Apart from that, the topography of the region should be considered too. For example, if the area is very hilly, it would need additional maneuvers than stated in the mission profile Figure 2.1. This could cause difficulties in flight and could require further modification on the design of the aircraft. However, major advantages of Aether are it can fly both vertically and horizontally, and it only requires vertiports on the land, which requires less space than runways for airplanes. Thus, geographical factors shall be taken taken in both negative and positive way.

- **Political climate** Political climate of the operating country or region encompasses aspects such as the openness of the government to new projects, funding possibilities from the government, regulations for infrastructure and airspace use, certification regulations in the area, etc. This can change drastically over time, so it is also important to carefully consider its prospects.

- **Socioeconomic status:** The socioeconomic status plays a crucial role in a success of the business. For the air taxi service to be feasible, the region's civil safety and security standards should be high. Also, since the price for the air taxi will at least as expensive as traditional public transport modes, there must be a sufficient number of people who can afford the travel. The economic condition of the area also cannot be ignored because not many people are in the "mood" of spending money for new technologies.

- **Social acceptance:** The last important factor to determine the success of the service is the social acceptance. A study on public acceptance of eVTOL shows that local residents have concerns about safety, noise etc [6]. It would be beneficial to analyse their cultural trends of recognition towards emerging technologies.

Considering the criteria mentioned above, several candidates for the operation city have come up.

- Amsterdam - It can provide smooth travel from Amsterdam city center or Schipol airport to the high tech campus in Eindhoven or Brussel, for example.

- London - It can provide a trip to cities around London, or a trip between two airports such as Luton and Gatwick.

- Philadelphia - It can provide travel to New York and Washington DC. There will be both both business use and tourism use.

- Los Angeles - It can provide travel to San Diego.

These candidate cities will be studied deeper in the further development stage, and the launch customer city will be determined. Should the business succeed in the first city, the service will be expanded to more area.

---

[15]http://starshorizons.ca/when-is-it-too-windy-to-fly/[Cited 26 January 2022]

Concept Trade Off

The following chapter explains the trade off performed in the midterm report that led to the decision of the final concept analysed in this report. Section 4.1 outlines the three concepts sketches which were analysed and compared with the selection criteria explained in Section 4.2. Finally, the chapter ends with a summary of the trade off process and the winning concept reveal in Section 4.3.

4.1. Concept Overview

After formulating the design option tree, a design space reduction was conducted to remove all unfeasible options and other options which were too complex. With the final options left, three distinct design were proposed which would be analysed in the midterm report phase. The first concept, sketched in Figure 4.1, portrays a blended wing body aircraft with tiltable rotors on the front and back of the fuselage. Figure 4.2 shows a design with tiltable rotors and a fuselage of similar shape as a light jet. Finally, Figure 4.3 depicts a multirotor design with coaxial rotors connected by a central fuselage section.
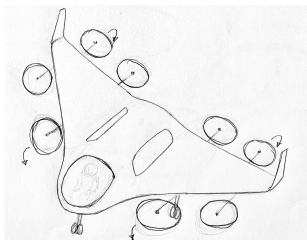
Figure 4.1: *Flying Wing sketch*
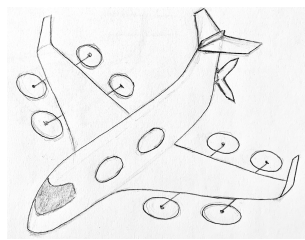
Figure 4.2: *Tiltrotor Aircraft sketch*
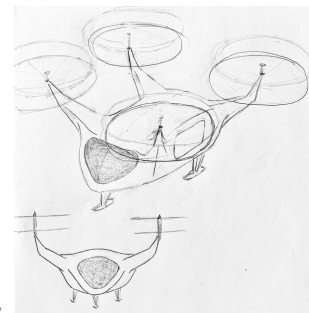
Figure 4.3: *Multirotor sketch*

4.2. Criteria Selection and Scoring

Before analysing each concept, a list of criteria had to be chosen such that a fair comparison could be made between the concepts. These stemmed from the important top level requirements, and discussion between the group members. The top level criteria chosen were sustainability, cost, passenger comfort, technology readiness level, and safety. All criteria except safety also included sub level criteria, which allowed a deeper analysis of each concept.

Before scoring each concept, the weights were assigned to each criteria and sub criteria. First, the weight of the top level criteria were decided by the group, and then a similar approach was taken to determine the weight distribution for the sub level criteria. All weights of the criteria and sub level criteria can be found in Table 4.2.

The last step for the trade off was to score each concept against the criteria. To do this, a grade scheme given in Table 4.1 was used to score each concept against. For each criteria a range of values were assigned to each score such that a final result would convert to a criteria score. Qualitative criteria such as passenger comfort used alternative methods to quantify the concepts such that they also had a score. Furthermore, a summary of the trade off methodology can be seen by the flowchart in Figure 4.4.
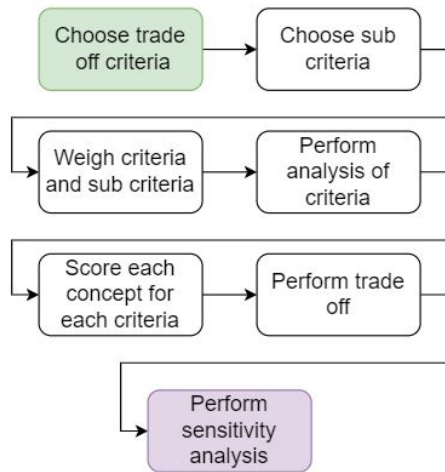
Figure 4.4: *Flowchart describing the process of performing the trade off methodology*

Table 4.1: *Criteria trade off scores with their respective qualitative definition*

Score	Qualitative description
1	Unacceptable
2	Correctable deficiency
3	Meets requirements
4	Surpasses requirements
5	Greatly exceeds expectations

4.3. Concept Trade Off

Once all scores for each sub criteria were calculated, a trade off matrix was made to summarise all the criteria and their respective score given for each concept, and can be seen in Table 4.2. The final scores show that the tiltrotor concept performs the best out of the three, and thus is the concept analysed in this report. Furthermore, a sensitivity analysis confirmed that the tiltrotor concept was the most robust and that results were not biased due to the criteria and weights. Note that changes have been made to the concept and thus the final design may not be representative of the design sketch in Figure 4.2.

Table 4.2: *Final trade off summary. Higher scores represent a better result.*

Top level criteria	Weight	Sub criteria	Weight	**Multirotor**	**Tiltrotor**	**Blended wing body**
Sustainability	16	Noise	9.4	3	2	2
		Energy consumption	6.6	2	4	4
Cost	20	Production cost	13.2	4	4	3
		Operational cost	6.8	3	4	5
Passenger comfort	27	Cabin comfort	12.7	4	3	4
		Trip time	14.3	3	4	4
Technology readiness level	13	Fuselage	4.7	4	5	3
		Propulsion	3.4	5	4	3
		VTOL configuration	5.1	5	3	2
Safety	24	Risk	N/A	3	4	4

	Total	341.6	368.9	357.3

5

Vehicle Specifications

This chapter outlines the specifications of the Aether aircraft. Firstly, the specification of the requirements is presented in Section 5.1 followed by a detailed description of the mission profile with all flight phases is described in Section 5.2. Then, the final layout description is presented in Section 5.3, where a review of number of rotors is described, along with the final technical drawings and renders of the aircraft. Finally, Section 5.4 describes the data handling block diagram which explains how the technical operation of the aircraft works.

5.1. Requirement Specifications

In this section the requirements specifications is presented. Firstly, the top level requirements are observed followed by the operational, performance, power & propulsion, cabin, structural, control & stability, and aerodynamics, respectively.

Table 5.1: *Top level requirements*

Code	Requirement	Reference	Type
TL-CON-VFS-01	The aircraft propulsion system shall be all electric.	VFS	Driving
TL-CON-VFS-02	The aircraft shall be accessible to people with disabilities of all types.	VFS	Driving
TL-CON-VFS-03	The aircraft shall be controlled by one pilot.	VFS	
TL-CON-VFS-04	The system shall be able to land vertically.	VFS	Driving
TL-CON-VFS-05	The system shall be able to take off vertically.	VFS	Driving
TL-CON-VFS-06	The aircraft shall have a range of 100 [$miles$] (161 [km]).	VFS	Driving
TL-TC-01	The aircraft shall be able to transport a maximum of 4 passengers.	VFS	
TL-TC-02	The aircraft shall be controllable throughout its mission.	B § 27.143(a)	Driving
TL-TC-03	The aircraft shall be longitudinally stable (Cm-alpha negative).		Key
TL-TC-04	The aircraft shall comply with all appropriate certification requirements.		Driving
TL-TC-05	The aircraft shall be designed to perform an emergency landing at any time.	VFS	
TL-TC-06	The noise of the aircraft shall not exceed <100> [dB].	Sustainability	
TL-TC-07	The noise of the aircraft, as perceived at ground level from an altitude of <100 m> shall not exceed <100> [dB].	Sustainability	
TL-TC-08	The noise of the aircraft perceived by the passengers shall not exceed 60 [dB].	Sustainability	
TL-CON-CRT-01	The aircraft shall not have design features that experience has shown to be hazardous or unreliable.	D § 27.601	
TL-CON-CRT-02	The Maximum Take Off Weight (MTOW) of the aircraft shall not exceed 3175 [kg].	A § 27.1(a)	
TL-CON-TIM-01	The aircraft shall be designed in 10 weeks.		
TL-CON-COS-01	The production cost of one aircraft shall be less than USD 3 million.	Market analysis	

Table 5.2: *Operational requirements*

Code	Requirement	Reference	Type
CON-VFS-OP-01	The aircraft shall be able to carry the baggage of all passengers.	VFS	
CON-VFS-OP-02	Each passenger shall be able to have one piece of checked baggage having total linear dimension of 158 [cm] and weighing up to 23 [kg].	VFS	
CON-VFS-OP-03	Each passenger shall be able to have one piece of carry on having dimensions $56x36x23$ [cm] and weighing up to 10 [kg].	VFS	
CON-VFS-OP-04	Each passenger shall be able to have one piece of personal item having dimensions $45x35x20$ [cm] and weighing up to 5 [kg].	VFS	
CON-VFS-OP-05	The aircraft shall be able to operate in urban environments.	VFS	
CON-VFS-OP-06	The aircraft shall be able to operate in suburban environments.	VFS	
CON-VFS-OP-07	The aircraft shall be able to operate in rural environments.	VFS	
CON-CRT-OP-01	The aircraft shall be protected against lightning induced effects.	D § 27.610(a)	
CON-CRT-OP-02	The never-exceed speed shall be no larger than 0.9 times the maximum speed allowed for structural integrity of the aircraft.	G § 27.1505(a)	
CON-CRT-OP-03	The maximum operating altitude, limited by structural, mission and functional characteristics, shall be established.	G § 27.1527	
CON-CRT-OP-04	The system shall be designed to minimize the possibility of immediate injury in the event of ditching.	§ 29.801(b)	
CON-CRT-OP-05	The system shall be designed such that egress after ditching must be possible for all passengers.	§ 29.801(b)	
CON-CRT-OP-06	Each crew and passenger area shall have means of rapid evacuation in case of a crash landing.	§ 29.803(a)	
CON-CRT-OP-07	Each crew and passenger area shall have means of rapid evacuation in case of fire.	§ 29.803(a)	
CON-CRT-OP-08	Passenger and crew doors which act also as emergency doors shall be accessible to all passengers and crew.	§ 29.803(b)	
CON-CRT-OP-09	Complete evacuation of the aircraft shall be possible within 90 seconds.	§ 29.803(e)	
CON-CRT-OP-10	The probability of the aircraft coming to rest on its side shall be essentially zero.	§ 29.807(c)	
CON-CRT-OP-11	Each emergency exit shall have means to open the door from the outside.	§ 29.809(b)	
CON-CRT-OP-12	Each emergency exit shall have means to open the door from the inside.	§ 29.809(b)	
CON-CRT-OP-14	Each emergency exit shall be visible from a distance equal to the width of the cabin.	§ 29.811(b)	
TC-OP-01	The aircraft shall house a flotation device used for water landings.	§ 29.801	
TC-OP-02	The aircraft shall be able to float in emergency situations and not sink during emergency water landing for at least 15 minutes.	§ 29.801	
TC-OP-03	Clear maintenance procedures shall be in place to help ensure the continued durability, integrity and functionality of the parts and systems.		
TC-OP-04	The battery level shall be known to the pilot at all times.		
TC-OP-05	The battery level of discharge shall be known to the pilot at all times.		

Code	Requirement	Reference	Type
TC-OP-06	The operational lifetime of the aircraft shall be at least 20 years.	Sustainability	
TC-OP-07	The aircraft shall be able to conduct 50,000 trips in its operational lifetime.	Sustainability	
TC-OP-08	The aircraft shall have means of allowing passengers to enter and exit the aircraft.		
TC-OP-09	The aircraft shall be able to communicate with Air Traffic Control.		
TC-OP-10	The aircraft's safety features in response to propulsion system failure shall be determined.	VFS	
TC-OP-11	The operational cost shall be less than USD 14 per mile.	Market analysis	

Table 5.3: *Performance requirements*

Code	Requirement	Reference	Type
CON-VFS-PER-01	The aircraft shall perform hover In Ground Effect (IGE) for 10 seconds.	VFS	
CON-VFS-PER-02	The system shall be able to vertically climb to 30.48 $[m]$ with Rate of Climb (ROC) of 0.8128 $[m/s]$.	VFS	
CON-VFS-PER-03	The system shall be able to hover Out of Ground Effect (OGE) at 30.48 $[m]$ for 10 seconds	VFS	
CON-VFS-PER-04	The system shall be able to perform steady climb to 609.6 $[m]$ Above Ground Level (AGL) at a climb gradient of 1:6 (9.46 degree angle of climb).	VFS	
CON-VFS-PER-05	The system shall be able to cruise at an altitude of 609.6 $[m]$.	VFS	
CON-VFS-PER-06	The system shall be able to conduct steady descent to 30.48 $[m]$ AGL at an angle of descent of 4 degrees.	VFS	
CON-VFS-PER-07	The system shall be able to perform a vertical descent to IGE with a rate of descent of <TBS> $[m/s]$.	VFS	
CON-VFS-PER-08	The aircraft shall be capable of continued flight following any single failure of the electrical distribution system.	VFS	Key
CON-VFS-PER-09	The aircraft shall be capable of IGE hover following any single failure of the electrical distribution system.	VFS	Key
CON-CRT-PER-01	The landing speeds shall guarantee minimum performance.	VTOL 2105.3(c)	
CON-CRT-PER-02	The aircraft shall be accelerated to Take-off Safety Speed (V_{toss}) while clearing any surface by 4.6 $[m]$ (15 $[ft]$).	VTOL 2115.2(b)	
CON-CRT-PER-03	Starting at the point at which the aircraft reaches 200 $[ft]$ above the take-off elevation, the aircraft shall be accelerated to the Final Take-off Speed (VFTO).	VTOL 2115.2(h)	
CON-CRT-PER-04	Starting at the point at which the aircraft reaches 200 $[ft]$ above the take-off elevation, the aircraft shall then be capable of a directional trajectory change with at least 3 $[deg/s]$.	VTOL 2115.2(h)	
CON-CRT-PER-05	Flying at V_{FTO} shall provide a manoeuvring capability of not less than 3 $[deg/s]$ of turn rate.	VTOL 2115.5(d)	
CON-CRT-PER-06	The aircraft operational speed range shall be established.	G § 27.1503(a)	
CON-CRT-PER-07	The available power shall correspond to the power available by the batteries.	B § 27.45(c)	
CON-CRT-PER-08	The steady rate of climb shall be determined with maximum continuous power on each rotor.	B § 27.65(a(1(i)))	
CON-CRT-PER-09	The steady rate of climb shall be determined with maximum weight.	G § 27.67(a)	

Code	Requirement	Reference	Type
CON-CRT-PER-10	The steady rate of descent shall be determined with maximum weight.	G § 27.67(a)	
CON-CRT-PER-11	The steady rate of climb shall be determined with the critical engine inoperative.	G § 27.67(b)	
CON-CRT-PER-12	The steady rate of descent shall be determined with the critical engine inoperative.	G § 27.67(b)	
CON-CRT-PER-14	The aircraft shall be able to transition from one flight condition to another without exceeding the limit load factor in normal conditions.	B § 27.141(b)	
CON-CRT-PER-15	The aircraft shall be able to transition from one flight condition to another without exceeding the limit load factor in one engine inoperative conditions.	B § 27.141(b)	
CON-CRT-PER-16	The aircraft shall be able to withstand load factors of -0.5 to +2.	D § 27.337(b)	
CON-CRT-PER-17	The aircraft shall be able to withstand loads from a 30 $[ft/s]$ gust for any flight condition.	D § 27.341	
CON-CRT-PER-18	Performance data shall be determined with a relative steady wind of 17 $[kts]$.	VTOL 2105.1.(a-b)	
CON-CRT-PER-19	The stall or minimum steady flight speed shall be determined.	B § 23.2110	
CON-CRT-PER-20	The climb performance after a critical loss of thrust in cruise shall be determined.	B § 23.2125a3	

Table 5.4: *Power & propulsion requirements*

Code	Requirement	Reference	Type
CON-VFS-PP-01	The system shall perform the mission with an idealized battery with an energy density of 400 [Wh/kg].	VFS	
CON-VFS-PP-02	No additional power sources shall be available during flight.	VFS	
CON-VFS-PP-03	The battery reserve energy shall be equal to at least 20 minutes of continuous draw of the power level at cruise condition.	VFS	
CON-CRT-PP-01	The aircraft shall have a power supply independent from the main lighting system to light the emergency exit signs.	§ 29.812(a)	
CON-CRT-PP-02	The aircraft shall have a power supply independent from the main lighting system to provide enough general lighting in the cabin.	§ 29.812(a)	
CON-CRT-PP-03	The emergency lighting shall provide the required level of illumination for at least 10 minutes after an emergency landing.	§ 29.812(e)	
CON-CRT-PP-04	The load distribution for lift/thrust unit designs shall be determined.	VTOL.2225.3	
CON-CRT-PP-05	Any single failure of an automatic power or thrust system shall not prevent continued safe flight and landing of the aircraft.	E § 23.2405b	

Table 5.5: *Cabin design requirements*

Code	Requirement	Reference	Type
CON-VFS-CA-01	The baseline configuration of the cabin interior shall be able to accommodate four adult passengers without disabilities.	VFS	Key
CON-VFS-CA-02	The configuration of the cabin interior shall be reconfigurable to accommodate no less than two adult passengers with disabilities.	VFS	Key
CON-VFS-CA-03	The cabin shall have a baggage compartment for checked baggage.	VFS	
CON-VFS-CA-04	For disabled passengers, the baggage compartment shall accommodate their required durable medical equipment in addition to their baggage.	VFS	
CON-CRT-CA-01	Handrails shall allow persons with disabilities to grasp them from outside the vehicle while starting to board, and to continue to use them throughout the boarding process.	ADA B § 1192.23	
CON-CRT-CA-02	The handrail shall have a cross-sectional diameter between 11/4 inches and 11/2 inches or shall provide an equivalent grasping surface.	ADA B § 1192.23	
CON-CRT-CA-03	Handrails shall not interfere with wheelchair or mobility aid maneuverability when entering or leaving the vehicle.	ADA B § 1192.23	
CON-CRT-CA-04	The wheelchair securement system shall be placed as near to the accessible entrance as practicable and shall have a clear floor area of 30 inches by 48 inches.	ADA B § 1192.23	
CON-CRT-CA-05	For each wheelchair or mobility aid securement device provided, a passenger shoulder harness shall be provided.	ADA B § 1192.23	
CON-CRT-CA-06	For each wheelchair or mobility aid securement device provided, a passenger seat belt shall be provided.	ADA B § 1192.233	
CON-CRT-CA-07	All aisles, steps, floor areas where people walk and floors in securement locations shall have slip-resistant surfaces.	ADA B § 1192.25	
CON-CRT-CA-08	Doorways shall have at least 20 lumen of illumination measured on the lift or ramp, when deployed at the vehicle floor level.	ADA B § 1192.31	
CON-CRT-CA-09	The vehicle doorways shall have outside lights which, when the door is open, provide at least 10 lumen of illumination on the street surface for a distance of 3 feet.	ADA B § 1192.31	
CON-CRT-CA-10	The aircraft shall provide sufficient external view so that the pilot can perform their task of safely controlling the aircraft flight path.	VTOL.2600.1.a & § 29.773(a(1))	
CON-CRT-CA-11	Optical distortions in the windshield, especially in the prime viewing areas shall be avoided.	VTOL.2600	

Code	Requirement	Reference	Type
CON-CRT-CA-12	The aircraft shall have a precipitation removing device for the windshield.	§ 29.775 & VTOL.2600.1b	
CON-CRT-CA-13	The external field of view shall be sufficient in day/night, and not impaired by precipitation or snow conditions.	VTOL.26001(d-e)	
CON-CRT-CA-14	Windshields and windows shall be made of material that will not break into dangerous fragments.	§ 29.775	
CON-CRT-CA-15	Cockpit controls shall be located to provide convenient operation, unrestricted movement of each control and to prevent confusion and inadvertent operation.	§ 29.777(a)	
CON-CRT-CA-16	Each external door shall be located to ensure that persons using the door will not be endangered by rotors, propellers, engine intakes, and exhaust when operating procedures are used.	§ 29.783(b)	
CON-CRT-CA-17	The surroundings of all seats designated for occupancy during takeoff and landing shall be free of sharp edges.	§ 29.785(a)	
CON-CRT-CA-18	The surroundings of all seats designated for occupancy during takeoff and landing shall be free of protuberances.	§ 29.785(a)	
CON-CRT-CA-19	The surroundings of all seats designated for occupancy during takeoff and landing shall be free of hard surfaces.	§ 29.785(a)	
CON-CRT-CA-20	Each occupant's seat shall have a combined safety belt and shoulder harness with a single-point release.	§ 29.785(c)	
CON-CRT-CA-21	If seat backs do not have a firm handhold, aisles shall contain hand grips or rails to let the occupants steady themselves while using the aisle in moderately rough air.	§ 29.785(d)	
CON-CRT-CA-22	Each non-PRM passenger seat and its supporting structure shall be designed for an occupant weight of at least 77 [kg].	§ 29.785(f)	Key
CON-CRT-CA-23	The cabin air shall be free of any hazardous or harmful gases.	§ 29.831(b)	
CON-CRT-CA-24	Emergency exit signs shall be placed above or next to emergency exits.	§ 29.811(c)	
CON-CRT-CA-25	The emergency exit signs shall have a minimum luminescence of 0.56 lumen per [m^2].	§ 29.811(d)	
CON-CRT-CA-26	Each occupant protection system shall not create a hazard that causes secondary injury to the passengers.	C § 23.2270d	
CON-CRT-CA-27	The cabin shall have readily located and easily accessible to emergency exits.	D § 23.2315a(2-3)	
CON-CRT-CA-28	The pilot, while seated, shall be able to easily access the fire extinguishing means in the cabin.	D § 23.2325f1	
TC-CA-01	Each PRM seat and its supporting structure shall be designed for an occupant weight of at least 90.72[kg] and a wheelchair weight of at least at least 113.4[kg].	Mass budget	Key
TC-CA-02	The cabin seats shall be able to accommodate booster seats approved for aviation use.	VFS	Key
TC-CA-03	The system shall be designed not to induce epilepsy.	Market analysis	Key
TC-CA-04	The cabin shall accommodate animals which fit in kennels of sizes 44[cm] × 30[cm] × 19[cm].	Market analysis	Key
TC-CA-05	The cabin shall have measures mitigating passenger infections from viruses.		Key
TC-CA-06	The temperature of the cabin shall remain within the range 18-25 [°C] during operation.	Market analysis	Key

Table 5.6: *Structural requirements*

Code	Requirement	Reference	Type
CON-VFS-STR-01	The aircraft length with rotors turning shall be no greater than 15.24 [m].	VFS	
CON-VFS-STR-02	The aircraft width with rotors turning shall be no greater than 15.24 [m].	VFS	
CON-CRT-STR-01	If outboard fins or winglets are included on the horizontal surfaces or wings of the aircraft, these surfaces shall be designed for their maximum load in combination with loads and moment exerted by the fins or winglets on the surfaces.	VTOL 2225.3.a	
CON-CRT-STR-02	In the event of an emergency water landing, the total lift, assumed to act through the centre of gravity during water entry, shall not exceed two-thirds of the design maximum weight.	VTOL 2270(c).1.a.4.	
CON-CRT-STR-03	The propeller blades shall be at minimum <20> [cm] from any other structural part of the aircraft.	D § 27.661	
CON-CRT-STR-04	The center of gravity limits shall lie within the extremes within which the structure is proven.	G § 27.27(b)	
CON-CRT-STR-05	The aircraft shall not have any excessive vibrations in any part or subsystem during operation.	B § 27.251	
CON-CRT-STR-06	The aircraft shall be able to sustain limit loads without permanent deformations.	C § 27.305(a)	
CON-CRT-STR-07	The aircraft shall be able to sustain ultimate loads without failure.	C § 27.305(b)	
CON-CRT-STR-08	Structures essential to a controlled landing shall be fireproof.	D § 27.861	
CON-CRT-STR-09	The design of the structure shall minimize the probability of fatigue failures.	D § 27.613(c)	
CON-CRT-STR-10	The structural design loads from asymmetric thrust resulting from the failure of a powerplant unit shall be determined.	C § 23.2215c	
CON-CRT-STR-11	The aircraft shall be designed to minimize hazards to the aircraft due to structural damage by fragments from a rotating part failure.	C § 23.2240d	
CON-CRT-STR-12	A factor of safety for each critical design value for each part shall be determined.	C § 23.2265a	
CON-CRT-STR-13	The aircraft shall have a means of stopping with sufficient kinetic energy absorption for landing conditions.	D § 23.2305b	
CON-CRT-STR-14	The aircraft shall be designed to protect the pilot and flight controls from propellers.	D § 23.2320a2	
CON-CRT-STR-15	The aircraft shall be designed to protect passengers from serious injury due to damage to windshields and windows.	D § 23.2320a2	
CON-CRT-STR-16	Equipment containing high-energy rotors shall be designed or installed to protect the passengers and aircraft from uncontained fragments.	E § 23.2550	
TC-STR-01	The aircraft shall have a landing system.	VFS	
TC-STR-02	The loads which the landing system will have to support shall be determined.		
TC-STR-03	The landing system shall prevent the aircraft from rolling over to its side.		
TC-STR-04	The landing system shall prevent the aircraft from tipping over.		
TC-STR-05	The landing system shall aid in providing a smooth deceleration during landing.		

Code	Requirement	Reference	Type
TC-STR-06	For the use of composite structures, failure due to fatigue loads shall be avoided throughout the operational life of the aircraft.		
TC-STR-07	Motor compartments shall be designed to resist vibrational loads.		
TC-STR-08	Motor compartments shall be fireproof.		
TC-STR-09	The landing gear shall be able to withstand the landing loads.		
TC-STR-10	The structure shall be able to support 1.5 times the limit load.		
TC-STR-11	The aircraft structure shall be able to withstand possible bird strikes without sustaining damage.		

Table 5.7: *Control& stability requirements*

Code	Requirement	Reference	Type
CON-CRT-STA-01	The aircraft shall be controllable during steady flight.	B § 27.143(a)	
CON-CRT-STA-02	The aircraft shall be controllable during takeoff.	B § 27.143(a)	
CON-CRT-STA-03	The aircraft shall be controllable during hover.	B § 27.143(a)	
CON-CRT-STA-04	The aircraft shall be controllable during climb.	B § 27.143(a)	
CON-CRT-STA-05	The aircraft shall be controllable during turning.	B § 27.143(a)	
CON-CRT-STA-06	The aircraft shall be controllable during landing.	B § 27.143(a)	
CON-CRT-STA-07	The controls shall prevent sudden motor operation when not commanded by the pilot.	VTOL.2400.a	
CON-CRT-STA-08	The landing speeds shall guarantee minimum controllability.	VTOL 2105.3.c.	
CON-CRT-STA-09	The aircraft shall maintain longitudinal trim.	B § 23.2140b	
TC-STA-01	The centre of gravity range for safe operation shall be determined.		Key

Table 5.8: *Aerodynamic requirements*

Code	Requirement	Reference	Type
CON-VFS-AE	Tip speeds of propellers shall not exceed 600 [ft/s].	VFS	
CON-VFS-AE	The blade characteristics of propellers shall be determined.	VFS	
CON-CRT-AE-01	The aircraft shall have controllable stall characteristics.	B § 23.2150a	
TC-AE	For any lifting surface that stalls within the operational envelope, the mitigation of these stall effects shall be determined.		

5.2. Vehicle Mission

Table 5.9 lists the profile of the flight with technical requirements or specifications given by the VFS.

Table 5.9: *Flight phases for the mission with respective performance requirements.*

Phase	Notes
IGE hover	10 s
Vertical climb	ROC = 0.8128 m/s
OGE hover	10 s
Climb	Climb angle = 9.46° Vertical distance = 579.12 m Horizontal distance = 8.282 km
Cruise	149.25 km
Descent	Descent angle = 4° Vertical distance = 579.12 m Horizontal distance = 3.368 km
OGE hover	10 s
Vertical descent	ROD = 0.8128 m/s
IGE hover	10 s
Reserve	20 minutes

5.2.1. Takeoff

The takeoff sequence involve three distinct phases. The first phase is the in-ground effect (IGE) hover, in which the aircraft hovers just above the ground that some of the ground effect resulting from the rotors are utilized to provide some lift. This phase lasts for 10 seconds before beginning the vertical climb phase. In the vertical climb phase, the aircraft climbs to an altitude of 100 feet above the ground. The rate of climb is specified by the VFS to be 0.8128 [m/s]. As the aircraft reaches the target altitude, it will start its out-of-ground effect (OGE) hover phase, in which no ground effect is present to bolster the lift. Similar to the IGE hover phase, this phase will also last for 10 seconds. During the takeoff, all six proprotors are in its upright position to produce an upward thrust.
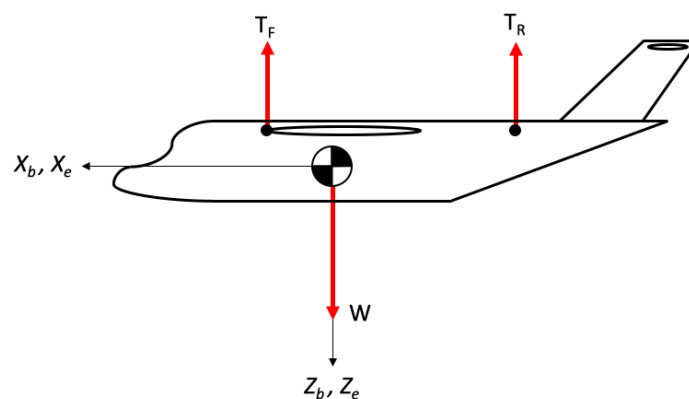

Figure 5.1: *Free body diagram of the aircraft at hovering phase.*

5.2.2. Transition to fixed wing: acceleration

The transition from a rotorcraft configuration to a fixed wing configuration first requires the aircraft to accelerate in order to gain airspeed for wing lift. In this part, the aircraft will fly parallel to the

horizon and gain airspeed until it reaches a sufficient speed for climb. During this process, the rotors are tilted forward at its optimal angle to accelerate and keep the aircraft level. The free body diagram for this phase is shown as in Figure 5.2. As the aircraft gains enough speed for climb, the elevators on the tail is controlled to pitch the aircraft nose upward. The main wing will begin to produce lift, and the aircraft will start gaining altitude. This is shown in Figure 5.3.
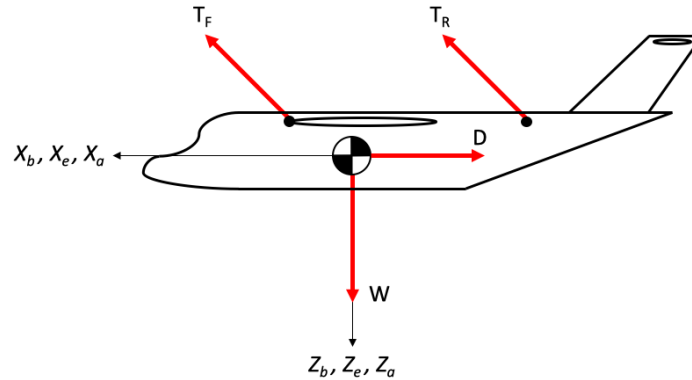
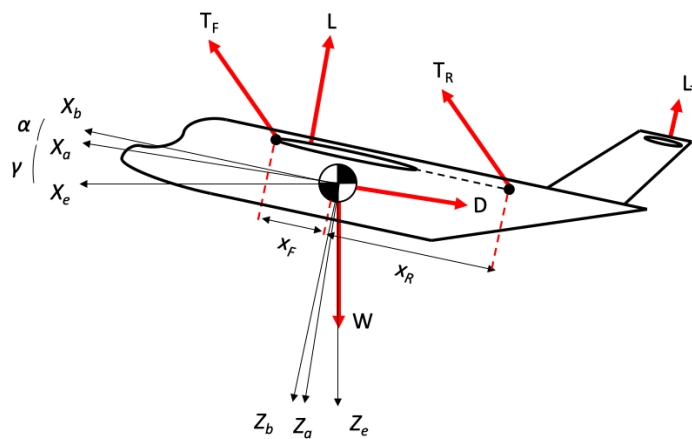**Figure 5.2:** *Free body diagram of the aircraft at acceleration in transition phase.*

Figure 5.3: *Free body diagram of the aircraft in transition phase after pitch up maneuver.*

5.2.3. Climb

At the climb phase, the rotors will tilt to become completely parallel to the aircraft. It is required that enough lift is produced from the wing to counter its weight. At this phase, the aircraft's transition to a fixed wing configuration is complete. The free body diagram for this phase is shown as in Figure 5.4.
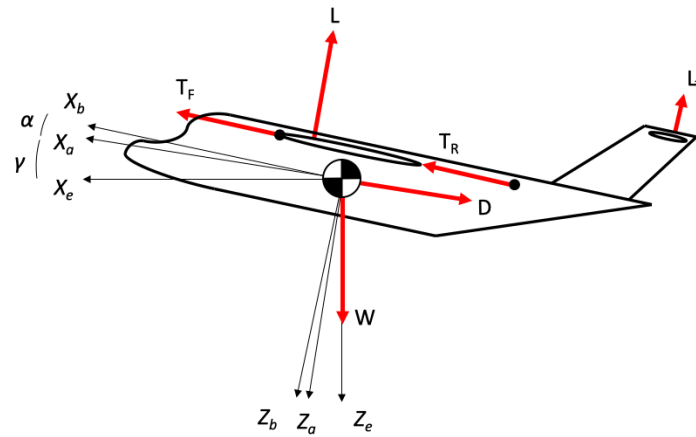
Figure 5.4: *Free body diagram of the aircraft at climbing phase.*

5.2.4. Cruise

The cruise phase is the most energy intensive phase of the flight, and therefore from a perspective of power consumption, it is crucial that the aircraft can fly as efficient as possible during the cruise. The free body diagram for this phase is shown as in Figure 5.5.
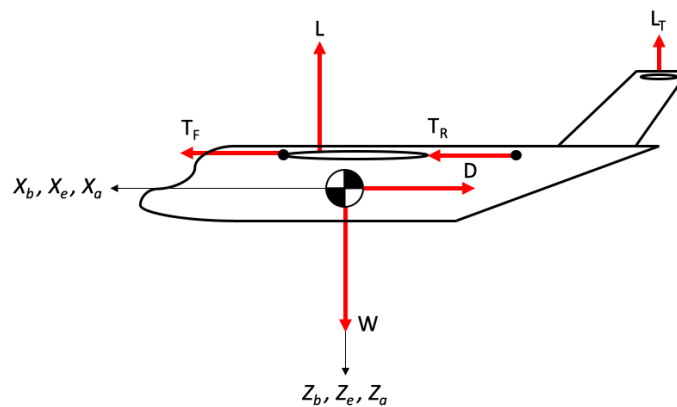

Figure 5.5: *Free body diagram of the aircraft at cruise phase.*

5.2.5. Descent

As the aircraft approaches the destination, it will start its descent approximately at a point of around 8 km from the destination, based on a descent angle of 4 degrees as indicated in the Request for Proposal [1]. This is shown in Figure 5.6.
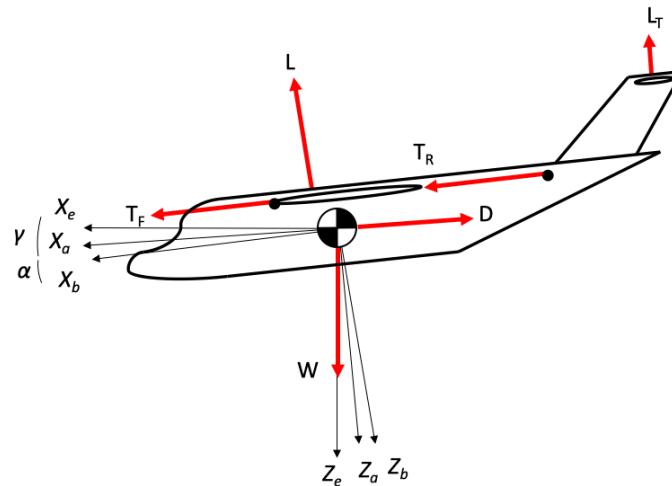
Figure 5.6: *Free body diagram of the aircraft at descent phase.*

5.2.6. Landing transition

The transition for landing involves a maneuver to switching the source of lift from the main wing to the proprotors as it tilts back to the upright position.

5.2.7. Landing

The landing sequence of the aircraft is as indicated in Table 5.9, and it consists of three phases: OGE hover, vertical descent and IGE hover. Similar to the takeoff sequence, the OGE hover will take place at 100 feet above the ground. The rate of descent is assumed to be the same as the rate of climb for takeoff. The forces involved are similar to that of the takeoff configuration.

5.3. Final Layout

The following section describes the final layout of the aircraft with technical and rendered drawings of the aircraft. Furthermore, a review of the numbers is present as the midterm report ended with the design having four rotors.

5.3.1. Review of number of rotors

At the end of the mid term report, the concept chosen included four rotors; 2 wing mounted and 2 fuselage mounted, and makes the whole aircraft similar to a quadcopter design. However, this concept has one major design flaw which relates to safety. Requirements CON-VFS-PER-08 and CON-VFS-PER-09 state that the aircraft should be able to continue safe flight and perform IGE hover with one rotor failure. With four rotors, as soon as one fails, there is an imbalance in torque coming from the one rotor spinning in the opposite direction of the other two, and as a result the whole quadcopter starts spinning[1]. This is visualised in Figure 5.7, which shows the typical direction which motors of a quadcopter spin, and also shows how one failure causes a resulting torque on the aircraft. It should be noted that the torque deficit cannot be compensated by the other rotor turning in the same direction as that would cause the whole quadcopter to tip over. While flight and hover are still possible, the spinning of the aircraft is still very dangerous for the passenger health and safety, and thus another rotor configuration had to be found.

---

[1]https://ethz.ch/en/news-and-events/eth-news/news/2013/12/new-algorithm-makes-quadrocopters-safer.html [cited 17 January 2022]
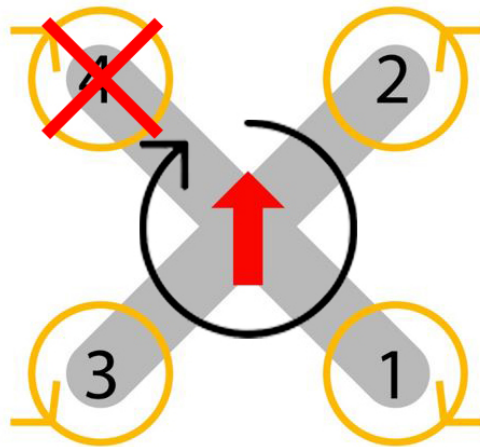
Figure 5.7: *Quadcopter rotor spin direction (yellow) and resulting system spin (black) with rotor failure.*[2]

As a result, two extra wing mounted rotors have been added which would mitigate the torque differential and stabilise the aircraft. Furthermore, the inner wing mounted rotors would have a longitudinal offset to the outside mounted rotors, increasing the effect that a hexacopter configuration would have. Studies[7][8] show that a hexacopter still has complete control during flight and hovering with one rotor failure, and thus adding two rotors would allow the aircraft to comply with requirements CON-VFS-PER-08 and CON-VFS-PER-09.

Besides safety, another benefit of this new configuration is that there is enough clearance between the ground and propellers when the rotors are put in the cruise condition. This has benefits of facilitating maintenance checks and also gives the possibility of performing non vertical emergency landings in case the mechanism responsible for transitioning the rotors malfunctions. On the other hand, due to the rotor radius decreasing, the power required for the different flight phases increases, and thus a larger total energy will be required, increasing operational costs and the mass of the battery. As there are more mechanism in the whole structure, the maintenance time and costs would as a result also increase. While the disadvantages are significantly impactful, the safety of the passengers is paramount, and thus the configuration of the six rotors is chosen.

5.3.2. Technical drawing
The following page presents the technical drawing of the Aether aircraft. The drawing includes the front, side, and top view in a 1:150 scale. The most important dimensions are also indicated, along with an isometric view of the aircraft in a 1:00 scale.
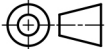
---

[2] https://www.getfpv.com/learn/fpv-essentials/how-to-setup-reversed-propellers/ [cited 17 January 2022]

2   1

B   B

A   A

Front view
Scale: 1:150

0.48

4.48

2.58

Side view
Scale: 1:150

1.80

2.49

1.09

9.15

Top view
Scale: 1:150

6.00

3000

1.38

5.64

0.50

15.00

Isometric view
Scale: 1:100
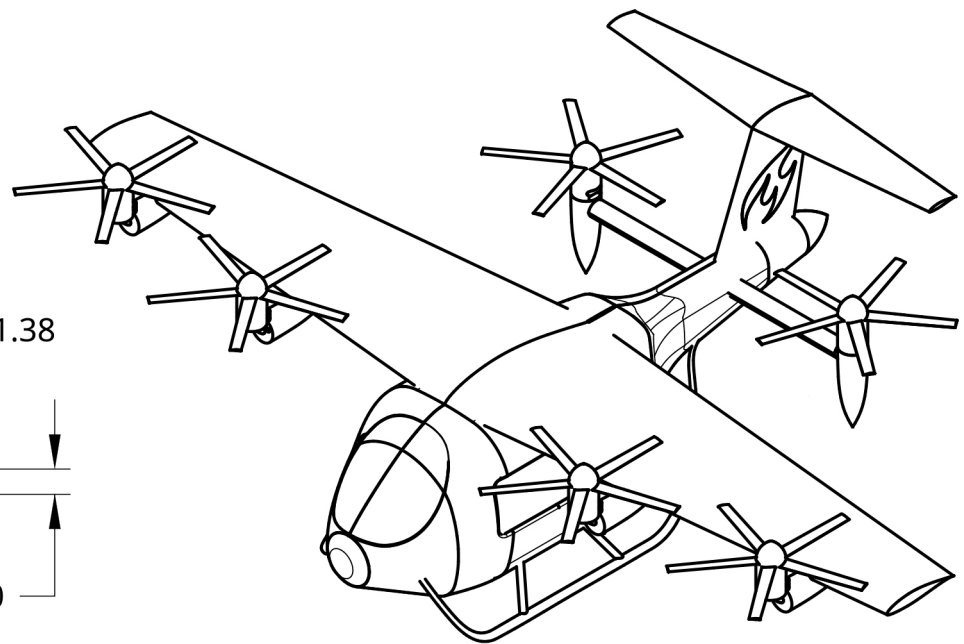
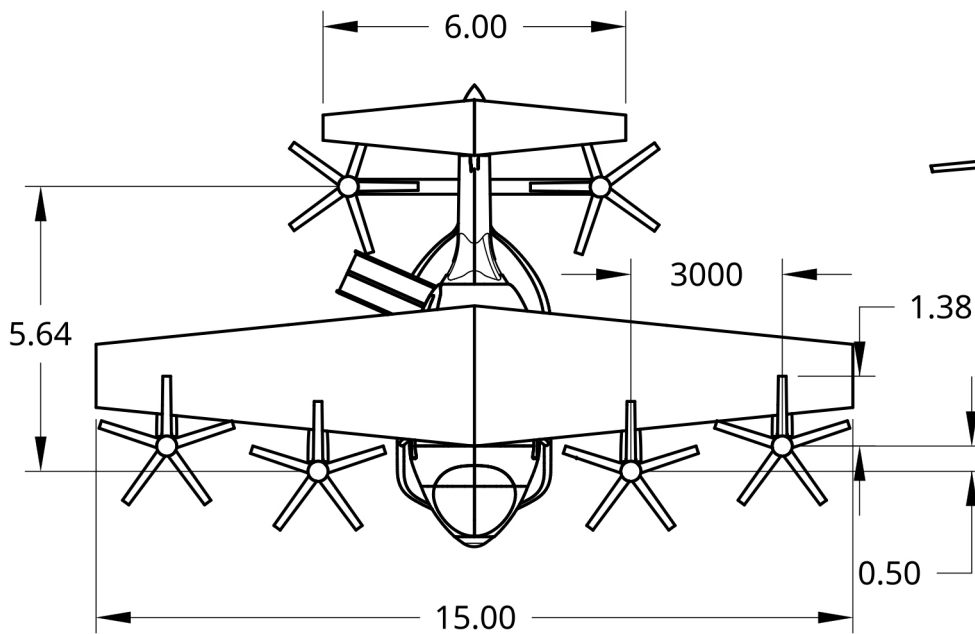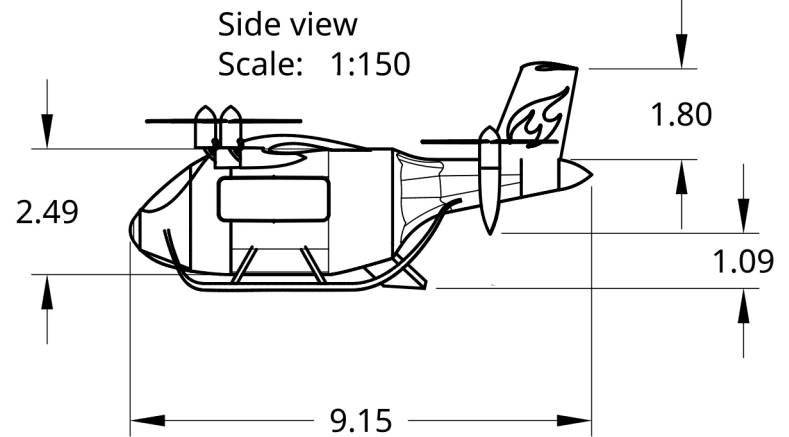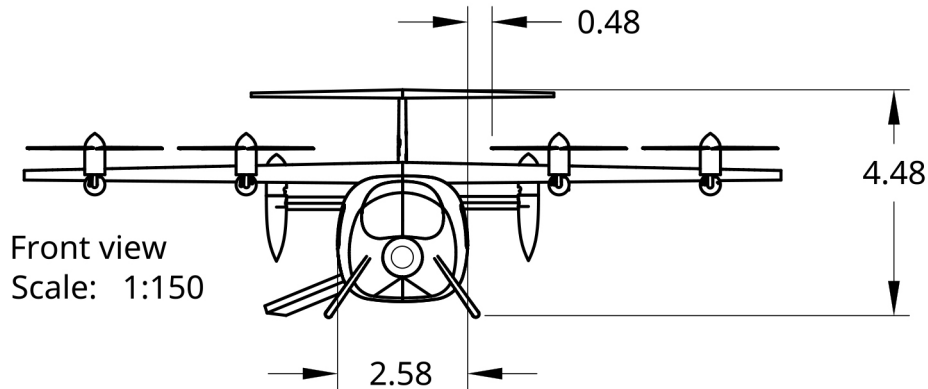|	NAME	DATE	TITLE	
UNLESS OTHERWISE SPECIFIED, DIMENSIONS ARE IN METERS				
DRAWN	JONATHAN TEGISCHER	20/01/2022	**AETHER v1.0**	
DO NOT SCALE DRAWING — CHECKED	ANTONIO GARCIA BULDER	20/01/2022		
BREAK ALL SHARP EDGES AND REMOVE BURRS — APPROVED	VASILEIOS ZYGOURIS	20/01/2022		
THIRD ANGLE PROJECTION — MATERIAL	Carbon Fiber (60%), Aluminium (20%), Other (20%)	FINISH --	SIZE A4 DWG NO.	**1.1**

MAXIMUM TAKE OFF WEIGHT: 2667.0 kg   OPERATIONAL EMPTY WEIGHT: 1963.0 kg   SHEET 1 of 1

2   1

5.3.3. Rendered drawings

With the design finished and technical drawing completed, a render of the aircraft can be made using the KeyShot10 software. Figure 5.8 shows the aircraft with the propellers in their hover configuration, while Figure 5.9 shows a render of the aircraft with the propellers as they would be in cruise.
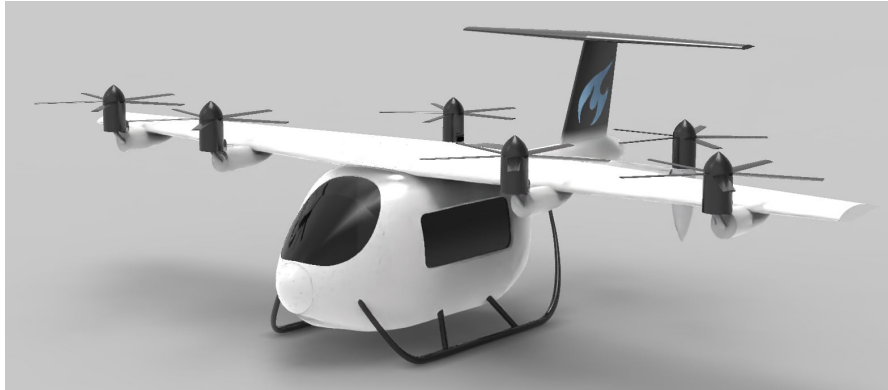
Figure 5.8: *Render of the Aether aircraft in its hover configuration.*
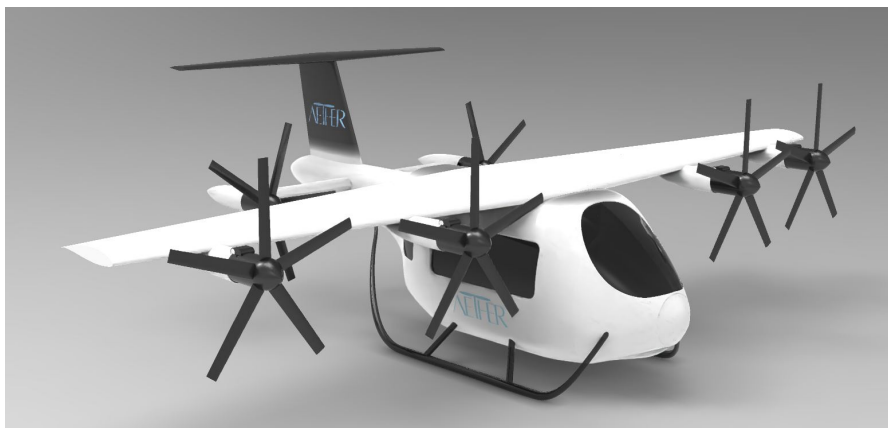
Figure 5.9: *Render of the Aether aircraft in its cruise configuration.*

5.4. Data Handling Block Diagram

The data handling block diagram is a representation of how the main data transfer in an Aether aircraft would flow. It explains how the hardware in the aircraft interacts with one another and which information is passed between data blocks. A top level simplification of the data handling block diagram starts with the control inputs, which are then processed and executed. Aircraft state determination then controls all aircraft parameters and sends feedback back to the control input block. The following page illustrates the data handling block diagram in detail. Blue boxes indicate the main physical functioning hardware for each top level data block, and white boxes represent the rest of the hardware. Text on arrows are the function that occurs between the two hardware blocks.

Data Handling Diagram

Top level data handling
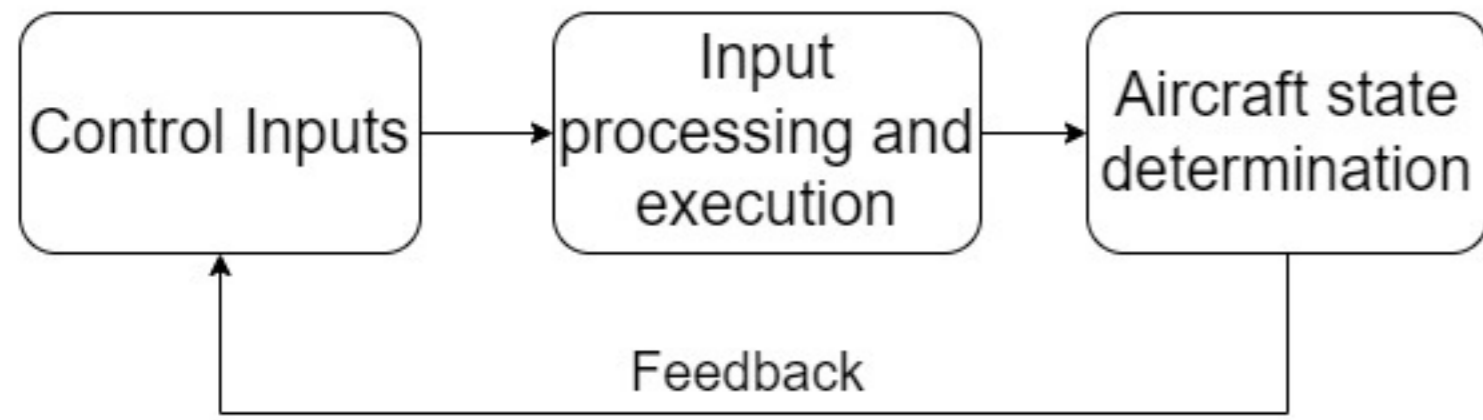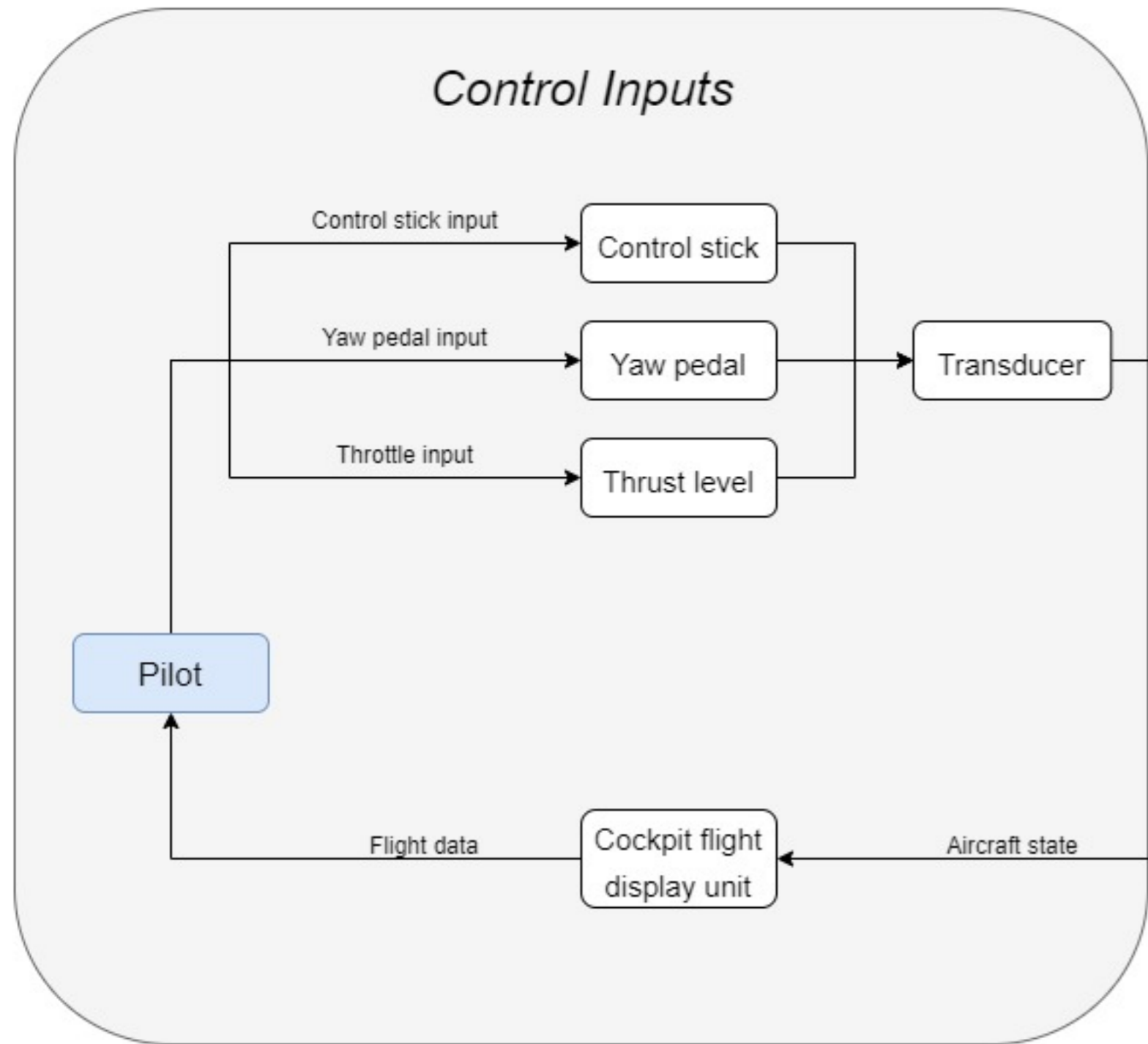
```
Control Inputs → Input processing and execution → Aircraft state determination
        ↑_____ Feedback _____|
```

Control Inputs

- Control stick input → Control stick
- Yaw pedal input → Yaw pedal
- Throttle input → Thrust level
- Control stick, Yaw pedal, Thrust level → Transducer
- Pilot
- Cockpit flight display unit → Flight data → Pilot
- Aircraft state → Cockpit flight display unit

Input Processing and Execution

- Flight control computer
- Control input settings → Power distribution unit
- Aileron input → Aileron actuator
  - Right aileron deflection → Right aileron
  - Left aileron deflection → Left aileron
- Elevator input → Elevator actuator
  - Elevator deflection → Elevator
- Throttle input / Yaw input → Electric motor controller
  - RPM differential → Electric motors

Aircraft State Determination

- True aileron deflection → Aileron sensors
- True elevator deflection → Elevator sensors
- True airspeed → Airspeed indicator
- Auxiliary traffic data → Air traffic detection system
- Sensor processing unit
- Aircraft attitude determination: Angle of attack sensors, Accelerometer, Gyroscope
- Aircraft position determination: GNSS, Altimeter, Barometric sensor

5.4.1. Control inputs

As no autopilot feature is present in the aircraft, all the inputs must come directly from the pilot. The pilot also receives information from the cockpit flight display unit which communicates relevant flight data. The pilot has three main inputs: control stick input, yaw pedal input, and throttle input.

The control stick input has the function of controlling the pitch and roll of the aircraft by controlling the elevator and aileron respectively. The yaw pedal controls the yaw of the aircraft using rotor rpm differential such that rotors on one side of the aircraft produce more thrust more than the other side, causing a turning motion around its z axis. Finally, the throttle input controls the thrust level by again increasing or decreasing the rpm of the rotors. All the physical inputs are converted into electrical signals using the transducer, which then send the data to the flight control computer.

5.4.2. Input processing and execution

This data handling block is responsible for processing the inputs given by the pilot and executes the appropriate actuator corresponding to the input. All the inputs from the pilot are collected in the flight control computer which sends the order of which control system or motor to activate to the power distribution unit. The power distribution unit (PDU) controls the electrical power going to the control surfaces and electric motors and controls the amount of actuation based on the input of the pilot which has been processed and converted by the flight control computer.

For the ailerons and elevator, a surge in power given from the PDU causes the control surface to actuate and perform its function based on the the current of the signal. Sensors then collect the actual deflection of the control surface to be sent to the sensor processing unit for verification. For the throttle and yaw inputs, the power distribution unit commands the electric motor controller to increase or decrease its RPM such that the desired output is achieved. The specifications of the electric motor controller are detailed in Chapter 9.

5.4.3. Aircraft state determination

The final major data block is the aircraft state determination, where sensors collect all the necessary data needed for safe flight. This data is then processed and compiled into useful data for the pilot. For the production of the sensors, purchasing off the shelf products is advised as opposed to manufacturing the sensors from scratch, as this would reduce the research and development time and cost significantly. Furthermore, many products are already used in aerospace applications, and therefore are reliable and tested thoroughly.

The aileron and elevator sensors are responsible for determining the true deflection of these control surfaces. This is important to measure in order to check whether there is a fault in a certain actuation system or if the flight control computer is receiving the inputs correctly.

The airspeed indicator is used to measure the true airspeed of the aircraft. This is achieved by calculating the difference between static and dynamic atmospheric pressure. This is can be achieved with pitot tubes which are commonly used in aerospace applications.

Another instrument important to the safety of the aircraft is the implementation of the air traffic detection system. This determines the location of other aircraft in the vicinity through their shared positional information from the GNSS system. Every 0.5 seconds, the position of each aircraft would

update and provide reliable information to the pilot[3]. This is important once AAM becomes common and multiple eVTOL aircraft will be flying above cities and vertiports will start to be more congested. Additionally, a system feature can be implemented to provide the pilot with the safest route to follow in case the aircraft is on a collision route with another aircraft.

For determining the position of the aircraft, a combination of Global Navigation Satellite System (GNSS), altimeter and barometric sensor sensors are used. The GNSS has similar capabilities to the Global Positioning System (GPS), but includes additional position determining systems and is able to accurately predict ones location with rapid feedback. The altimeter is a tool used to measure the altitude of the aircraft. This can be done using radar, where radio waves are projected towards the ground and the time to reflect back indicates ones altitude. The barometric sensor is responsible for measuring the atmospheric pressure, which is another effective way to calculate and verify the altitude of the aircraft.

The last set of sensors are used to determine the attitude of the aircraft, and involves a combination of accelerometers, gyroscopes, and angle of attack sensors. The accelerometer is used to measure the accelerations in the aircraft which can arise from turbulence or due to control surface actuation's. This is useful to check that the ultimate loads are not exceeded. Furthermore, low and high frequency vibrations can also be detected by the accelerometer and is important to monitor any natural frequencies which could develop in the wings or rotors. Gyroscopes are used to determine an aircraft's attitude and aid the pilot in controlling the aircraft. Finally angle of attack sensors measure the angle of attack of the aircraft. For an eVTOL aircraft this is especially important as some flight phases such as hovering are unstable and thus pilot inputs are the only factor keeping the aircraft stable. Thus angle of attack indicators are important for stability and controllability purposes.

5.4.4. Reliability

Reliability of these systems is a very important factor that needs to be taken into consideration. If any of the control blocks fails and no contingency plan is present, the aircraft is put in a dangerous flying state. If any control input fails or the input processing and execution malfunctions, the aircraft will be less controllable. If any sensor of the aircraft state determination block fails, the pilot would be given incorrect data and detrimental flight decisions could be made.

For this reason, sensors will be usually coupled with a backup sensor which continually verifies that the primary sensor is correct. As the flight control computer is such an integral part of the data handling block and responsible for the actuation of the control surfaces, these are often accompanied by one or two redundant computers which can take over in case of failure. A complete restart of the system can also be made in case of a software glitch. Finally, as the control inputs are mechanical, these can be designed such that the reliability is high enough and a second set of controls is not required.

---

[3] https://aireon.com/services/global-air-traffic-surveillance/ [cited 19 January 2022]

5.5. Spec Sheet

MTOW	2667 [kg]
Passengers + Pilot	5 passengers
Passenger mass	100 [kg]
Range	100 [miles]
Flight Time	56 [min]
Operating Altitude	4000 [ft]
Cruise Speed	49 [m/s]
Vertical Climb Speed	0.813 [m/s]
Vertical Descent Speed	0.813 [m/s]
Wing Span	15 [m]
Rotor Radius	1.4 [m]
Disk Loading	73 [Kg/m^2]
Noise	86 [dBA]
Maximum Tip Speed	182 [m/s]
Hover Power Required	580 [kW]
Maximum Power Required	588 [kW]
Battery Mass	520 [kg]
Battery Energy Density	400 [Wh/kg]
Battery Cell Type	Li-ion
Materials of Structure	CFRTP and Al-Li 2198

6

Design Methodology

The following chapter describes the design methodology used to design the Aether aircraft. Section 6.1 gives an overview of all the subsystems in the aircraft, and Section 6.2 describes the method to size and design all the subsystems. Finally, Section 6.3 outlines the ways in which the subsystems will be verified and validated.

6.1. Subsystem Overview

To begin the design of each subsystem, an outlook on the subsystem design and its objectives shall be identified to get a clear understanding of what exactly must be sized. The following explanations provide a brief overview of all the subsystems of Aether, and are structured in the order as in the report.

Cabin design: The cabin design focuses on the passenger experience and aims at fulfilling their needs according to the structural and mission constraints. As requirement TL-CON-VFS-02 demands that the aircraft shall be accessible to people with any type of intellectual or physical disability, a heavy focus is put into designing the cabin such that the aircraft is inclusive and accessible to everyone. Furthermore, a focus is put into the logistical side of the cabin in order to fit all luggage, comfortably accommodate the pilot in the cockpit, and simplify the boarding procedures for the PRM at the vertiports.

Propulsion & performance: This subsystem is analyses the power requirements that the aircraft will need for every phase of flight. Once these are found, the rotor tilting mechanism is analysed such that the transition phase is mechanically backed up and designed for. The class I and class II mass estimations are run through a python script and converged in order to come up with a final MTOW and OEW. Finally, an analysis is made on the propeller design an extensively sizes all the characteristics of the blade.

Powertrain: The powertrain subsystem designs the high voltage battery interface and sizes all electronic components in Aether. A focus is put on the motors and battery of the aircraft due to their importance and connection to flight performance. An electrical block diagram along with the hardware and software interfaces detail out all electrical connections and relations that are required to have a functioning aircraft.

Aerodynamics: This subsystem analyses the effects of the air on the aircraft while it is in motion. In particular, the wing is of high interest for optimising cruise performance, while the empennage focuses on meeting requirements for the stability and control of the aircraft. The drag of the fuselage is also relevant for stability and performance purposes. Finally, a noise analysis is performed to comply with certification requirements.

Structures & materials: This subsystem sizes exterior structural components and verifies the structural rigidity of the structure based on the ultimate loads given by certification. The structures analysed in detail are the boom connecting the back motor to the fuselage and the wing box. In combination with these analyses the materials are chosen for the structure and individual subsystems, and a final analysis of the landing gear is also discussed.

Stability and control: To begin the analysis of this subsystem, the reference frames and equations of motion are evaluated such that a consistent framework can be used for the stability and control

of the aircraft. In order to analyse the static stability, a potato diagram is constructed along with a scissor plot, while the eigenmodes of the short period and phugoid motions are calculated as part of the dynamic stability of the aircraft. With the flight dynamics and stability cases analysed, a MATLAB script is written which models a controller for the cruise and hover flight phases. Finally, the more complex transition flight phase is also analysed and modelled such that it can also be controlled by a MATLAB script.

6.2. Design Procedure

This section outlines the steps that are taken during the design of each subsystem. The following is a general outline and is not necessarily always followed. The six steps are as follows:

1. **Analyse requirements and assumptions:** The first step to designing a subsystem is to analyse the requirements that need to be met. Sorting through the requirements and categorising them based on importance and complexity is also very useful to identify which requirements can be met easily and which requirements will need to have more effort put into to meet them. Additionally, the assumptions relevant for the subsystem shall be determined.

2. **Identification of subsystem sizing:** Based on the analysis of the requirements, the parts of the subsystem which need to be sized can be identified. As this is still part of conceptual design, the sizing does not have to be incredibly detailed and thus only the crucial parts to meet the requirements shall be sized. More minute and detailed parts can be left out for the preliminary and detailed design phase.

3. **Preliminary sizing:** In this step the components which need to be designed for are calculated and sized. This involves calculating the actual mass, power, size, performance etc. characteristics which were identified in step 2.

4. **Integration:** After the main components are sized, it is integrated in the sub or main assembly, and a check is made whether it fits and is compatible with other components. For power sizing and other non physical components this step can be substituted by verifying whether the sizing integrates with the main mission requirements.

5. **Verification and validation:** After the integration, the component sized shall be verified and validated to check whether the method of designing is correct and is consistent with literature or similar proven tests. A more detailed explanation of the method for verifying and validating the subsystems can be found in Section 6.3.

6. **Iteration/optimisation:** Lastly, steps 1-5 are iterated and improved upon by optimising the component and subsystem. For air travel, the weight of the aircraft can have snowballing effects on the power and cost budgets, and thus minimising the component weights and size has favourable effects. In most cases this is done using a Python or Matlab script in order to save time.

6.3. Verification & Validation

The following section describes the methods that are used to verify and validate subsystems in the aerospace industry. Then, it outlines the specific methods which are applicable to Aether and how the limitation of resources and time affects which verification and validation techniques can be used.

6.3.1. Verification

Verification determines "if a simulation model accurately represents the chosen physical model" [9]. This means that this process checks whether a model is producing expected results based on the constraints and assumptions. There are four main ways to verify a model, and they are as follows:

Inspection: This method of verification works by just inspecting whether a component meets the requirements. This can be made easily with dimensions, cost analysis, and other simple parameters.

Analysis: The method of analysing to verify involves making mathematical calculations to prove a model is correct. This will be the most common method of verifying used for the subsystems.

Demonstration: This method relies on having a physical model created such that a physical demonstration can be made on it. Due to time and resource constraints, a physical model of a subsystem or the aircraft cannot be made and thus this method will not be practised.

Testing: The last method relies on having either a physical or representative model to perform tests on. Due to the lack of resources and time this method will as well not be used to verify parts of the aircraft.

For the models that are created in Python and Matlab, unit testing will be performed in which a small section of the code base is isolated and tested. It is estimated that for every 1000 lines of code, 10-20 of those contain errors, which can lead to errors in the rest of the software[1]. Due to this, it is paramount to test as much of the code written such that these mistakes can be avoided. This type of unit testing is done for small formulas and calculations which can be tested quickly. The most common method of unit testing is to change an input and predicting the output based on theory or knowledge on a formula. If the output of the software is consistent with the expected output, the section of the code can be considered to be verified.

While this method tests smaller sections of the code, it is important to also verify the integration, and this is done using system tests. This analyses whether larger chunks of the software also output results similar to those expected by analysis. A small change is made in one formula and the altered result is recorded and compared. With the combination of unit and system tests, it can be assumed that the code is verified and thus the model itself as well.

Finally, requirement verification is performed through the use of a compliance matrix. This shows which requirements have and been met and also the ones which were not met and have to be analysed in the next phase of design. This testing will be performed mainly through the use of inspection as a cross reference will only be required to justify the compliance of each requirement. The compliance matrix can be found in Section 15.1.

6.3.2. Validation

Validation determines "if the simulation results accurately represent the physical problem" [9]. This means that validation is the process of determining whether a model is correct when put into the real world environment.

---

[1] https://labs.sogeti.com/how-many-defects-are-too-many/ [cited 18 January 2022]

Validation is most commonly performed using three main methods: Experience, Analysis, and Comparison. Experience is the process of validating a model from an engineer's experience in the field. It is possible that a certain component is common to many projects, and thus experience with the component can determine whether the model is correct or not. As this type of design project is new to all group members, this type of validation is not recommended as a wrong judgement or assumption can be dangerous once the aircraft is operational. Analysis is the process of using computer software or real life testing of a part or subsystem to check whether it is performing its function as intended. Due to the complexity of finite element modelling (FEM) software and the scarcity of time, this method is used only in the structures and materials subsystem for simple parts. The last and most common method of validation is through the use of comparison. This method involves taking results from a model and comparing them with real life test data already validated. Another method of achieving this is by inputting characteristics of a aircraft or component which has already been tested and validating whether the model reproduces the results of the real test. As this method is the least resource and time intensive method, it shall be used for all the subsystems.

II

FINAL CONCEPTUAL DESIGN

Passenger Experience

The design of Aether is passenger oriented. This means that the most important aspect when designing is the passenger. Safety is also of major importance, but so is passenger comfort. In this section, the design of the cabin is explained. Firstly, the requirements and passenger needs derive to the main cabin sizing parameters. These are then used for the main cabin design and cabin layout as well as the specific seat design which is also explained in detail. Finally, other specific detail design parameters are explained.

7.1. Passenger Needs

Passengers with Reduced Mobility (PRM) have extensively varied needs, especially when considering the vast description of PRM used in this design. To better understand the requirements of the cabin for each of these passengers, PRM were divided into different personas or PRM categories. These personas were categorised according to the different special needs they may have during air travel. The following main personas are identified as:

- Wheelchair or stretcher user

- Passenger requiring full-time assistance

- Portable oxygen concentrator user

- Limited strength passenger (eg. muscle atrophy, elderly,...)

- Blind and/or visually impaired

- Deaf and/or hearing impaired

- Blind and deaf

- Intellectually disabled (eg. Down syndrome, autism,...)

In the first stage of the cabin design, the main focus is on preliminary sizing. Therefore, initially in this chapter there will be a special focus on verifying how much space each of the personas' special needs will require. This will be defined in detail in the following section.

Firstly, some research was carried out in the field of PRMs. It has been found that at least 6.8% of people with a disability in the U.S.A. are not able to live independently and need full-time assistance [1], which would mean that these passengers require travelling with their personal aid. A similar value of 8% has been found for PRM in the Netherlands [2].

Secondly, for the wheelchair or stretcher users it is important they have wide aisles and doors to move around. It is preferable if they do not have to use an aisle chair and do not have to move from their wheelchair to the passenger seat [3]. Furthermore, there must be enough space in the cabin

---

[1] https://www.1800wheelchair.com/faq/how-much-does-a-wheelchair-weigh/ [cited 24 November 2021]

[2] https://www.cdc.gov/ncbddd/disabilityandhealth/infographic-disability-impacts-all.html[cited24November2021]

[3] https://www.npr.org/sections/health-shots/2019/12/10/786559969/wheelchairs-on-planes-why-cant-passengers-use-their-own-onboard?t=1637745818671&t=1638697374404 [cited 6 December 2021]

to accommodate medical equipment, such as portable oxygen concentrators, crutches and white canes, and assistance animals. Lastly, it is also crucial for the cabin to be high enough so that PRMs such as blind passengers, passengers on crutches or passengers with limited strength, are able to board the aircraft easily and without difficulties. Since these needs are related to cabin dimensions, they are taken into account during the initial sizing of the cabin. Other PRM needs are taken into consideration further in this chapter during the detailed design of the cabin.

Some important initial design choices were made with the use of the personas research:

- An assistant shall be included as part of the PRM configuration of the aircraft, differing with the VFS payload configuration requirement.

- PRM seats should be able to accommodate a wheelchair attached to the chair using chest and waist seat belts: Research has shown passengers requiring a wheelchair experience high levels of physical and psychological discomfort when being changed of wheelchair during travel[4].

- Door containing ramp is placed in the back of the cabin for easy access by wheelchair.

The above design choices mean that a chair shall be designed able to fit and safely hold a wheelchair in place. The detailed design of the PRM chair is explained further in Section 7.3. Furthermore, an aisle fitting a wheelchair will be necessary together with enough space for a wheelchair to be able to parallel park from the aisle.

7.2. Cabin Sizing Parameters

Based on the categories and design choices explained in the previous section, the sizing parameters were researched to be able to construct a preliminary sizing of the cabin layout.

Firstly, the VFS requires this vehicle to transport two PRM or four non-PRM both including their luggage. As explained in the previous section, one of the design choices based on research, is to modify this requirement to transporting two PRM with one assistant or four PRM both including their luggage.

The dimensions needed for the wheelchairs are based on the accessibility criteria for PRM set by ETSI [10]. These guidelines define the space a wheelchair will occupy as the dimensions shown in Figure 7.1. These dimensions are used to define the width of the PRM chair, since the PRM chair will need to envelop the wheelchair.
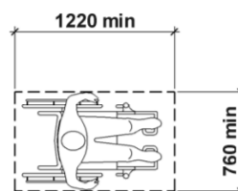

Figure 7.1: *Dimensions of space occupied by a wheelchair in minimum "min" millimeters. [10]*

---

[4]https://www.npr.org/sections/health-shots/2019/12/10/786559969/wheelchairs-on-planes-why-can
t-passengers-use-their-own-onboard?t=1637745818671&t=1638697374404 [cited 6 December 2021]

Secondly, the length of the PRM area, also defined later as the PRM seat pitch, is found from Figure 7.2, which identifies this area as the area required for wheelchair parallel parking.
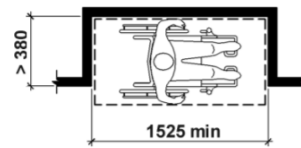

Figure 7.2: *Dimensions of parallel parking space required by wheelchair in minimum "min" millimeters. [10]*

Following this value, Figure 7.3 is used to determine the width of the aisle, as it provides the necessary clearance required by the wheelchair. All the values are shown in the figures are given in minimum "min" millimeters.
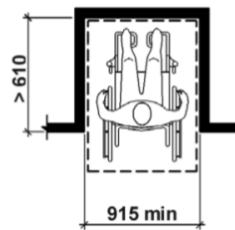

Figure 7.3: *Dimensions of forward parking space required by a wheelchair in minimum "min" millimeters. [10]*

For the non-PRM seat dimensions and cockpit dimensions, the data provided on seats for general aviation aircraft on the Aerospace Design and Systems Engineering Elements lecture slides is used. The values of these dimensions are listed in Table 7.1 as: seat pitch non-PRM, seat width non-PRM, cockpit height and cockpit length.

The dimensions of a typical stretcher are assumed from data coming from a single manufacturer [5].

The carry-on luggage and personal item dimensions are taken from the VFS requirements.
In Table 7.1, all values used for preliminary cabin sizing are listed together with their reference. Values with an asterisk in the reference column are the following assumed values:

- Cabin height: This value is taken from anthropometric data as the height of a 95th percentile male [6]. As stated previously, it is desired to allow PRM to be able to stand inside the cabin.

- Folded seat length PRM: This value is assumed from general aviation data on seat thickness.

- Cockpit width: This value is estimated from general aviation data for small aircraft.

- Medical equipment dimensions: This value is estimated from sources found during research on the personas. The average dimensions of a portable oxygen concentrator are used. It is assumed that this will be the largest piece of medical equipment a PRM will carry together

---

[5]https://www.airmedicstretchers.com/products.php [cited 6 December 2021]
[6]ttps://www.hermanmiller.com/research/categories/white-papers/the-evolution-of-anthropometrics-and-user-control/ [cited 6 December 2021]

with a wheelchair. As an example, if a passenger would bring crutches or a white cane, this could be secured in the PRM area.

Table 7.1: *Cabin sizing parameters. Values with an asterisk (*) in the reference column are explained in the list above.*

Parameter	Size [m]	Reference
Cabin height (from floor)	1.88	*
Seat width non-PRM	0.46	ADSEE information
Seat width PRM	0.76	ETSI guidelines
Seat pitch non-PRM	0.81	ADSEE information
Seat pitch PRM	1.525	ETSI guidelines
Folded seat length PRM	0.2	*
Aisle width	0.915	ETSI requirement
Medical equipment (length x width)	0.3 x 0.3	*
Cockpit height	1.219	ADSEE information
Cockpit length	1.092	ADSEE information
Cockpit width	1	*
Checked luggage (height + width + length)	1.58	VFS requirement
Carry-on luggage (height x width x length)	0.56 x 0.23 x 0.36	VFS requirement
Personal item (height x width x length)	0.45 x 0.2 x 0.35	VFS requirement
Stretcher length	1.93	Manufacturer data [7]
Stretcher width	0.53	Manufacturer data [7]
Door width	0.915	ETSI guidelines

Using these values, the sizing of the cabin was performed. This can be observed in Figure 7.4, which show a scaled version of the top view of the entire cabin, and the widest cross-section of the cabin, respectively. The configuration chosen is a diagonal positioning of the PRM seats to allow for a narrower aisle. The door in the back of the fuselage allows for easy boarding and disembarking. The space in the cabin to make the turn from the door to the aisle and vice versa also follow ETSI guidelines for wheelchair turning. Similarly, there is enough space inside the cabin to perform a turn of 180 degrees in the cabin, according to the regulations. As can be observed, there are two PRM seats and two non-PRM seats. The PRM seats can also be used for passengers with full mobility. This type of seats are sized according to the ETSI guidelines for passengers in a wheelchair to be able to parallel park. Once in place, this extra space can then be used to place additional equipment such as oxygen concentrators, other medical equipment, personal items or assistance animals. In Figure 7.4, the front view shows the cross-section of the widest part of cabin. Here, a more square-like structure can be observed rather than a circular cross-section, in order to allow for sufficient cabin height above the seats.

---

[7] https://www.airmedicstretchers.com/products.php [cited 6 December 2021]
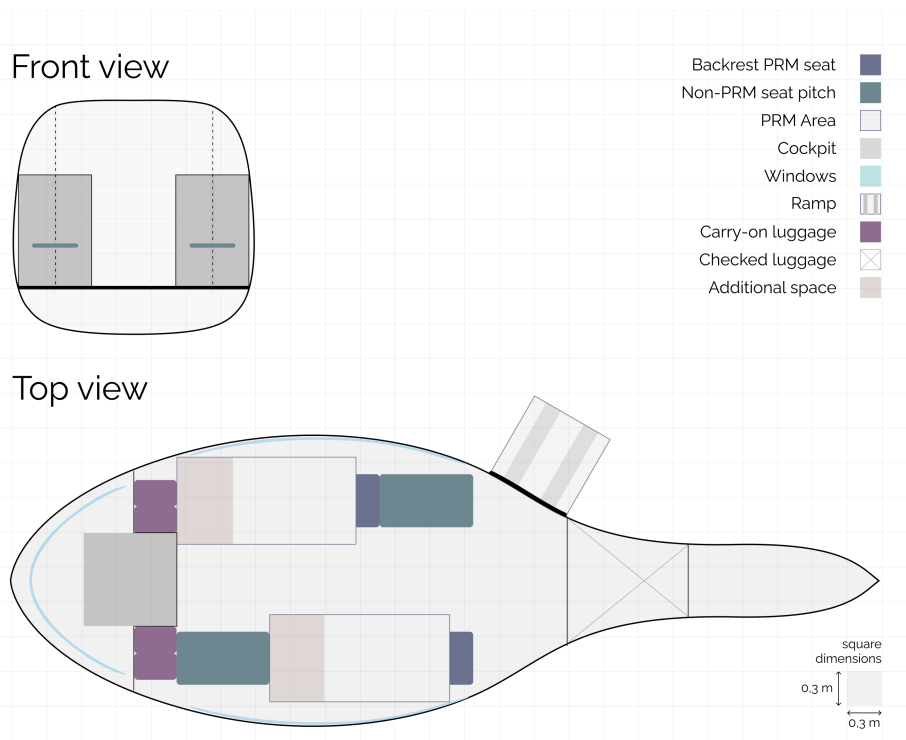
Figure 7.4: *Scaled sketch of the front and top view of the cabin.*

7.3. Detailed Cabin Design

Based on the personas into which PRM are categorized and the cabin design requirements that are based on client needs and certification, the detailed cabin design is done. For the initial cabin dimensioning, the needs of wheelchair or stretcher users, portable oxygen concentrator and other medical equipment users, the visually impaired and passengers with limited mobility were given the greatest emphasis. This is because the needs of these personas defined the upper limits of the cabin size and mass. In the detailed cabin design, besides the interior cabin design and the entry to and exit from the eVTOL, the needs of PRM that have hidden disabilities are also considered.

To allow wheelchair users and other medical equipment users, such as portable oxygen concentrators, easy access into Aether without assistance, ramps are deployed at the doors of the aircraft. The ramp is hidden under the cabin floor during flight and is deployed using an automated system controlled by the pilot when the aircraft is on the ground. The railing which has a diameter of 11/4 [in] allows people who have difficulty going up the ramp to rest and get support. This value complies with certification for PRM and is small enough to allow people to easily hold on to the railing. The ramp dimensions similarly comply with EC certification. In addition, the ramp floor has some texture that prevents the slipping of wheels and allows blind people to feel the ground the walk on. For the latter reason, there is also some texture on the railing. The textures of the railing and ramp get smoother as the PRM ascends which signifies to the blind person that they are getting closer to the door of the eVTOL.

Inside the cabin, the floor will still be textured in order to allow blind or visually impaired people to improve their orientation and get a better feel of the path they are walking on. According to CON-CRT-CA-21, the aisles do not need to have hand grips or rails given that the seat backs have a "firm handhold". The seats are equipped with such handholds to allow PRMs to easily move around the aisle. Portable oxygen tanks are supported by attachments to the ground such that they do not

move around during take-off and landing. However, the PRM still has the possibility to remove the attachments and move around with the portable oxygen tank in case of emergencies or if they need to change spots during cruise. Lighter medical equipment such as crutches and white canes are stored next to the PRM seat in a container resembling an umbrella stand.

To accommodate the needs of not only the visually impaired but also the intellectually disabled, the surrounding environment of the interior cabin should be relaxing. This would help reduce stress levels for PRM with anxiety, Down syndrome, autism, etc. In order to achieve a relaxing environment, appropriate colours and lighting are used. A neutral colour palette for the cabin interior was found to be particularly useful. Next, the lighting in the cabin must be adjustable to reduce stress levels for people with intellectual disabilities and mental disorders while making sure that people with visual impairment can see clearly. For this, an upper and lower limit is set to the light intensity. The lower limit for lighting is given by aircraft certification and regulations for PRM transport. These are the following requirements: CON-CRT-CA-08, CON-CRT-CA-09 and CON-CRT-CA-25. Flashing lights are avoided to not induce epilepsy as stated in TC-CA-05. It is important that there are clear exit signs and lights near the exit signs in order to allow visually impaired passengers to find their way out during an emergency. For blind people, announcements are done through speakers in order to guide them towards the exit. It should also be mentioned that people with guide dogs are allowed to keep their pets in the cabin throughout the flight. There is enough space around the PRM seats to place emotionally assisting pets and guide dogs even for PRM who sit on wheelchairs, have portable oxygen concentrators. Finally, high-quality ventilation filters are used to avoid airborne infections and keep immunosuppressed PRM safe. These are a part of the heating, ventilation and air conditioning (HVAC) system.

In order to improve passenger comfort during flight, several accessories are added to the cabin interior. Cup holders are attached to the PRM and non-PRM seats to let passengers enjoy their beverage of choice during flight. Head rests are also featured to allow passengers to rest and nap. These also decrease discomfort in the neck and shoulder areas. Lastly, in-flight entertainment (IFE) is provided with headphones and screens. These are noise-cancelling headphones that can also be used when IFE is not turned on. IFE includes not only media such as music and audiobooks but also relaxing music that can help passengers meditate and decrease their stress levels during flight.

As previously stated, the cabin has two PRM seats and two non-PRM seats. The design of the non-PRM seats follow commercial aviation standards. The specific dimensions can be observed in Table 7.2. Since the PRM seats will also be used by passengers with full mobility, the design of these seats include a seat as described for the non-PRM seats but with a bigger backrest and a foldable seat and armrests. This allows for passengers travelling in a wheelchair to stay in their wheelchairs for commodity. This way their chair can be placed against this backrest secured with a safety mechanism. This type of seat allows for all type of wheelchairs (manual, manual tilt, electric, and scooter). For security, this seat is equipped with a special system located on the floor of the cabin to safely secure the wheelchair in place [11]. Additionally, the seat is also equipped with a belt connected to the backrest for passenger safety. These seats are designed for comfort and allow for independence and autonomy for all type of passengers.

Table 7.2: *Seat sizing parameters.*

Parameter	Size
Seat depth	45.7 [cm]
Seat height	45.5 [cm]
Seat width	46.0 [cm]
Backrest height	72.0 [cm]
Armrest length	41.0 [cm]
Armrest height	15.0 [cm]
Armrest width	5.0 [cm]
Seat clearance	2.0 [cm]

The design of the PRM seat can be observed in Figure 7.5, Figure 7.6, and Figure 7.7. This figures show the three positions of the seat. Firstly, the seat extended position for a passenger which does not use a wheelchair and can thus make use of the seat. Then the folded seat is shown, and finally the folded seat with a wheelchair placed against the backrest. As can be observed this allows for passengers travelling in a wheelchair for maximum independence, avoiding changing to a chair or wheelchair. For a better overview, an artistic impression of the interior of the cabin can be observed in Figure 7.8. For passengers travelling in a stretcher, one of these PRM seats can be folded forward in order to fit the stretcher on that space. The system which holds wheelchairs can also be used to safely attach these stretchers.

Figure 7.5: *PRM seat extended for use of a passenger without a wheelchair. [12]*

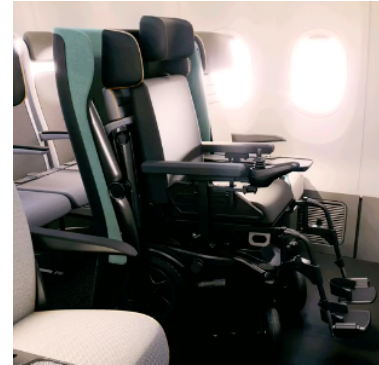**Figure 7.6:** *PRM seat folded for use of a passenger with a wheelchair. [12]*

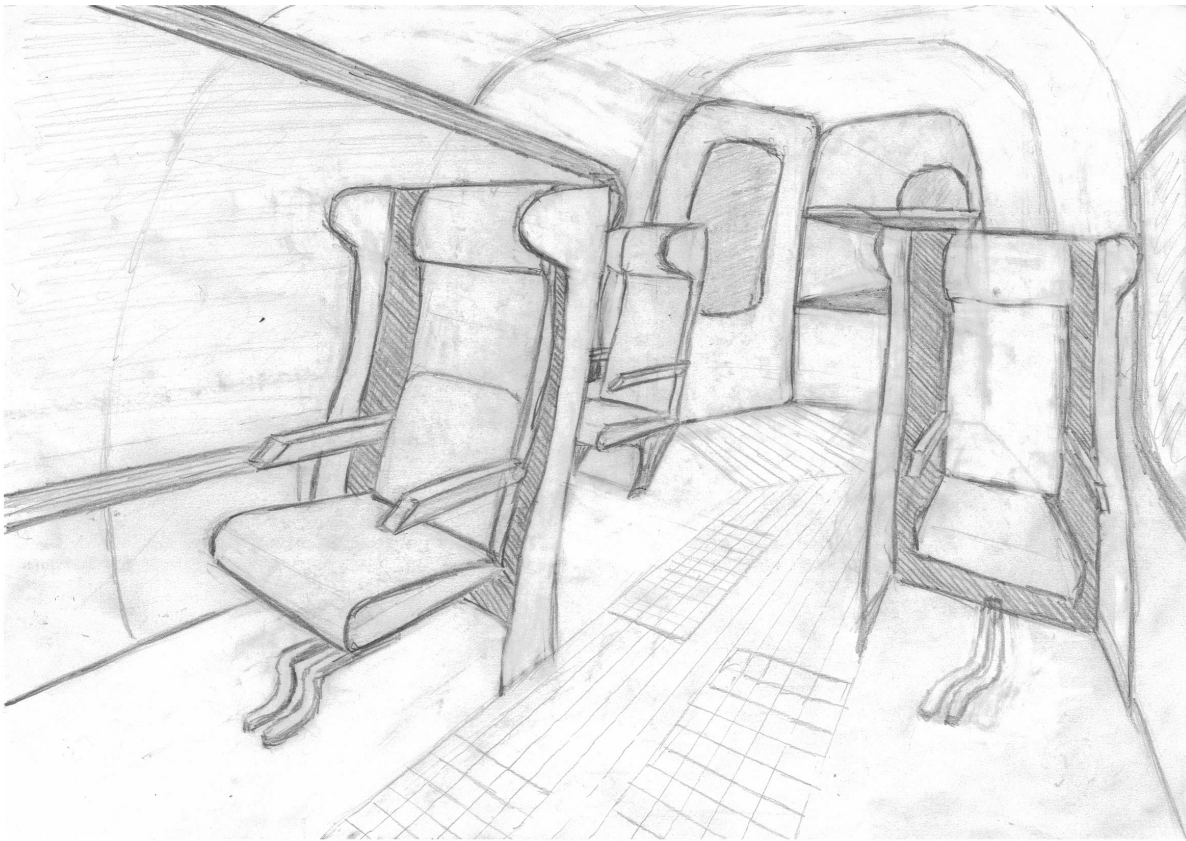**Figure 7.7:** *PRM seat folded with a wheelchair allocated. [12]*

Figure 7.8: *Artistic impression of cabin interior*

To accommodate the passengers' luggage, which include for each passenger a personal item, one piece of carry-on luggage, and one piece of checked luggage, two different compartments were designed. The personal items are located underneath the passengers seat or by their feet. As can be observed in Figure 7.4, the carry-on luggage is located in two compartments located on both sides of the cockpit and the checked luggage is located in the tail cone at the back of the cabin. The carry-on luggage can have a maximum weight of 10 [kg] and maximum dimensions of 56x36x23 [cm] according to VFS requirements. The compartments for this type of luggage have a dimension of 58 [cm] deep, 40 [cm] high, and 50 [cm] wide. This allows to place two pieces of carry-on luggage in each compartment. However, for this compartment, it was crucial to size it without taking view out of the pilot's field of view. This way, the height of the compartment was found taking into account a minimum over side angle of 35 [deg], taken from the horizontal down. This is the minimum side field of view angle that the pilot must have on each side of the cockpit for safety. This way, this angle allows for a maximum compartment height of 70 [cm]. The checked luggage compartment located in the tail cone, is designed to carry four pieces of 23 [kg] with a maximum linear dimension (width+height+length) of 158 [cm] each. This compartment has a varying cross-section along its length due to the tail cone shape. The frontal surface has a width of 1.2 [m] and a height of 1.3 [m]. The back surface has a width of 0.7 [m] and a height of 1.15 [m]. With a distance of 1.50 [m] deep, this allows for the accommodation of all the checked luggage.

8

Propulsion & Performance

This chapter describes the propulsion subsystem of the aircraft. The chapter first reviews the aircraft properties which are easily sized. Then the estimation of aircraft mass is conducted, and is followed by an extensive analysis of the power requirements for each flight phase of the aircraft. As one of the notable features of this aircraft is that the proprotors may tilt, this chapter will also describe its tilting mechanism. After these key points are evaluated, the chapter will revisit the calculations of mass for the propulsion subsystem. Finally, a detailed design of the propeller is presented.

8.1. Aircraft Properties
This section elaborates on some of the aircraft properties that drive or constrain the propulsion subsystem design.

8.1.1. Wing profile
The wing area is based on the MTOW and the maximum wing loading. The maximum wing loading may be calculated from the stall speed, based on the maximum lift coefficient of the selected airfoil, as presented in Table 10.1 of Chapter 10. The initial estimation from the Midterm Report used an MTOW of 3175 $[kg]$ [13], and as the power calculations (which are to be introduced in the proceeding sections) progress, a new iterated value of MTOW is calculated. Likewise, the wing area will be updated according to the new MTOW.

$$S = \frac{W}{(W/S)_{max}} \tag{8.1}$$

As a result, the final wing area of this aircraft is determined to be 27.51 $[m^2]$. The wing span is provided by the VFS to be 15.24 $[m]$, and using this wing area, the wing has an aspect ratio of 8.44 with a root chord of 2.50 $[m]$, a tip chord of 1.12 $[m]$ and a mean aerodynamic chord (MAC) of 1.90 $[m]$.

8.1.2. Propeller sizing
The size of the propeller was determined geometrically using the maximum possible radius with consideration for clearances between propellers and the fuselage. The radius of the propeller is determined to be 1.384 $[m]$. As mentioned in Subsection 5.3.1, the aircraft has 6 proprotors with equal radii.

8.2. Power Calculations
The calculation for power is crucial for the design of the aircraft. It plays a large role in determining the total mass of the aircraft as well as the size of some major components such as the wing. This section shows the process in which the power generated from the propulsion subsystem is calculated and the sizing of various components for this system.

The process to calculate the power is an iterative process that involves estimating the power as a result of the maximum takeoff weight and vice versa. Power is calculated for each phase of flight: IGE hover, OGE hover, vertical climb, vertical descent, transition, climb, descent, cruise and reserve. Moreover, the sizing of the battery for propulsion is dependent on the total energy consumption, which is the sum of the product of power consumption and operation time for each phase. For the

most part, power is based on the MTOW and other aircraft parameters, which are also based on the MTOW. The following sections describe the process in which power is calculated for every phase.

8.2.1. OGE and IGE hover

The calculations used in this section were obtained from [14] [15] [16]. Based on the blade element theory, the hover power is calculated as a sum of two components: induced drag power and profile drag power.

$$P_{hover} = \frac{1}{FOM}P_{i,hover} + P_{prof} \tag{8.2}$$

The induced drag is a rearward component of lift, and it is dependant on the thrust required (i.e. the weight of the aircraft), the air density and the total disk area. The total disk area is calculated based on the geometrical limitations of the aircraft, that four rotors must fit within the span of the main wing with clearances taken into account. For simplicity, it is assumed that all rotors have the same size. Induced drag power for OGE hover may be determined with Equation 8.3.

$$P_{i,hover} = \sqrt{\frac{T^3}{2\rho A}} \tag{8.3}$$

On the other hand, profile drag is the result of air friction on the blade element of the propeller. The profile power is dependant on the profile drag coefficient, solidity of the blade, tip speed of the blade, the length of the blade and the air density. Profile drag power may be determined using Equation 8.4. It is worth noting that this formula is also applicable for other rotorcraft phases of flight.

$$P_{prof} = \frac{1}{8}C_{Dp}\rho V_{tip}^3 \frac{(N_b c)^2}{\pi} \tag{8.4}$$

IGE hover power may be calculated from OGE hover power as the induced drag power are related through Equation 8.5.

$$\frac{T}{T_{inf}} = \frac{1}{1 - \frac{1}{(\frac{4Z}{r_{propeller}})^2}} \tag{8.5}$$

Similar to the OGE hover power, the IGE hover power is also a sum of the induced drag power with FOM correction with a value of 0.7 and the profile power. The initial FOM value was 0.6, but this was later changed to be 0.7, as this resulted in very high power requirement values.

8.2.2. Vertical climb and descent

Vertical climb power may be calculated as a combination of climb power, induced power and profile power.

$$P_{climb} = \frac{1}{FOM}P_{i,climb} + P_{c,climb} + P_{prof} \tag{8.6}$$

$$P_{i,climb} = T_h(\sqrt{\frac{1}{4}Vc^2 + V_h^2} - \frac{1}{2}V_c) \tag{8.7}$$

$$P_{c,climb} = V_c T_h \tag{8.8}$$

Similarly, vertical descent power is calculated as a combination of the three powers mentioned previously, but with a negative sign on the rate of climb.

8.2.3. Transition

The transition of configuration from a rotorcraft to a fixed wing aircraft first involves an acceleration of the aircraft to lift off speed. The required power upon acceleration is driven by this requirement. This target lift off speed is determined using equations of motion for the aircraft at a steady climb.

$$\frac{W}{g}\frac{dV}{dt} = Tsin(\beta) - D \tag{8.9}$$

$$\frac{W}{g}V\frac{d\gamma}{dt} = Tcos(\beta) - W \tag{8.10}$$

The distance for horizontal acceleration can be expressed using the initial climb speed and the average acceleration as in Equation 8.11.

$$s = \frac{V_{initial}^2}{2\bar{a}} \tag{8.11}$$

The initial climb speed may be estimated based on the stall speed as in Equation 8.12.

$$V_{initial} = 1.05V_{stall} \tag{8.12}$$

Using Equation 8.9, the average acceleration may be estimated as in Equation 8.13.

$$\bar{a} = \frac{g}{W}(\bar{T}sin(\beta) - \bar{D}) \tag{8.13}$$

The average thrust and average drag is estimated at the point of average speed. This value is conventionally expressed in terms of the initial climb speed as in Equation 8.14.

$$\bar{V} = \frac{V_{initial}}{\sqrt{2}} \tag{8.14}$$

Using the above relations, the tilt angle may be expressed as in Equation 8.15.

$$tan(\beta) = \frac{V_{initial}^2}{2Sg} + \frac{\bar{D}}{W} \tag{8.15}$$

8.2.4. Climb and descent

The equations of motion for climb are as shown in Equation 8.16 and Equation 8.17.

$$\frac{W}{g}\frac{dV}{dt} = Tcos(\alpha_T) - D - Wsin(\gamma) \tag{8.16}$$

$$\frac{W}{g}V\frac{d\gamma}{dt} = L + Tsin(\alpha_T) - Wsin(\gamma) \tag{8.17}$$

In order to determine the required thrust for a steady climbing flight, Equation 8.16 may be rearranged and expanded for thrust.

$$T_{clm} = \left(C_{D0} + \frac{1}{\pi ARe}\left(\frac{2Wcos(\gamma)}{\rho V_{clm}^2 S}\right)^2\right)\frac{1}{2}\rho V_{clm}^2 S + Wsin(\gamma) \tag{8.18}$$

The descent power may be calculated in a similar manner, but with the sign of the weight component reversed. The formula for vertical descent thrust is as in Equation 8.19.

$$T_{clm} = \left(C_{D0} + \frac{1}{\pi ARe} \left(\frac{2W cos(\gamma)}{\rho V_{clm}^2 S} \right)^2 \right) \frac{1}{2} \rho V_{clm}^2 S - W sin(\gamma) \tag{8.19}$$

8.2.5. Cruise and reserve

Using the free body diagram shown in Figure 5.5, the equations of motion for cruise flight may be derived as in Equation 8.20 and Equation 8.21.

$$\frac{W}{g} \frac{dV}{dt} = T cos(\alpha_T) - D - W sin(\alpha_T) \tag{8.20}$$

$$\frac{W}{g} V \frac{d\gamma}{dt} = L - W cos(\alpha_T) \tag{8.21}$$

Using a small angle approximation, the required power for cruise flight may be derived as in Equation 8.22.

$$P_{r,cruise} = (C_{D0} + \frac{1}{\pi ARe}(\frac{2W}{\rho V_{cruise}^2 S})^2) \frac{1}{2} \rho V_{cruise}^3 S \tag{8.22}$$

In order to maximize cruise range, the design point for cruise should be selected at the point in which drag is minimized. This can be done by taking a derivative of drag to velocity, and equating the result to 0. Using this equation, the optimal velocity can be calculated. This can be shown graphically on a power-velocity graph as in Figure 8.1, found in the succeeding subsection. The tangent point of the cruise curve and the tangent line extending from the origin is the point at which velocity is optimal for maximum range. As a result, the optimal cruise velocity was determined to be 49.77 $[m/s]$, with a required power of 155.159 $[kW]$. Additionally all other power curves and points may be shown on this graph.

8.2.6. Power values summary

Figure 8.1 shows the power curves and points for the aircraft. The graph shows the power required at each phase of the mission for a range of airspeed. It is worth noting that since hover, vertical climb and vertical descent phases are operated at zero airspeed, the dashed lines seen in the graph are reference points for comparison with other phases. Moreover, the black dashed line is shown as a tangent line to determine the optimal design point for the cruise phase. In addition, Table 8.1 shows a list of the maximum power required for each phase of flight and its associated duration and energy consumption. From this table, it can be seen that the most power intensive phase is the transition. On the other hand, the cruise phase is the most energy intensive phase even as its power consumption is in fact the lowest out of all phases, because the bulk of operation time is spent on cruise. Therefore in terms of minimizing battery size, power efficiency is the most crucial phase.
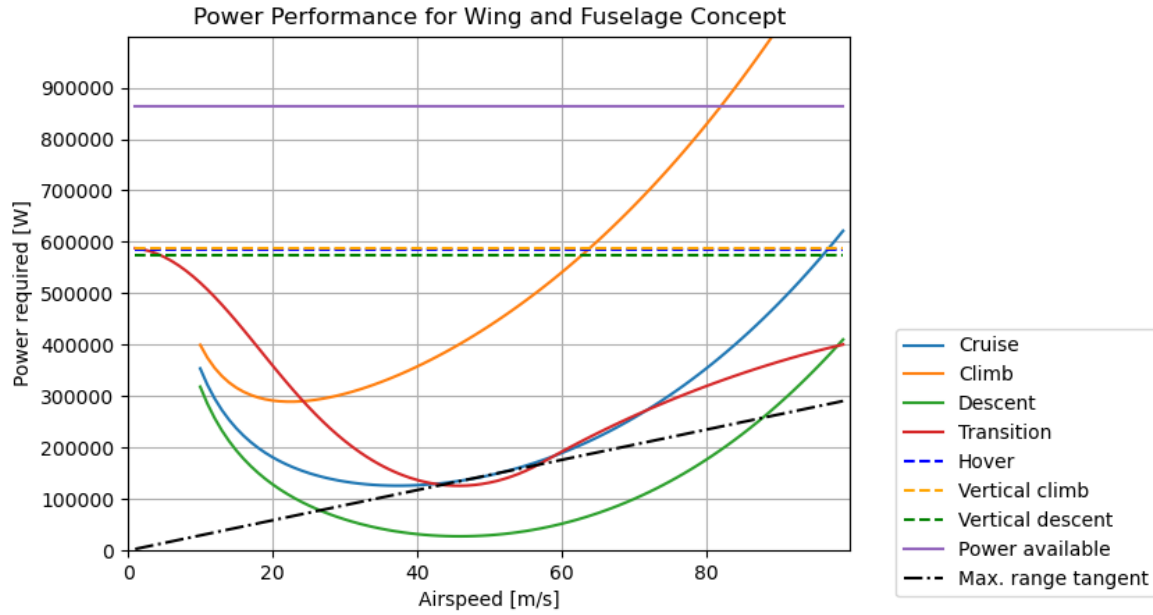
Figure 8.1: *Power Performance Curves.*

Table 8.1: *Power values for each phases of flight.*

Phase	Power required [kW]	Duration [s]	Energy consumption [Wh]
P_{IGE}	564.836	20	3138
$P_{vertical\ climb}$	586.781	38	6112
P_{OGE}	580.292	20	3224
$P_{transition}$	587.665	8	1308
P_{climb}	475.351	62	8178
P_{cruise}	144.241	3033	121515
$P_{descent}$	35.401	154	1514
$P_{vertical\ descent}$	574.208	38	5981
$P_{reserve}$	126.554	1200	42185

8.3. Mass Calculations

To perform the mass calculations of the aircraft a class I and class II weight estimation are used and described in detail in the following subsections. The results of these estimations is allowed to converge, leading to a final value for the MTOW and OEW (Operative Empty Weight) of the aircraft.

8.3.1. Class I weight estimation

The class I estimation estimates that mass of the propulsion subsystem based on the power required and the mass density of components. The mass of other subsystems is estimated based on mass fractions, and the sum of each subsystem mass estimations are then used as the MTOW to be iterated.

$$MTOW = \frac{M_{propulsion} + M_{payload} + M_{battery}}{1 - (MF_{structure} + MF_{subsystems} + MF_{avoinics})} \qquad (8.23)$$

The payload mass was estimated to be 704 $[kg]$. The mass fractions of the components are highlighted in Table 8.2.

Table 8.2: *Summary of mass fractions used in Class I estimation.*

Mass fractions	
Structures	0.3
Avionics	0.05
Other subsystems	0.1

The mass estimation of the battery and the proprotor components are elaborated in Chapter 9. The general formula for each proprotor is as follows.

$$M_{proprotor} = M_{motor} + M_{inverter} + M_{propeller} \qquad (8.24)$$

It is worth mentioning that the mass of the cowling of the proprotor is not included. The final mass of a single proprotor is 40.5 $[kg]$. The breakdown of this mass is shown in Section 8.4, Subsection 9.2.1 and Subsection 9.2.2.

8.3.2. Class II weight estimation

The class II weight estimation uses sets of semi empirical relations, based on aircraft baseline geometry and an estimation of the maximum load factors. For this aircraft, the class II weight estimation given by Jan Roskam is used, which can be found in [17]. It is important to note that Roskam uses imperial units, therefore all the calculations below are performed in such units and converted to SI units in Table 8.3 including all the parameters and final values.

Firstly, the wing weight W_{wing} is estimated using the following relation for cantilever wings:

$$W_{wing} = 0.04674 W_{TO_1}{}^{0.397} S_{wing}{}^{0.360} n_{ult}{}^{0.397} AR_{wing}{}^{1.712} \qquad (8.25)$$

Where W_{TO_1} is the class I estimated maximum takeoff weight, S_{wing} is the surface area of the wing, n_{ult} is the design ultimate load factor and AR_{wing} is the aspect ratio of the wing.

The fuselage weight W_f is estimated using the equation for high wing aircraft:

$$W_f = 14.86 W_{TO_1}{}^{0.144} \left(\frac{l_{fn}}{p_{max}}\right)^{0.778} l_{fn}{}^{0.383} N_{pax}{}^{0.455} \qquad (8.26)$$

Where l_{fn} is the fuselage length, p_{max} is the fuselage maximum perimeter and N_{pax} is the number of passengers. It is important to note that the number of passengers used is chosen to be five, due to the fact that it is assumed that this equation relates to an average weight for a passenger, which is not the case for this aircraft design, due to the PRM weight. This value has been raised to an equivalent value for a larger amount of passengers with an average weight.

To estimate the weight of the empennage of the aircraft, the following equations following the Cessna method are used. These apply to relatively low performance aircraft with a maximum speed below 200 $[kts]$. To find the final value for empennage weight, the calculated values for the horizontal tail weight W_h in Equation 8.27 and vertical tail weight W_v in Equation 8.28 should be added together.

$$W_h = \frac{3.184 W_{TO_1}^{0.887} S_h^{0.101} A_h^{0.138}}{57.5 t_{rh}^{0.223}} \qquad (8.27)$$

Where S_h is the surface area of the horizontal tail, A_h is the aspect ratio of the horizontal tail and t_{rh} is the horizontal tail maximum root thickness.

$$W_v = \frac{1.68 W_{TO_1}^{0.567} S_v^{1.249} A_v^{0.482}}{15.6 t_{rv}^{0.747} cos\Lambda_{1/4_V}^{0.882}} \qquad (8.28)$$

Where S_v and A_v are the surface area and the aspect ratio of the vertical tail respectively, t_{rv} is the vertical tail maximum root thickness and $\Lambda_{1/4_V}$ is the vertical tail sweep at a quarter chord.

The empennage weight is calculated as follows:

$$W_{emp} = W_v + W_h \qquad (8.29)$$

hlTo calculate the rotor group weight, the values calculated in Chapter 9 are used. This is done because the equations given by Roskam are less accurate and since they are not attuned to the rotor type of the aircraft being designed, namely an electrically powered tiltrotor. The rotor group can be defined as shown in Equation 8.30 as the sum of the weight of the proprotors placed near the root of the wing $W_{r_{root}}$, the weight of the rotors placed near the tip of the wing $W_{r_{tip}}$, the weight of the rotors placed in the rear of the aircraft $W_{r_{rear}}$ and the battery weight $W_{battery}$.

$$W_r = W_{r_{root}} + W_{r_{tip}} + W_{r_{rear}} + W_{battery} \qquad (8.30)$$

hlNext, to estimate the weight of the landing gear, similarly to the rotor weight, a different reference to Roskam is used. This is due to the fact that the aircraft being designed will take off and land similarly to a helicopter, with the use of skids. Therefore the Roskam approximation for an aircraft landing gear with wheels is not used and instead, Equation 8.31 found in [18] is used. This relation applies to skid-type landing gears for a gross weight of less than 7000 [lbs].

$$W_{lg} = 0.035 W_{TO_1} \qquad (8.31)$$

To estimate the weight of the fixed equipment of the aircraft, the following equations from Roskam found in [17] are used. The weight of the fixed equipment is a summation of the following subsystem weights:

- The flight controls W_{fc}

- The electric system W_{els}

- Instrumentation avionics and electronics W_{iae}

- The air-conditioning and de-icing system W_{api}

- The auxiliary power unit W_{APU}

- The furnishing W_{fur}

- The auxiliary gear W_{aux}

- The paint W_{pt}

The equations used for these parameters are defined as follows:

$$W_{fc} = 1.08 W_{TO_1}^{0.7} \tag{8.32}$$

$$W_{els} = 0.0268 W_{TO_1} \tag{8.33}$$

$$W_{iae} = 40 + 0.008 W_{TO_1} \tag{8.34}$$

$$W_{api} = 0.018 W_{TO_1} \tag{8.35}$$

$$W_{APU} = 0.004 W_{TO_1} \tag{8.36}$$

$$W_{fur} = 0.412 N_{pax}^{1.145} W_{TO_1}^{0.489} \tag{8.37}$$

$$W_{aux} = 0.01 W_{OE_1} \tag{8.38}$$

Where W_{OE_1} is the operative empty weight estimated during the class I weight estimation.

$$W_{pt} = 0.004 W_{TO_1} \tag{8.39}$$

Then adding all the different fixed equipment components, the value for W_{feq} can be found:

$$W_{feq} = W_{fc} + W_{els} + W_{iae} + W_{api} + W_{APU} + W_{fur} + W_{aux} + W_{pt} \tag{8.40}$$

Finally, adding all the different components of the class II weight estimation, the class II weight estimation for the empty operative weight can be found:

$$W_{OE_2} = W_{feq} + W_{lg} + W_r + W_{emp} + W_f + W_{wing} \tag{8.41}$$

To find the class II maximum takeoff weight estimation, the following equation is used:

$$W_{TO_2} = W_{OE_2} + W_{payload} \tag{8.42}$$

Where $W_{payload}$ is the payload weight.

As a reminder of the previously performed calculation for the payload weight, the following equation is used for the heaviest passenger configuration which is known to be two passengers with reduced mobility (including their wheelchairs), one non-PRM passenger (helper) and one pilot. The pilot only carries one personal item with them in the aircraft. This leads to the following equation:

$$W_{payload} = 3W_{check-in} + 3W_{carryon} + 4W_{personal} + 2W_{PRM} + W_{Non} + W_{pilot} \tag{8.43}$$

Where $W_{check-in}$ is the weight of one piece of check-in luggage, $W_{carryon}$ is the weight of one piece of carry-on luggage and $W_{personal}$ is the weight of one personal item. These three values are defined as stipulated by the VFS guidelines.

The weight of a non-PRM, which also includes the pilot, is assumed to be 88.45 [kg], as stipulated by the FAA's newest regulations [19]. The weight of a PRM is seen as the weight of the PRM in addition to the weight of an electric wheelchair, which is the heaviest equipment expected in the aircraft. These weights added to each other culminate in a PRM weight of 204.1 [kg]. The reason behind the

decision to board passengers in their own wheelchair and include an assistant in the configuration are explained in Chapter 7.

Finally, the class II weight estimation and payload parameters discussed in this subsection and the outputs of their equations are listed in Table 8.3.

Table 8.3: *Class II weight estimation and payload parameters and output values.*

Parameter	Symbol	Value	Units
Class I estimated maximum takeoff weight	W_{TO_1}	2667	kg
Class I estimated empty operative weight	W_{OE_1}	1963	kg
Wing surface area	S_{wing}	27.5	m^2
Design ultimate load factor	n_{ult}	2.5	-
Wing aspect ratio	AR_{wing}	7.38	-
Fuselage length	l_{fn}	9.15	m
Fuselage maximum perimeter	p_{max}	7.854	m
Number of passengers	N_{pax}	4	-
Horizontal tail surface area	S_h	8.253	m^2
Horizontal tail aspect ratio	A_h	4	-
Horizontal tail max root thickness	t_{rh}	0.196	m
Vertical tail surface area	S_v	3.8	m^2
Vertical tail max root thickness	t_{rv}	0.324	m
Vertical tail aspect ratio	A_v	0.7	-
Vertical tail quarter chord sweep angle	$\Lambda_{1/4_V}$	0.175	rad
Wing weight	W_{wing}	236	kg
Fuselage weight	W_f	181	kg
Empennage weight	W_{emp}	153	kg
Rotor group weight	W_r	756	kg
Landing gear weight	W_{lg}	93.3	kg
Flight controls weight	W_{fc}	213	kg
Electric system weight	W_{els}	71.5	kg
Instrumentation avionics and electronics weight	W_{iae}	39.5	kg
A-C and de-icing system weight	W_{api}	48.	kg
Auxiliary power unit weight	W_{APU}	10.7	kg
Furnishing weight	W_{fur}	82.2	kg
Auxiliary gear weight	W_{aux}	19.6	kg
Paint weight	W_{pt}	10.7	kg
Fixed equipment weight	W_{feq}	495	kg
Class II estimated empty operative weight	W_{OE_2}	2084	kg
Payload weight	$W_{payload}$	704	kg
Class II estimated maximum takeoff weight	W_{TO_2}	2788	kg

Using the value for the empty operative weight for the class I weight estimation W_{OE_1} and allowing it to converge with the now calculated empty operative weight for the class II weight estimation W_{OE_2}, a new value can be found which can be used in the upcoming calculations for the CG range (Center of Gravity range) in Chapter 12.

The final convergence values of the class I and class II weight estimation are found in Table 8.4.

Table 8.4: *Converging values for the maximum takeoff weight and empty operative weight.*

Parameter	Symbol	Value	Units
Convergence value maximum takeoff weight	W_{TO_3}	2700	kg
Convergence value empty operative weight	W_{OE_3}	1995	kg

The payload weight remains the same as shown in Table 8.3, as it is a fixed value given by the mission.

8.4. Propeller Design

The following section presents the analysis and selection of the propeller blades. The main characteristics of the blade concern the airfoil, twist, solidity, chord length, number of blades, and taper.

8.4.1. Airfoil

When choosing the airfoil for the blades, the value of $\frac{C_L}{C_D}$ will want to be maximised. This ensures that the maximum amount of lift or thrust is produced for the least amount of drag, which is favourable for efficiency purposes. As less work is required, this ultimately reduced the amount of energy required for operation, and in the long term will mean that the operational costs would lower. The methodology used to choose the most appropriate airfoil was to first collect a set of airfoils which could be viable for the purpose of this mission. Four sets of airfoils were chosen: Airfoils used in tiltrotors which don't fall under the first generation airfoil category, airfoils used in helicopters for low to medium Reynolds numbers, common airfoils used in aircraft propellers, and second generation helicopter airfoils as given by [20]. In total, 11 airfoils are compared. With the tip speed known, the blade analysis will be made for cruise conditions as this the longest phase of the mission.

With the 11 airfoils chosen, a design space is created to measure the $\frac{C_L}{C_D}$ at specified radial positions of the blade. Since the speed varies along the blade radial position, the Reynolds number also consequently varies, and using a validated software, the airfoils can be analysed. The design space consists of four radial positions along the blade, represented by $\frac{r}{R}$. For each radial position the corresponding Reynolds number is calculated and the airfoil with the highest $\frac{C_L}{C_D}$ is chosen, given that it is at an angle which does cause the airfoil to stall. The pitch angle is also noted down, as this will be basis for which the linear twist will be chosen from. The results are tabulated in Table 8.5.

Table 8.5: *Results of the airfoil analysis for various radial positions of the blade.*

$\frac{r}{R}$	**0.2**	**0.5**	**0.75**	**1.00**
Re	2.95e5	7.34e5	1.1e6	1.47e6
Best Airfoil	Clark X	Clark X	Clark X	Clark X
$\frac{C_L}{C_D}$	87.9	114.5	124.7	131.5
Pitch	5.25	4.5	4.5	4.00

It is evident from the results that the Clark X airfoil performs the best in all radial positions. The Clark X airfoil is part of the Clark family of airfoils, and it often undermined by the more commonly used Clark Y airfoil. However, the Clark Y was considered in the trade off and still performed worse. Figure 8.2 shows the profile of the airfoil Comparing its performance to the NACA0012 first generation helicopter blade airfoil which has a $\frac{C_L}{C_D}$ at the 0.75 radial position of 77.5 shows that the Clark X airfoil performs 61% better. As mentioned earlier, this has significant advantages for the power

requirements which ultimately reflect on the operational costs favourably. Furthermore, having the same airfoil along the span of the blade also benefits the manufacturing process as mixing airfoils increases complexity and thus would be more prone to errors.
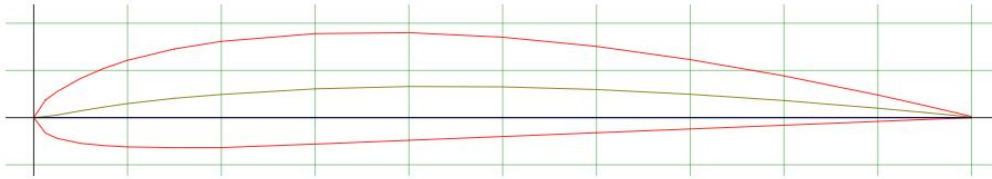

Figure 8.2: *Profile of the Clark X airfoil.*[1]

To better understand the performance in the third dimension, the aerodynamic characteristics of the entire blade are represented by the airfoil at the 0.75 radial position. This position is taken as it most closely represents the characteristics of the entire blade, and saves the effort of doing lengthy CFD analysis of the entire blade. The polar plots are shown in Figure 8.3.
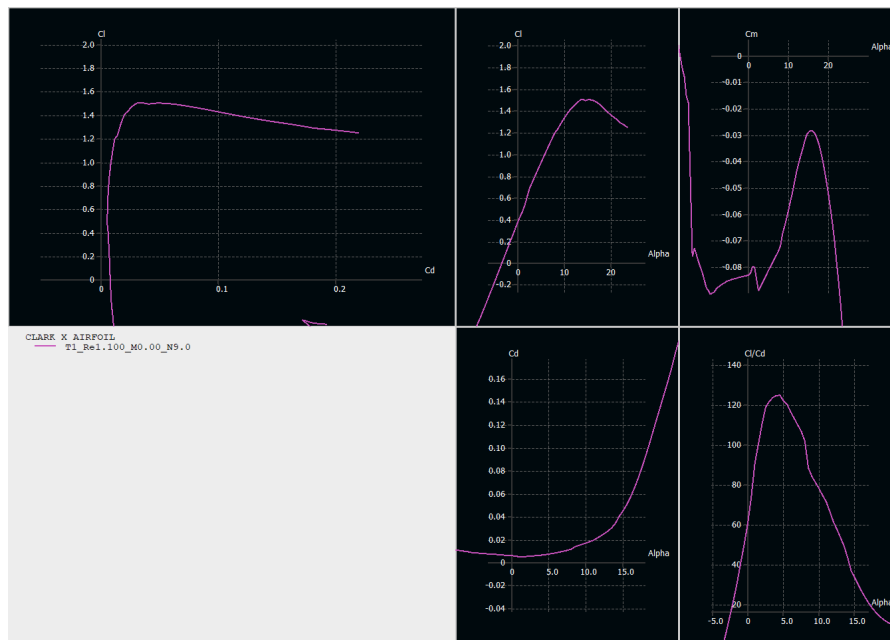
Figure 8.3: *Polar plots of the Clark X airfoil at a radial position of 0.75*

8.4.2. Twist

Blade twist is an important parameter to be considered as the Reynolds number along the airfoil differ and thus to maximise the performance of the blade, twist can be applies to compensate for the Reynolds number changing. While aircrafts have high twist, helicopter propellers omit high twist angles due to difference in advancing and retreating blade causing stall for highly twisted blades, which also increases oscillatory behaviour. Following the requirement CON-CRT-STR-05, vibrations in the aircraft shall be minimised, and therefore it makes sense to have lower twist angles.

As seen in Table 8.5, the pitch of the airfoil for each radial position which maximises the $\frac{C_L}{C_D}$ is already

---

[1] http://airfoiltools.com/airfoil/details?airfoil=clarkx-il [cited 25/01/2022]

given. Ideally, this non linear twist would be used as it gives the twist with the highest performance characteristics, but requirements from the VFS state that the twist shall be assumed to be linear[1]. In order to adhere to this requirement, a linear trendline is made between the 0.2 and 1.00 radial positions and then the twist is calculated such that the pitch in the aforementioned radial positions is met. Using this method, the blades have a pitch of 5.56 deg with a twist of $-1.56\,\text{deg}/\frac{r}{R}$. To calculate the pitch at a desired radial position, Equation 8.44 can be used.

$$\theta_{r/R} = -1.56\frac{r}{R} + 5.56 \tag{8.44}$$

Using Equation 8.44, the new pitch angle's can be calculated for the remaining two radial positions. Consequently, the $\frac{C_L}{C_D}$ also change slightly. The results of the airfoil analysis with linear twist are tabulated in Table 8.6.

Table 8.6: *Results of the airfoil analysis for various radial positions of the blade with linear twist.*

$\frac{r}{R}$	**0.2**	**0.5**	**0.75**	**1.00**
Re	2.95e5	7.34e5	1.1e6	1.47e6
Best Airfoil	Clark X	Clark X	Clark X	Clark X
$\frac{C_L}{C_D}$	87.9	114.3	124.6	131.5
Pitch	5.25	4.78	4.39	4.0

Compared to the results with non linear twist, the changes in the $\frac{C_L}{C_D}$ are insignificant as they have a less than 1% in difference. Nevertheless, these new values must be used such that the requirement of the VFS is adhered to. Since the twist is analysed and optimised for cruise conditions, it is expected that the power required for hovering would increase. As twist in blades increases, it more closely represents ideal twist, and therefore increases the figure of merit for hovering[15]. To take advantage of this, blades are normally highly twisted in rotorcrafts which have higher hovering time requirements. For the mission of Aether, only 40 cumulative seconds of hovering are required or about 1% of the mission duration, and therefore it is not needed to design the propellers for this purpose. Due to this, the figure of merit decreases, consequently increasing the induced power, which ultimately increase the power and weight budgets of the mission.

8.4.3. Solidity

The rotor solidity is the ratio of the blade area to the rotor area. The higher the solidity, the closer it represents an ideal disc used in the disc actuator theory, and the equation to calculate it is seen in Equation 8.45.

$$\sigma = \frac{Nc}{\pi R} \tag{8.45}$$

As both the number of rotors and number of blades is not known yet, an alternate method will have to be used. An empirical method used for helicopter design is used, where the solidity for level flight, angled turn, and in the case of a gust is analysed, and then the highest solidity is chosen. For level flight, the flight speed according to the FAR 29.175(b) certification shall be taken to be $1.1V_{ne}$. For the angled turn, FAR29.251 require the analysis be made at a turn of 30 deg at V_{ne}. Lastly, FAR29.341 set the gust velocity at $30\,ft/s$ and at a flight speed of $1.1V_{ne}$. Using the advance ratio and Figure 8.4, the thrust coefficient over solidity ratio is obtained for each condition, and found to be 0.14 for level flight, 0.145 for turn, and 0.17 for the transient pullup. With the constraints listed previously from certification, the solidity's are calculated for each condition, and the highest solidity is chosen as it

is considered the critical condition. Results show that the solidity in transient pullup is the highest, and a final solidity of 0.180 is obtained.
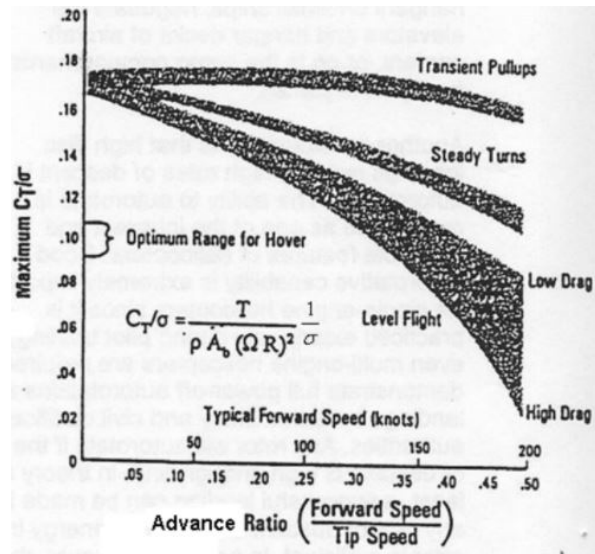

Figure 8.4: *Empirical method of choosing thrust coefficient over solidity ratio.[14]*

8.4.4. Number of blades and chord length

With the solidity, Equation 8.45 can be used to make a design space for various number of blades and chord length combination. Normally, helicopters follow a rule of having an aspect ratio between 14 and 20[14]. However, with a solidity of 0.18, the minimum amount of blades possible to fulfill this requirement would be 8, which would greatly increase the weight of the aircraft. As the majority of the flight time is in cruise, the aspect ratio rule can be omitted, and a trade off has to be made between the reduction of number of blades, and the consequential increase in induced drag. When reducing the number of blades to 4, a 97% increase in induced drag is created as compared to 8 blades, and using 5 blades already sees a reduction to 52% increase in induced drag. It was determined that for a reduction in weight, this increase in drag is considered acceptable. This would increase the hover power required, but as the majority of the flight time is in cruise, the overall increase in energy required would not increase significantly. Thus, 5 blades are used per propeller, and consequently a chord of length of 0.156 is used.

8.4.5. Other blade characteristics

For the taper, the most commonly used taper in aircraft design is 0.8 as it increases L/D performance and is favourable for strength considerations. Therefore a taper of 0.8 is used for the blades of the propellers. For the material of the blade, Toray BT250E-6 was chosen. This material is a cure epoxy prepreg, has a density of 1.20 [g/cc], and is designed for rotorcraft blade and propeller structures [21]. With the current blade dimensions, each blade weighs 2.80 [kg], therefore having a total propeller mass of 13.99 [kg], given that 5 blades are present.

8.4.6. Summary of results

To summarise, all the characteristics of the proprotors are tabulated in Table 8.7.

Table 8.7: *Summary of all the characteristics of the proprotor blades.*

Blade characteristics	
Airfoil	Clark X
Twist	-1.56
Pitch	5.56
Solidity	0.180
Chord length [m]	0.156
N blades	5
Taper	0.8
Mass [kg]	2.80

8.5. Verification and Validation

The wing geometry was verified by limits and inspection of dimension values. If was verified that the tip chord length does not exceed the root chord length and the mean aerodynamic chord length. Moreover, the render shows that the wing area is not disproportionate to the fuselage dimensions. For the propeller dimensions, it was verified that the dimensions in the span wise direction does not exceed the limit specified by the VFS. This verification includes the fuselage width at the propeller positions and the clearances between the propellers and the fuselage.

The power performance analysis was first verified by inspecting the power performance curves. The power curves for the fixed wing aircraft resembles a conventional curve for propeller aircraft. The transition curves follow a curve similar to a cruise phase of a rotorcraft, and as the aircraft travels in a similar manner, the shape of the curve is verified. Moreover, the location of each curves relative to one other were examined to ensure that the values are consistent throughout the analysis. The mass calculations were verified by conducting a class I and class II estimation and comparing the final MTOW value to examine the convergence. Moreover, the battery mass based on total energy consumption showed that its ratio to the MTOW is approximately 0.195, which is an acceptable value for an eVTOL aircraft.

For the propeller design, one immediately noticeable characteristic which is unlike any other propeller is the low twist. Usually the velocity of the blades towards the root of the blade is considerably lower than at the tip, and thus twist is applied such that the thrust is equal at the root and the tip, and the change in velocity is effectively compensated for. Helicopters have a twist of 8 degrees, and this is still considered to be low compared to aircraft propeller aircraft. As the blade that was chosen for Aether only has a twist angle of 1.56, this shows that the propeller is likely not a correct propeller design.

Despite the design not being consistent with proven and validated propellers, the method chosen for the twist is correct using the basis that a maximum $\frac{C_L}{C_D}$ is wanted for the various radial positions. It is expected that the low twist, although being in the most efficient state, will have low thrust performances as the maximum $\frac{C_L}{C_D}$ does not represent a high overall C_L of the blade. To conclude, while the method of designing the blade is robust and verified, comparing the final result with literature and real life blades show that the blade cannot be validated, and thus a redesign of the blades is recommended. A possible method to achieve this is to use one of many propeller design software's available, and to then again verify and validate the new design.

9

Powertrain Subsystem

This chapter describes the powertrain subsystem that includes the motors and battery which power the propellers and the auxiliary systems of the eVTOL. Firstly, the architecture of the powertrain, including the electrical block diagram is presented. Then, the components, namely the motor, inverter and high voltage battery pack, of the powertrain are sized. Finally, summary tables for the specifications of the powertrain components are given.

9.1. Powertrain Architecture

This section presents the structure of the powertrain including the relationships between the different components. The design of the powertrain was based on the needs of the different systems of the eVTOL. Based on these needs, the group worked backwards through each component that was required to satisfy each need with the final goal of choosing the correct battery parameters. During the design, factors such as decreasing waiting times between trips and ease of manufacture were also considered.

The powertrain consists of two separate subsystems: the one powered by the high voltage (48 [V]) battery and the one powered by the low voltage (12 [V]) battery. The high voltage subsystem's purpose is to power flight by giving the required power to the tilt rotors. The low voltage subsystem's main goal is to provide power to the other subsystems of the aircraft. Since the VTOL is fully electric, automated subsystems and components are fully powered with batteries. Five such subsystems and components were identified: lighting, doors, in-flight entertainment (IFE), heating, ventilation and airconditioning (HVAC) system and avionics as shown in Figure 9.1.
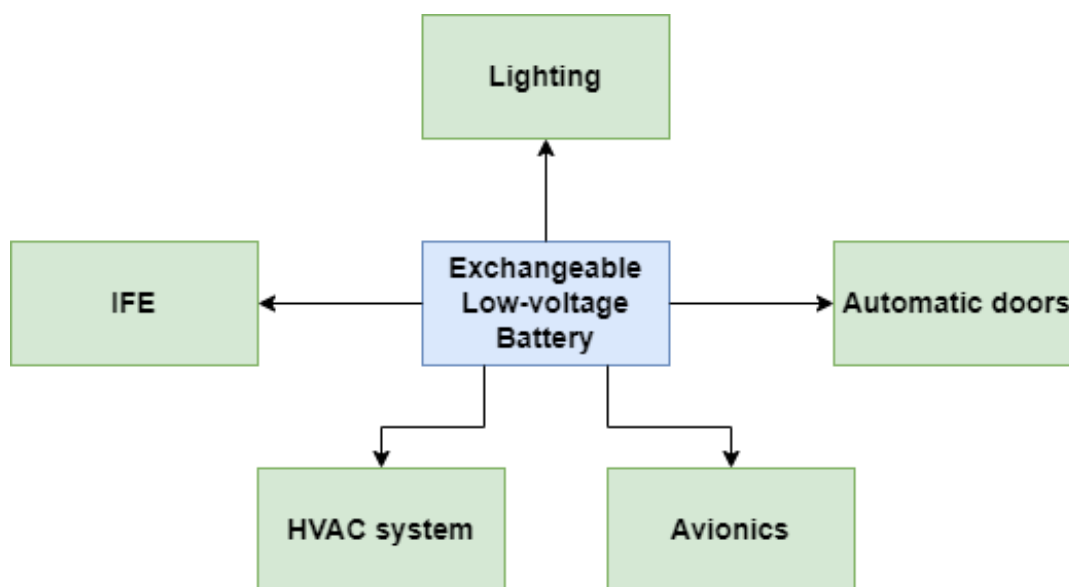

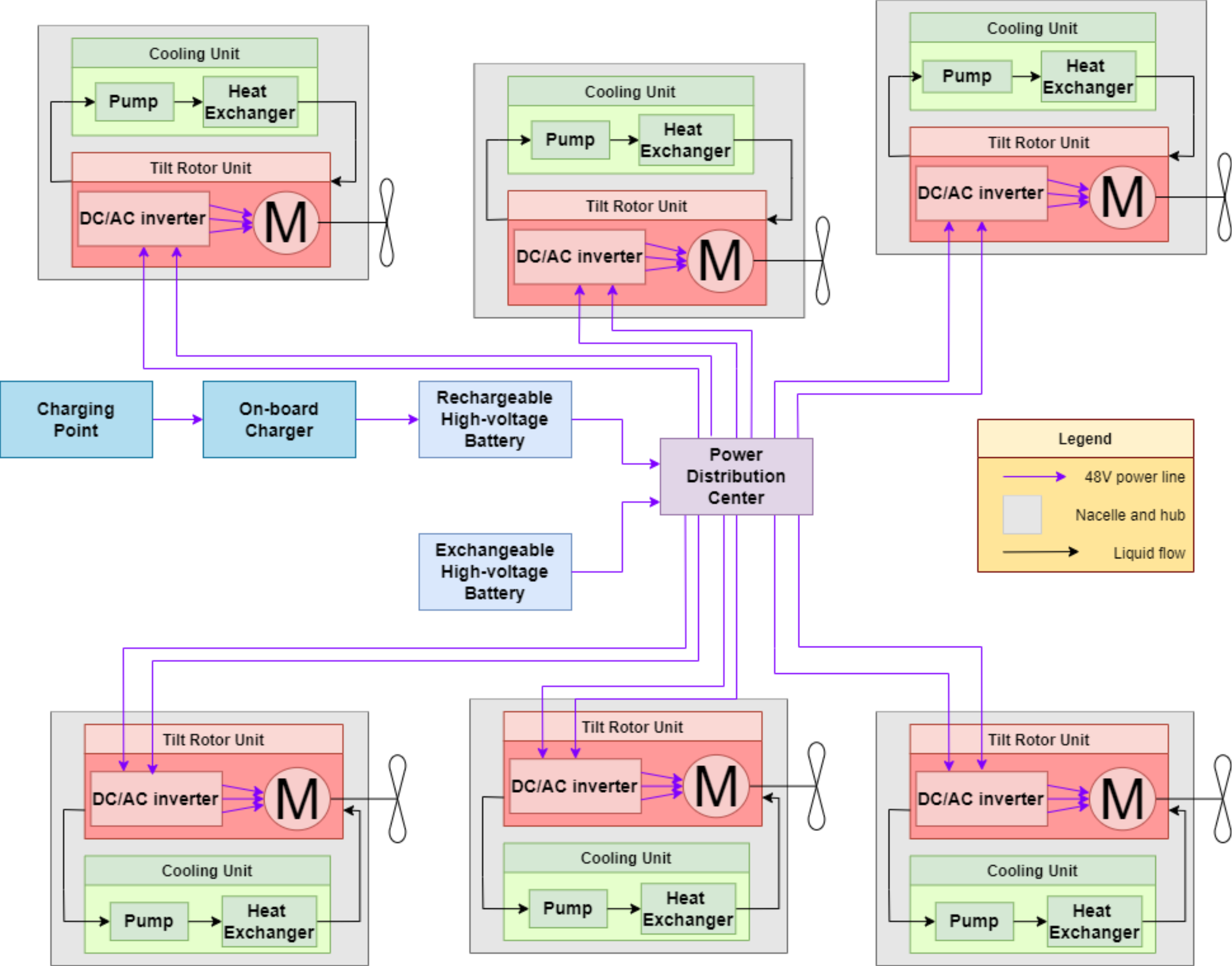**Figure 9.1:** *Electric block diagram for low voltage subsystem*

These are found within the cabin and do not have high power requirements. Therefore, the low voltage battery is sufficient to power these subsystems. It should be noted that the subsystems are connected to the battery in parallel such that the failure of one subsystem does not affect the func-

tioning of the other subsystems. Another contribution to safety is that subsystems such as emergency are not connected to the high voltage battery that powers the rotors. Therefore, for example if there is rotor failure or main battery failure, emergency lighting still works for emergency landings. The low voltage battery pack is placed in the undercarriage of the eVTOL, and it is exchangeable between trips. Placing the low battery pack in the undercarriage makes it accessible for maintenance staff when it needs to be changed between trips. In addition, by choosing exchangeable batteries the need for charging components within the aircraft are removed and waiting times between trips are decreased.

Further design may be done to improve the low voltage battery subsystem design. By checking the minimum required power for each of the five subsystems, the power that has to be delivered by the low voltage battery can be calculated. Based on this, the mass and volume of the low voltage battery pack can be found. For this stage of the design, these calculations are assumed to be negligible. This is because the mass contributions by the low voltage battery pack are not considered to be significant enough to have a large effect on the overall mass of the eVTOL.

The high voltage (HV) power subsystem is powered by a rechargeable high voltage battery pack and an exchangeable high voltage battery pack. The rechargeable battery pack is located in the wing of the eVTOL. The exact location is in the wing as close to the root chord as possible such that the moment of inertia of the aircraft is not increased dramatically. This location also facilitates access to the charging station. When charging the rechargeable HV battery pack, the power goes through the charging point and reaches the on-board charger. The exchangeable HV battery pack is placed in the undercarriage. This facilitates accessibility between trips for maintenance staff, making it easier to train new staff for performing the battery exchange. Most of the battery pack will be exchangeable and placed in the undercarriage. The rest of the battery pack will be rechargeable and placed in the wings. The initial design choice was to only have a rechargeable battery pack. However, it was discovered that the number of trips per day could be doubled by adopting a hybrid solution. This is due to the fact that the time for recharging is reduced, so waiting times between trips are decreased. This results in a significant increase in revenues and thus return on investment, makes the aircraft more attractive for investors. The power from the two battery packs reaches the power distribution center which is connected in parallel to the power units of the six tilt rotors. Therefore, the failure of one rotor does not damage the entire system, improving robustness and reliability. The power unit of each tilt rotor is equipped with a package of DC/AC inverter and motor and the cooling unit package that consists of pump and heat exchanger. The inverter and motor can be packaged in the same unit because they both have the same diameter as seen in Section 9.2. This makes manufacturing easier since the same package can be mass produced and repeated for each tilt rotor, leading to a more serviceable design. The inverter chosen in Subsection 9.2.2 has three outlets for the three-phase motor and two outlets for the power distribution center. This is reflected in the electrical block diagram. The cooling unit consists of a pump and heat exchanger, with liquid being used for cooling. The inverter and motor are compatible for liquid cooling. Further investigation has to be made on the type of coolant and the temperature of the coolant that has to be used. It should also be underlined that the batteries do not have a cooling unit due to the assumption by the VFS that an ideal battery that does not overheat is used. The cooling unit and tilt rotor power unit is fully encased by the nacelle for the rear tilt rotors that are attached to the fuselage. For the front tilt rotors, half of the motor remains a little outside the nacelle. This is due to the front of the nacelle (the hub part) tilting.

The electrical block diagram for the HV battery subsystem is shown on the next page.

Cooling Unit
- Pump → Heat Exchanger

Tilt Rotor Unit
- DC/AC inverter → M

Charging Point → **On-board Charger** → **Rechargeable High-voltage Battery**

Exchangeable High-voltage Battery

Power Distribution Center

Legend
- → 48V power line
- ▢ Nacelle and hub
- → Liquid flow

9.2. Motor and Inverter

This section explains how the motor and inverter are sized and what design choices are made.

9.2.1. Motor

The sizing of the motor is based on the highest power required throughout the flight, namely the transition phase at takeoff as it can be seen on Table 8.1. Since the transition has a duration greater than $10-20$ [s], the motor's continuous power is used. The continuous power of the motor shall be able to meet with the power requirements given here. In addition, efficiency values needs to be taken into account, as there are some energy loss in the shaft as well as the propeller. A mechanical efficiency of 0.98 and a propeller efficiency of 0.75 was used. In order to find the critical power requirement per rotor, the transition power required that takes into account the efficiencies is divided by the six tilt rotors.

In order to size the motor, the specific power of an existing motor was used to determine the mass based on the maximum continuous power required. The *Wright Motor* from Wright Electric was selected. This motor is currently developed specifically for a full-electric passenger aircraft to be available in the future. The motor may be scaled for a power of up to 4 [MW] and has a specific continuous power of 10 [kW/kg]. [1] [2] Dividing the critical power by the specific motor power results in the mass of the electric motor. With these motor specifications, the total mass of the six motors for this aircraft is 93 [kg].

The nominal torque is defined as the "maximum permissible continuous torque that may act on the output shaft". [3] The nominal torque of the rotor is calculated based on the maximum nominal rotation and maximum continuous power that the motor can have during operation. In Chapter 8 the vertical climb phase with a front rotor maximum rotation of 1203 [rpm] and power required per rotor of 174.43 [kW] was shown to satisfy this criteria. In order to be safe, the maximum rotation of the front motors is chosen to be 1300 [rpm]. The nominal torque of the four front motors is thus calculated to be 1281.23 [$N \cdot m$] using Equation 9.1.

$$Power[W] = Torque[N \cdot m] \cdot Speed[rpm] \cdot \frac{2 \cdot \pi}{60} \tag{9.1}$$

The dimensions of the motor are also based on volumes of existing motors. Motor dimensions were not available for the *Wright Motor*, but other existing motors may be used with differences in continuous power taken into account. The *Emrax 348* motor has a diameter of 348 [mm] and a length of 104.6 [mm]. The continuous power of this motor is 210 [kW]. Using these values as a reference, it can be estimated that the volume of the front motors for this aircraft is 0.04407 [m^3], in which the length is 350.7 [mm] given a diameter of 400 [mm].

The maximum rotation of the two rear tilt rotors is 844 [rpm]. In order to be safe, the maximum rotation of the rear motors is chosen to be 900 [rpm]. Using Equation 9.1 the nominal torque is found to be 1850.76 [$N \cdot m$]. The torque is the cross product of the force and perpendicular distance from the center to the force. The same motor can be used for the rear rotor as for the front rotor. However, adjustments need to be made in order to make up for the increase in nominal torque. The nominal torque in the rear rotor has increased by a factor of 1.44. Increasing the length by the same amount leads to 506.59 [mm] which makes up for the increase in nominal torque. Another option would have been to use a gearbox. This option was not preferred because the gearbox introduces

---

[1] https://www.weflywright.com/technology#motors
[2] https://www.magnix.aero/services
[3] https://hilba.net/en/faq-items/what-is-a-nominal-torque-and-what-is-the-maximum/

losses in power and increases the mass of the tilt rotor power unit more than making the motor longer.

9.2.2. Inverter

The sizing of the inverters are also based on a similar approach to the motor. The critical power required per tilt rotor is the same as in Subsection 9.2.1. The magniDrive 100 inverter unit produced by magniX is selected. The specific output power of this unit is 14.2 $[kW/kg]$. [4] By dividing with the critical power required per rotor, the mass of the inverter is found. The total mass of the six inverters is 65.67 $[kg]$.

The inverter has a specific volume of 20 $[kW/L]$. [5] With this specific volume, the volume of the inverter for the aircraft is 0.04651 $[m^3]$, in which the length is 370.2 $[mm]$, given a diameter of 400 $[mm]$.

9.3. High Voltage Battery Sizing

This section describes how the high voltage battery is sized. This mainly involves calculating the battery mass and battery volume.

9.3.1. Battery mass

The battery mass is estimated based on the specific power density, given by the VFS. The VFS requires the battery to have a specific power density of 400 $[Wh/kg]$. Using the power requirement and duration for each phase of flight as highlighted in Table 8.1, the energy consumption of each phase of flight can be calculated. The maximum amount of energy consumption, including reserve time, is used to determine the battery mass for the propulsion subsystem. The formula for battery mass is as follows.

$$M_{battery} = \frac{E_{IGE} + E_{OGE} + E_{vertical-clm} + E_{vertical-des} + E_{transition} + E_{clm} + E_{des} + E_{cruise} + E_{reserve}}{\lambda_{battery}}$$

$$(9.2)$$

As a result, the battery mass is estimated to be 520 $[kg]$.

9.3.2. Volume

Following TC-PP-05, the dimensions of the battery have to be calculated and should be consistent with the energy density of the battery. One study collected the energy and volumetric density of 25 batteries of electric vehicles and plotted them against the year of manufacturing, ultimately coming up with a statistical trendline analysing the relationship between the year of battery manufacturing and volumetric density of a cell[22]. The equation describing the relationship is given by Equation 9.3.

$$\rho_V = 27.79Y - 55553 \tag{9.3}$$

With the start of operation set for 2030, the volumetric density of lithium ion is estimated to be 860.7 Wh/L. With a total battery energy of 205.1 kWh, the total volume of the battery is 4.19 m^3. This is also consistent with the energy density trendline given by the study, as plugging in 2030 for

---

[4]https://www.aviationtoday.com/2020/01/30/wright-electric-begins-1-5-mw-engine-development-program-186-seat-commercial-airliner/
[5]https://www.weflywright.com/technology#motors

the regression of the energy density gives a value of $404.5 Wh/kg$, which is only a $4.5\ Wh/kg$ difference to the energy density used for Aether. Compared to a Tesla battery, with a volumetric density of $250\ Wh/L$, the volume for the aircraft is significantly large, but due to the higher energy density this is expected.

Initially the idea was to place the battery in the undercarriage such that it has the least amount of effect on the aircraft's moment of inertia, but limitations of undercarriage space mean that some of the battery will have to be placed elsewhere. The only other place with available space for the battery is the wing, and thus the remaining volume of the battery is placed in the wing as close to the root chord as possible such that the moment of inertia of the aircraft is not increased dramatically. A large percentage of the battery (about three-fourths) will be placed in the undercarriage and will be exchangeable. The rest of the battery will be rechargeable and will be placed in the wings.

9.4. Powertrain Specifications Summary

This section presents a summary of the specifications for the components designed. The input parameters used for sizing the components in this chapter are presented in Table 9.1. Then, the specifications of the inverter and motor are shown in Table 9.2.

Table 9.1: *Input parameters*

	Inputs
Motor power/mass [kW/kg]	10
Inverter power/mass [kW/kg]	14.17
Motor efficiency [%]	95
Maximum rotation [rpm]	1203
Preq critical per tiltrotor [kW]	174.43

Table 9.2: *Inverter-motor outputs*

(b) *Motor specifications*

	Outputs
Total motor mass [kg]	93
Mass of one motor [kg]	15.5
Maximum rotation front [rpm]	1300
Nominal torque front [$N \cdot m$]	1281.23
Output power [kW]	126.96
Volume [L]	44.07
Length front [mm]	350.7
Diameter [mm]	400
Maximum rotation rear [rpm]	900
Nominal torque rear [$N \cdot m$]	1850.76
Length rear [mm]	506.59

(a) *Inverter specifications*

	Outputs
Total inverter mass [kg]	65.67
Mass of one inverter [kg]	10.94
Volume [L]	46.51
Length [mm]	370.2
Diameter [mm]	400

10

Aerodynamics

This chapter presents the aerodynamic design and the aerodynamic characteristics of the aircraft. Section 10.1 presents the methodology followed for selection of the wing airfoil and its characteristics. Section 10.2 presents a basic qualitative approach to the rotor/wing and rotor-on-rotor interaction during hover. Section 10.3 presents the methodology for determining the aerodynamic characteristics of the wing, while Section 10.4 presents the basic sizing of the empennage. Section 10.5 presents a methodology for determining the drag generated by the fuselage. Lastly, Section 10.6 presents the noise calculations for the rotorcraft phases of the flight.

10.1. Wing Airfoil

The first step in the design of the wing is the sizing of the airfoil. The selection of an airfoil from the existing designs is chosen over the design of a novel one due to the abundance of data and experimental measurements on existing airfoils. The selection criteria and the airfoil characteristics are presented below.

10.1.1. Selection procedure

Airfoil selection is based on aerodynamic requirements and objectives [23] [24]. Airfoil design objectives, among others, are:

- High lift coefficient C_l

- Low drag coefficient $C_{d_{min}}$

- High lift to drag ratio $\frac{C_l}{C_d}$

- High lift curve slope C_{l_α}

- Negative (and low value of) pitching moment coefficient C_m

Airfoils of the NACA 6 and 7 Series were considered, due to their increased chord-wise length of laminar flow compared to the 4 and 5 digit NACA airfoils [25]. The airfoils selected are based on availability of data (polar diagrams) and performance characteristics [26]. The airfoils considered are:

- NACA 747A315 [1]

- NACA 747A415 [1]

- NACA 63(2)-615

- NACA 63-412

The airfoils were compared for a Reynolds number of ($Re = 1 \cdot 10^6$), with the NACA 6-Series airfoils outperforming the 7-Series ones in all of the objectives presented in Subsection 10.1.1. Therefore, further analysis on the NACA 6-Series airfoils is required in order to select the optimal one for this specific mission.

---

[1] http://airfoiltools.com/airfoil/details?airfoil=naca747a315-il [cited 24 December 2021]
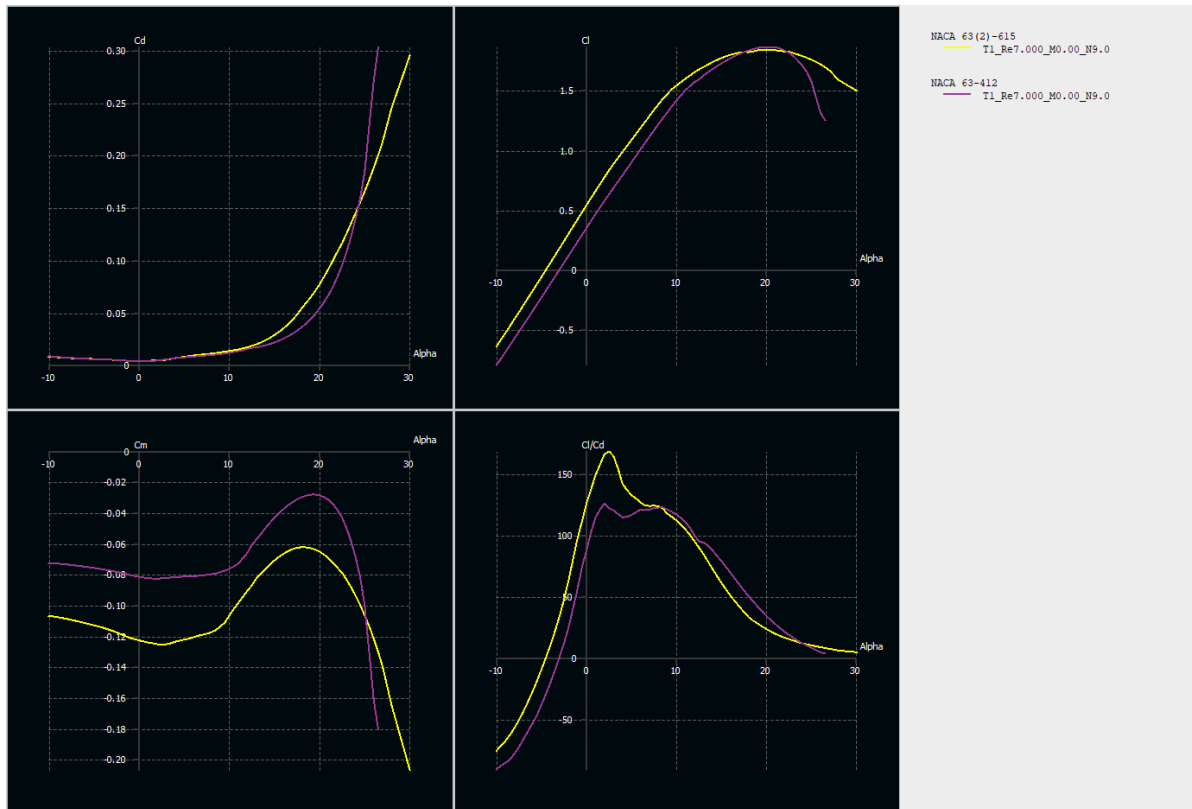
Figure 10.1: *Polars for airfoil comparison for wing tip Reynolds number*

For further sizing, preliminary results from Chapter 8, such as MTOW, cruise velocity and preliminary wing sizing (chord length for Reynolds number) are required.

The airfoils are compared for chord lengths of $c_{root} = 2.5$ [m] and $c_{tip} = 1.12$ [m], from preliminary wing design, at cruise conditions, resulting in a Reynolds number for the root of $8.5 \cdot 10^6$ and $3.8 \cdot 10^6$ for the tip.

The airfoil characteristics are shown in Figure 10.1 using the XFLR5 software. It is shown that NACA 63(2)-615 airfoil outperforms the NACA 63-412 one in terms of highest $\frac{C_l}{C_d}$, lowest C_m, and has higher C_l at low angles of attack. The C_d vs α polar shows that NACA 63(2)-615 has a better performance in terms of drag only for the range $\alpha = 2 - 4°$ compared to NACA 63-412.

Given these results, the NACA 63(2)-615 airfoil is selected.

10.1.2. Airfoil characteristics

The airfoil polars are presented for the root and tip Reynolds numbers, as shown in Figures 10.2 to 10.5.
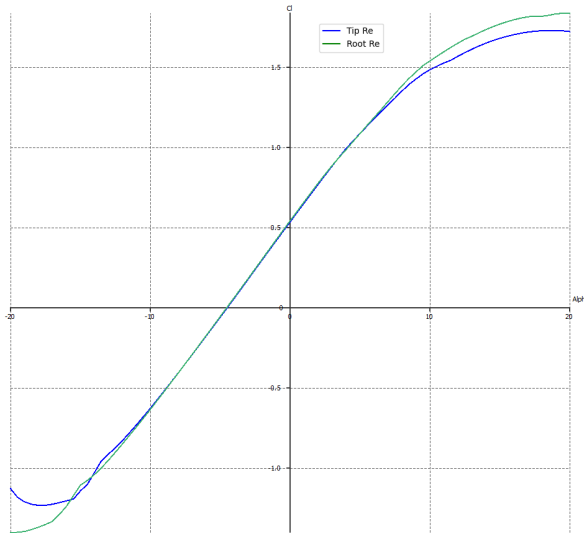
Figure 10.2: *Lift polar*
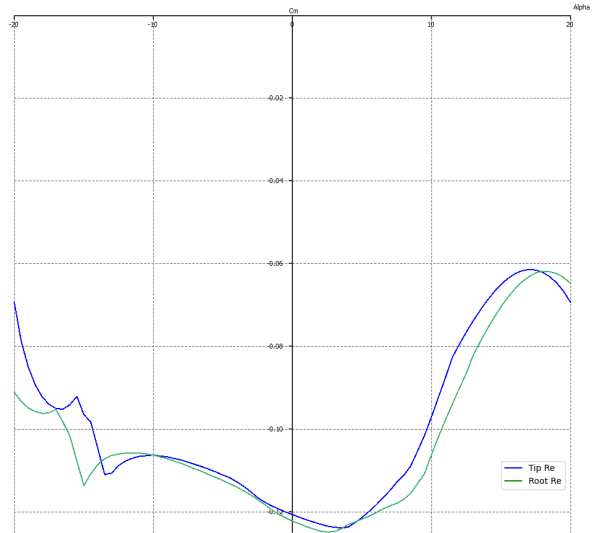
Figure 10.3: *Pitching moment coefficient vs α*
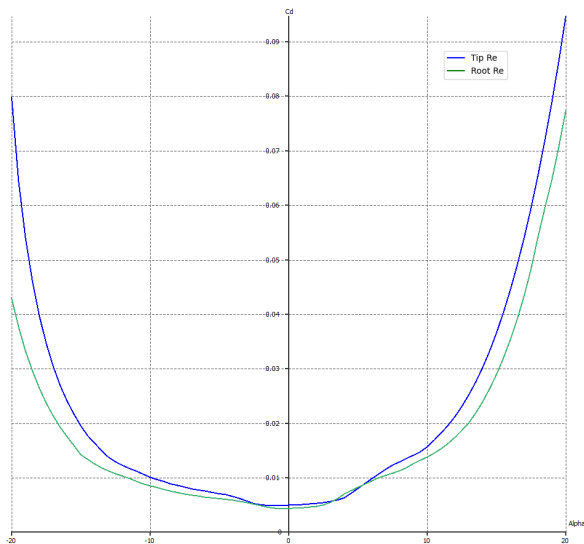
Figure 10.4: *Drag polar*
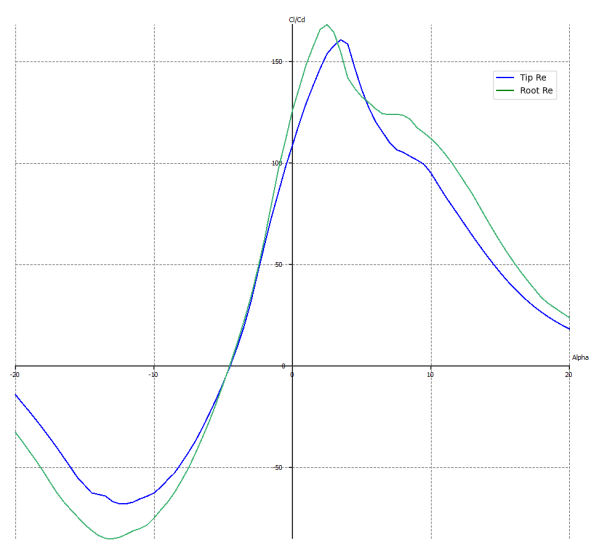
Figure 10.5: *Lift-to-drag coefficient ratio vs α*

From Figures 10.2 to 10.5, the observations presented in Table 10.1 can be made:

Table 10.1: *NACA 63(2)-615 aerodynamic characteristics for Re = 3,000,000.*

Characteristic	Value	Notes
$\alpha_{C_{l=0}}$	-4.5	
$C_{l_{\alpha=0}}$	0.535	
$C_{l_{max}}$	1.73	$\alpha = 18.5°$
Updated C_{l_α}	$0.54 + 0.11\alpha$	$\alpha = [-10, 6]$
$C_{d_{\alpha=0}}$	0.0047	
$C_{d_{min}}$	0.005	
$(C_l/C_d)_{max}$	160	

10.2. Hover Aerodynamic Analysis

During hover, literature suggests that wing-on-rotor and rotor-on-rotor interactions are the main influences on rotor performance [27].

The presence of the wing presents a substantial disturbance on the rotor inflow, leading to an inflow momentum deficit of about 15%; flow recirculation occurs due to the wing's presence on the downwash of the rotor, not allowing the wake to develop. The effect can be seen in Figure 10.6.

The other influence on rotor performance is the rotor-on-rotor interaction. This is particularly important due to rotor proximity, as it leads to rotor thrust loss.

The further analysis of these phenomena required to be able to conclude the effect they have on the performance of the current configuration is out of the scope of this report.
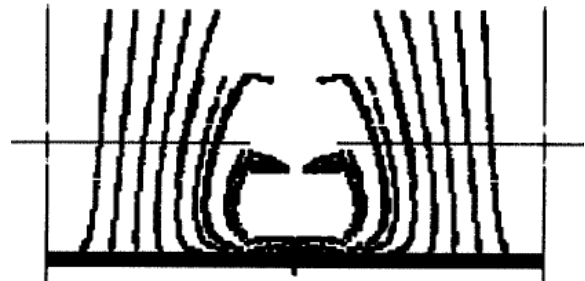
Figure 10.6: *Wing/Rotor fountain effect prediction [27]*

10.3. Wing Analysis

After the selection of the airfoil, the wing can be designed. The basic wing geometry and the preliminary results and assumptions are presented in Subsection 10.3.1 and the wing aerodynamic analysis is presented in Subsection 10.3.2.

10.3.1. Preliminary results & geometry

A preliminary design choice for this aircraft has to do with the wing's vertical position. A high-wing configuration has been chosen to allow for higher clearance between the wing-mounted rotors and the ground. It also, however, lowers the amount of ground effect due to increased clearance. Furthermore, the wing is assumed to have no sweep, as this would increase the complexity of the nacelle design; the nacelle needs to be long enough so that the rotor blades do not damage the wing. No twist is also assumed, as it has the disadvantage of lift reduction [26]. For the rotor-wing interaction it is assumed that the rotor axis is on the chordline and the effect of wake contraction can be considered to be negligible. As a simplification, the effect of the nacelle on the flow is not taken into account.

10.3.2. Aerodynamic analysis

The tool for aerodynamic analysis extends Prandtl's Lifting Line Theory [28] with the inclusion of the effect of the propeller on the wing [29] [27].

A sample discretization of the wing and the stations nomenclature used in the calculations are shown in Figure 10.7 [28].

The method is presented sequentially.
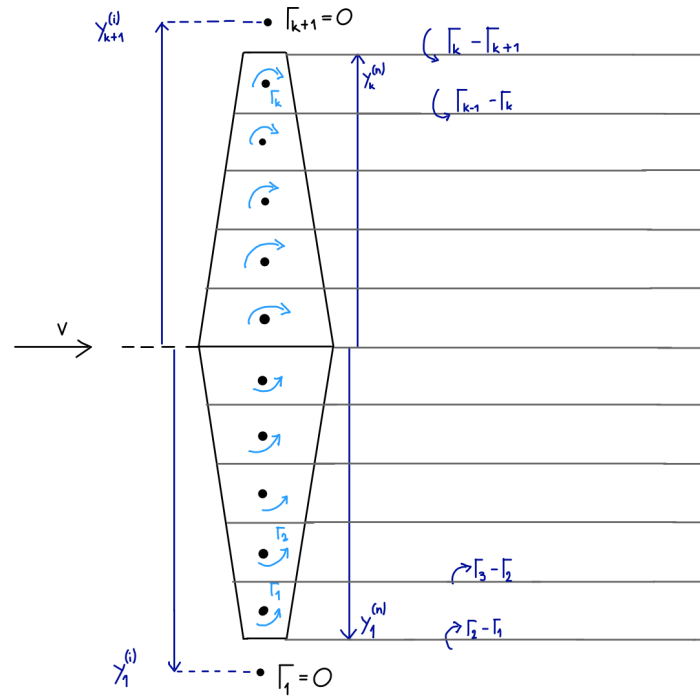
Figure 10.7: *Definition of wing and dimensions for aerodynamic analysis [28]*

Circulation

The Kutta-Joukowski theorem in Equation 10.1 relates lift to the circulation distribution.

$$L(y_n^i) = \rho v_\infty \Gamma(y_n^i) \tag{10.1}$$

The circulation $\Gamma(y_n^i)$ is calculated based on an initial estimate for lift, shown in Equation 10.2, and an assumption of elliptic distribution for lift and circulation, as shown in Equation 10.3. Γ_0 is determined by matching Equation 10.1 and Equation 10.2 (preliminary C_l is assumed to be $2\pi\alpha$).

$$L = \frac{1}{2}\rho v_\infty^2 S \cdot 2\pi\alpha \tag{10.2}$$

$$\Gamma = \Gamma_o \sqrt{1 - \left(\frac{2y}{b}\right)^2} \tag{10.3}$$

Effective angle of attack

The effective angle of attack, as defined by Equation 10.4, describes the angle of attack seen by the wing due to freestream and propeller induced velocity.

$$\alpha_{eff}(y_n) = \alpha - \alpha_i = \alpha_{wing} + \arctan\frac{w_i}{v_\infty + v_i} \tag{10.4}$$

The induced velocity is calculated based on the horseshoe vortices along the lifting line and includes the effect of the proper induced velocity, as shown in Equation 10.5 [28].

$$w_i(y_n) = v_{i_{propeller}} - \frac{1}{4\pi}\sum_{i=0}^{k}\frac{\Gamma_{i+1} - \Gamma_i}{y_i - y_n} \tag{10.5}$$

Propeller induced velocity

The effect of the propeller on the wing is determined using the Vortex Ring method [29], where the wake is modeled by ring vortices. For modelling purposes, it is assumed that the propeller is close to the chordline so that wake contraction is negligible. It is also assumed that the vortex strength Γ_{ring} is the same for all rings. The effect of the nacelle on the flow is not considered. For this iterative method, the induced velocity is determined by Equation 10.6, with inputs from Equations (10.7) to (10.10). The propeller angle of attack α_{prop} is originally assumed to be 2° [2]. [29] [27]

$$v_{induced} = \frac{C_T^1(\Omega R)A_{eff}}{2\sqrt{\mu^2 + \lambda^2}} \tag{10.6}$$

$$C_T^1 = \frac{4C_T}{\pi^3} \tag{10.7}$$

$$\mu = \frac{v_\infty cos\alpha_{prop}}{\Omega R} \tag{10.8}$$

$$\lambda = \frac{v_\infty cos\alpha_{prop} + v_i}{\Omega R} \tag{10.9}$$

$$A_{eff} = \frac{1}{1 - (\text{root cutout})^2} \tag{10.10}$$

The iterative process for the determination of the induced velocity requires an initial estimation, which is shown in Equation 10.11.

$$v_{induced_i} = \frac{1}{2}\left(-v_\infty cos(\alpha_{prop}) + \sqrt{(v_\infty cos\alpha_{prop})^2 + \frac{2T}{\rho A_{disk}}}\right) \tag{10.11}$$

Updated circulation distribution

The wing C_l distribution is estimated from the lift curve slope, based on the linear range of the graph in Figure 10.8 ($\alpha = [-10, 10]$), shown in Equation 10.12:

$$C_l(\alpha_{eff}) = 0.426 + 0.09\alpha_{eff}(y_n) \tag{10.12}$$
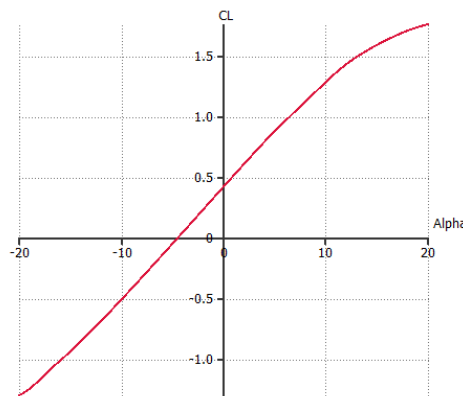

Figure 10.8: *Wing lift polar*

The circulation is updated according to Equation 10.13.

2https://www.thaitechnics.com/propeller/prop_intro.html [cited 20 Janurary 2022]

$$\Gamma_i = \frac{1}{2}(v_\infty + v_{i_{propeller}})c(y_i)C_l(a_{eff}) \tag{10.13}$$

The new circulation distribution is calculated with Equation 10.14 and is based on the difference between the outputs of Equation 10.3 and Equation 10.13. A damping factor DF of 0.05 is assumed [28].

$$\Gamma = \Gamma_{n-1}(1 - DF) + \Gamma DF \tag{10.14}$$

Finally, the final values for lift and drag can be computed from Equation 10.15 Equation 10.16 [28].

$$C_{D_i} = \frac{2}{(v_\infty + v_{induced})S_{wing}} \sum_{i=1}^{b} (\Gamma(y_i) - \Gamma(y_{i-1})) \tag{10.15}$$

$$C_{D_i} = \frac{2}{(v_\infty + v_{induced})S_{wing}} \sum_{i=1}^{b} (\Gamma(y_i) - \Gamma(y_{i-1}))a_{eff}(y_n) \tag{10.16}$$

10.3.3. Wing results

Wing optimization is done through a Python script based on the Lifting Line Theory adaptation model presented in this section. The code is constructed with methods and functions used in SUAVE [30] and Aerosandbox [31] for their respective aerodynamic analysis, in combination with the calculations for the rotor induced velocity.

Preliminary values for root chord, wing area and aspect ratio are provided from the Power calculations in Chapter 8. Further constraints for the model are:

- lift during cruise must equal the vehicle's weight,

- MTOW remains fixed,

- the wing is not swept.

The analysis shows that the optimal range for α_{prop} is $2-3°$. Furthermore, the optimal cruise angle of attack α for minimized drag is 3°. The induced velocity of the propeller on the wing, as calculated with the method presented, is in the order of $1-3$ $[m/s]$. The performance of the wing is affected, as the drag sees an 8% increase, while the lift to drag ratio increases much less, in the order of 2%.

The final values for the wing are presented in Table 10.2. An illustration of the designed wing is presented in Figure 10.9.

Table 10.2: *Wing characteristics*

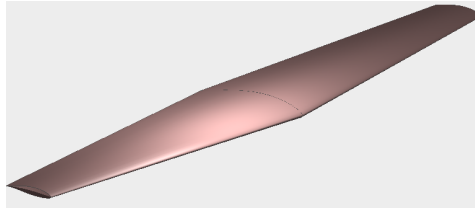| Parameter	Value	Unit
Wing Aspect Ratio	8.4	-
Wing Area	27.5	$[m^2]$
Wing Span	15	[m]
Wing Taper Ratio	0.45	-
Wing Root chord	2.5	[m]
Optimal α_{cruise}	3.5	°
Wing L/D	18	-
Wing Loading	97	$[kg/m^2]$

Figure 10.9: *Wing design*

10.4. Tail Design

Following the wing, the tail is designed. Requirements on tail surface area are provided by and further analyzed in Chapter 12. The first aspect to be considered prior to the sizing of the tail is its configuration, presented in Subsection 10.4.1. The sizing of the horizontal and vertical tail are presented in Sections 10.4.2 to 10.4.3.

10.4.1. Tail configuration

The tail configurations considered were limited to the conventional tail, a T-tail and a V-tail, as all the other configurations are combinations of the ones previously mentioned [26]. One of the main points regarding the choice of configuration is the clearance with respect to the position of the rear rotor and its inflow: a lower horizontal tail does not have enough clearance with the rear rotors, as shown in Chapter 5. Furthermore, literature suggests that a T-tail remains undisturbed from the wing flow and has less interference drag compared to a V-tail or a conventional tail design.

For the above reasons, a T-tail configuration was chosen.

10.4.2. Horizontal tail design

From Chapter 12, the requirements for a tail airfoil are specified. Namely, the airfoil needs to be symmetric with low thickness. Based on these requirements and general aviation common used airfoils, the NACA 0010 airfoil is selected [26].

The aspect ratio of the horizontal tail is suggested to be half of the wing's respective value, leading to $AR = 4$. Literature suggests typical values for taper ratio should be in the $0.4 - 0.5$ range [32]. With that information, the horizontal tail geometric characteristics can be calculated using Equation 10.17 and Equation 10.18. The optimization library from [31] is used to optimize the horizontal tail for minimized span [33].

$$b_h = \sqrt{AR \cdot S_h} = AR \cdot MAC \qquad (10.17)$$

$$c_{r_h} = \frac{3}{2} MAC \frac{1 + \lambda_h}{1 + \lambda_h + \lambda_h^2} \qquad (10.18)$$

The properties of the horizontal tail are shown in Table 10.3.

10.4.3. Vertical tail design

The vertical tail airfoil shall be symmetric. It is common practice in general aviation to use similar airfoils for vertical and horizontal tails, hence the NACA 0010 is also used for the vertical tail [33]. The vertical tail area is provided by Equation 12.12 from the control section. From literature, it is suggested that T-tail configurations have an aspect ratio range of $0.6 - 1.2$ for the vertical tail and a taper ratio in the range of $0.6 - 1$. Provided these constraints, using Equation 10.17 and Equation 10.18 adapted for the vertical tail and using, once again, the optimization library from [31] to optimize for span and root chord, the vertical tail sizing results are provided.

The properties of the vertical tail are shown in Table 10.3.

Table 10.3: *Horizontal and Vertical tail characteristics*

	Horizontal Tail	Vertical Tail	
Parameter	Value	Value	Units
Area	9.15	4.9	m^2
Aspect ratio	4	0.7	-
Span	6	1.86	m
Taper ratio	0.47	0.6	-
Root chord	1.96	3.2	m
MAC	0.93	2.66	m
Sweep angle	0	35	°

10.5. Fuselage Drag

Another important parameter to be calculated is the drag force produced by the fuselage. This drag value will later be needed, along with other values, to model the stability of the aircraft in Chapter 12.

It is already known that the fuselage drag can be calculated with Equation 10.19.

$$D_{fuselage} = \frac{1}{2}\rho V_\infty^2 S C_{D_{fus}} \tag{10.19}$$

Where ρ is the density of air during cruise, V_∞ is the freestream velocity during cruise, S is the wing area of the aircraft and $C_{D_{fus}}$ is the drag coefficient of the fuselage, which is the only unknown in this equation.

A method for the approximation of this unknown value $C_{D_{fus}}$ is found in [34] and is described in this section. First, to identify the components in this fuselage drag coefficient, the different drag contributions due to the fuselage are identified:

- Friction drag

- Form and base drag

- Drag due to lift, or induced drag

- Interference drag

- Compressibility or wave drag

The fuselage drag coefficient can then be defined to be:

$$C_{D_{fus}} = C_{D_{0f}} + C_{D_{bf}} + C_{D_{Lf}} \tag{10.20}$$

Where:

- $C_{D_{0f}}$ is the fuselage zero-lift drag coefficient

- $C_{D_{bf}}$ is the fuselage base drag coefficient

- $C_{D_{Lf}}$ is the drag coefficient due to the lift of the fuselage

Firstly, the drag coefficient due to the lift of the fuselage, or $C_{D_{Lf}}$, can be assumed to be zero since the aircraft will not be flying at supersonic speeds.

Since there is no base area on the fuselage of the aircraft, the fuselage base drag coefficient, or $C_{D_{bf}}$, can also be assumed to be zero.

The only parameter left to calculate is the fuselage zero-lift drag coefficient, or $C_{D_{0f}}$ which is calculated using Equation 10.21 from [34].

$$C_{D_0 f} = R_{w_f} C_{f_f} \left\{ 1 + \frac{60}{(l_f/d_f)^3} + 0.0025(l_f/d_f) \right\} \frac{S_{wet_f}}{S} \tag{10.21}$$

Where R_{w_f} is the wing-fuselage interference factor, C_{f_f} is the turbulent flat plate friction coefficient, l_f/d_f is the fuselage fineness ratio and S_{wet_f} is the wetted area of the fuselage.

To calculate C_{f_f}, Equation 10.22 is given in the previously cited source [34].

$$C_{f_f} = \frac{0.455}{(log R_{N_f})^{2.58}} (0.144 M_f^2)^{0.58} \tag{10.22}$$

Where M_f is the Mach number of the fuselage and R_{N_f} is the fuselage Reynolds number which can be calculated with Equation 10.23.

$$R_{N_f} = \frac{\rho V_\infty l_f}{\mu_{air}} \tag{10.23}$$

Where ρ and V_∞ are the same values previously shown in Equation 10.19, l_f is the length of the fuselage and μ_{air} is the dynamic viscosity of air at 20 degrees Celsius at 4000 ft in m^2/s.

Furthermore, to find the wing-fuselage interference factor R_{w_f} in Equation 10.21, the figure below is used which is found in [34] together with the previously calculated Mach number M_f and fuselage Reynolds number R_{N_f}.
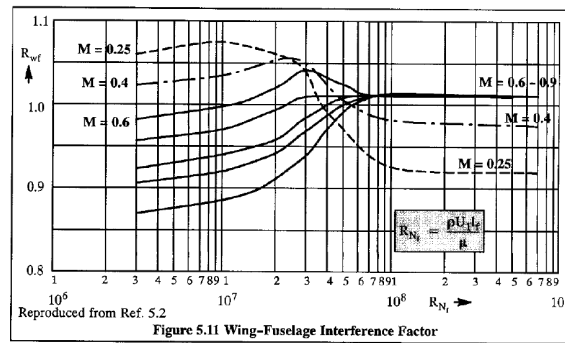
Figure 10.10: *Fuselage-wing interference factor [34]*

Another important parameter yet to be calculated is S_{wet_f}, also known as the wetted area of the fuselage. This value can be calculated using Equation 10.24.

$$S_{wet_f} = S_{wet_c} + S_{wet_{nose}} + S_{wet_{tail}} \tag{10.24}$$

Where S_{wet_c} is the wetted area of the constant part of the fuselage, $S_{wet_{nose}}$ is the wetted area of the nose of the fuselage and $S_{wet_{tail}}$ is the wetted area of the tail of the fuselage. The last two parameters can be calculated using the equations found in [35], namely:

$$S_{wet_{nose}} = 0.75\pi d_f l_{nose} \tag{10.25}$$

$$S_{wet_{tail}} = 0.72\pi d_f l_{tail} \tag{10.26}$$

Where d_f is the maximum fuselage diameter, l_{nose} is the length of the nose and l_{tail} is the length of the tail, all three values in meters.

Finally, to calculate S_{wet_c} or the wetted area of the constant part of the fuselage, the equation for the surface area of a cylinder is used:

$$S_{wet_c} = 2\pi \frac{d_f}{2} l_c + 2\pi \frac{d_f}{2}^2 \tag{10.27}$$

Where l_c is the length of the constant part of the fuselage.

To conclude this section, a table containing all the different parameters is given with the final value for drag in Table 10.4.

Table 10.4: *Values used in fuselage drag calculation.*

Parameter	Symbol	Value	Units
Length of fuselage constant part	l_c	4	m
Diameter of fuselage	d_f	2.5	m
Length of fuselage nose	l_{nose}	1.85	m
Length of fuselage tail	l_{tail}	3.3	m
Wetted area of fuselage constant part	S_{wet_f}	61.72	m^2
Fuselage Mach number	M_f	0.1603	-
Wing-fuselage interference factor	R_{w_f}	1.065	-
Dynamic viscosity of air in cruise condition	μ_{air}	$1.76637x10^-5$	m^2/s
Freestream velocity during cruise	V_∞	55	m/s
Air density during cruise	ρ	0.0669	kg/m^3
Turbulent flat plate friction coefficient	C_{f_f}	0.0896	-
Fuselage zero lift drag coefficient	$C_{D_{0f}}$	0.5311	-
Fuselage lift drag coefficient	$C_{D_{Lf}}$	0	-
Fuselage base drag coefficient	$C_{D_{bf}}$	0	-
Fuselage drag coefficient	$C_{D_{fus}}$	0.5311	-
Wing surface area	S_{wing}	27.5	m^2
Fuselage drag	$D_{fuselage}$	3927	N

Using this value for fuselage drag, further calculations can be performed for the stability and control of the aircraft in Chapter 12.

10.6. Noise Analysis

Noise calculations are conducted based on the method presented in [36], where rotational (harmonic) and vortex noise are estimated for a rotorcraft. The method has been adapted to account for all rotorcraft phases (hover, vertical climb and descent).

10.6.1. Rotational noise

Rotational noise occurs at discrete frequency values (integer multiples of the blade passing frequency). The overall sound pressure level for rotational noise is presented at Equation 10.30. Rotational noise is comprised of loading noise, caused by thrust generation, presented in Equation 10.28, and thickness noise caused by finite blade thickness, presented in Equation 10.29. [36] [37].

$$P_{m_l} = \frac{mN_b\Omega}{2\sqrt{2}\pi a(\Delta S)}\left(T\cos\theta - Q\frac{a}{\Omega R_e^2}\right)J\left(\frac{mN_b\Omega}{a}R_e\sin\theta\right) \tag{10.28}$$

$$P_{m_t} = \frac{-\rho(mN_b\Omega)^2 N_b}{3\sqrt{2}\pi(\Delta S)}ctR_eJ(\frac{mN_b\Omega}{a}R_e\sin\theta) \tag{10.29}$$

$$SPL = 10log\left(N_r\frac{P_{m_l}^2 + P_{m_t}^2}{P_{ref}^2}\right) \tag{10.30}$$

m is the harmonic number, N_b is the number of rotor blades, N is the number of rotors, Ω is the rotor angular velocity, a is the speed of sound, R_e is the effective rotor radius (defined as 0.8 R, is the rotor thrust, Q is the rotor torque (as calculated from blade element theory), c is the blade chord and t is the maximum blade thickness. J_{mB} is a Bessel function of the first kind of order mB. Loading noise is dependent on the location of the observer with respect to the rotational axis of the blades. The argument of the Bessel function suggests that when the observer angle θ between the rotational axis and the observer is 180° (so the observer is directly below the rotorcraft), $P_{m_l} = 0$. θ relates to the distance ΔS between the rotor and the observer according to Equation 10.31, which is based on Figure 10.11.

$$\theta = \arccos\left(-\frac{y}{\Delta S}\right) \tag{10.31}$$
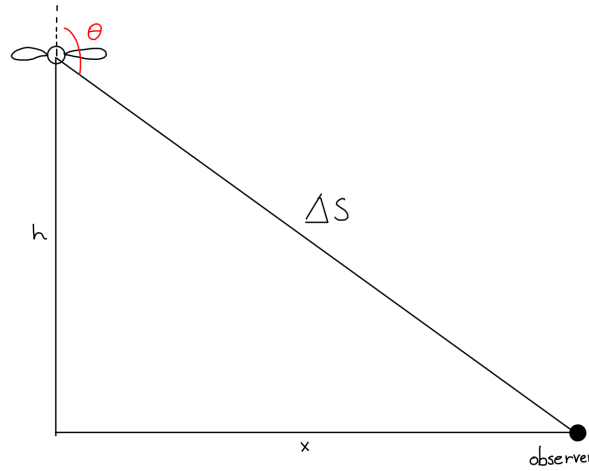

Figure 10.11: *Observer position and observer angle [36]*

10.6.2. Vortex noise

Vortex noise is calculated according to Equation 10.32.

$$SPL = 20log\left[K_2\frac{\Omega R}{\rho(\Delta S)}\sqrt{\frac{NT}{s}\left(\frac{T}{A}\right)}\right] \tag{10.32}$$

K_2 is a constant equal to $1.206 \cdot 10^{-2}$, and $\frac{T}{A}$ represents the disk loading per rotor.

10.6.3. Results

The noise results are presented in Table 10.5. Rotational noise is calculated for vertical climb conditions.

Table 10.5: *Noise results*

Parameter	Value	Unit
Rotational noise	86	$[dBA]$
Vortex noise	48.5	$[dBA]$
Peak frequency	4.7	$[kHz]$

10.7. Verification & Validation

This section presents the verification and validation procedures used for the aerodynamic analysis of Aether.

10.7.1. Wing design

The libraries and methods used for the wing analysis are based on Lifting Line theory, a theory that has already been validated. The results obtained from the tools used were further verified by hand calculations for a smaller number of panels (4), providing the same output.

Parameter	Tool	XFLR
C_l	0.683	0.655
C_d	0.028	0.03

Another verification test conducted was the convergence to a specific oswald factor for elliptic lift distribution. The output was tested against a hand-written analytical model. With an expected answer of 1, the numerical model's output was 0.9999835. This deviation is still acceptable for a numerical model.

Further validation of the outputs of the tools can be done when comparing with the results from XFLR5, which offers the possibility for using Vortex Lattice Method. The parameters compared are the lift and drag coefficient for cruise conditions.

10.7.2. Tail design

he tail sizing is verified by analytical methods. Given the same input, the methods provided the same numerical results.

11

Structures & Materials

Aether's structural design is a fundamental aspect of its design. The failure of any of its structure due to fatigue could result in a catastrophic crash. For this reason it is crucial to design a structure that can be able to withstand all loads acting on the aircraft during all flight phases and maneuvers. However, an overly designed structure would cause a loss in performance as well as an unnecessary increase in the aircraft weight. Additionally, this would significantly increase the overall costs. For this reason, an optimum structure design is desired by reducing its weight to a minimum while still being able to withstand all the loads ans stresses. This chapter aims to explain the preliminary design and analysis of Aether's structure. Firstly, Section 11.1 explains the general overview of the design of the structure, followed by the material selection. Then, the preliminary design and analysis of the main structures is shown in Section 11.3 and Section 11.4. Finally, verification and validation procedures are performed in Section 11.5.

11.1. Manoeuvre Diagram

The first step to conduct the structural analysis of Aether was to perform a manoeuvre load diagram. A load diagram shows the maximum loads to be designed for in terms of velocity. The maximum loads are obtained during certain maneuvers which the structure must bear. These loads are then used for the design of the structure. The maximum and minimum loads are depicted in this type of diagram. Figure 11.1 shows the preliminary load diagram of Aether. Together with the data obtained from other departments such as cruise velocity or stall speed and taking a maximum load factor of 2.5 and a minimum load factor of 1 this diagram was constructed. In a later stage of the design the maximum load factor is substituted with that found from specific maneuvers such as a pull-up maneuver.
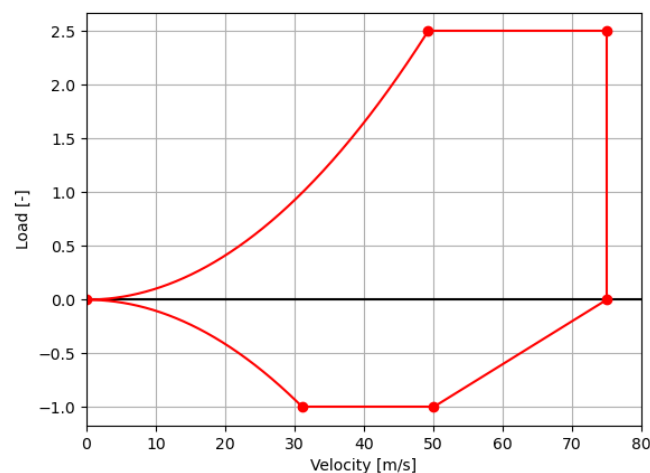

Figure 11.1: *Manoeuvre load diagram of Aether.*

11.2. Material Selection

For the selection of the materials to be used in the structure of Aether, a trade-off was performed. This was done taking into account sustainability as well as density of the material as the most important characteristics, besides their overall properties. Since Aether is a VTOL vehicle saving weight is crucial. The two materials that were taken into account are Carbon Fibre Reinforced Polymer (CFRP) and the Aluminum Alloy Al-Li 2198.

In terms of material strength, aluminium alloys tend to perform better than composites. In the context of aircraft structures, it is often important that the material exhibits strength against various loads as a result of maneuvers at high speeds, landing or pressurization. However for this application, it is the case that loads are not as high compared to commercial airliners that travel at high altitudes. The landing process is rather less rough as it hovers just above the ground before landing, and the cabin does not need to be pressurized as the cruise altitude is 4000 feet above sea level (1219 meters). Therefore, from a weight reduction perspective it is a better design choice to select composites instead of aluminium alloys for this particular application, as this material tends to be lighter.

For these reasons it was concluded that CFRP would be the best material in terms of material properties and in order to safe as much weight as possible. The specific CFRP chosen is Carbon Fiber Reinforced Thermo-Plastic (CFRTP) which means that instead of using the usual thermosetting as a resin, thermoplastic is used as the impregnating material[1]. This allows for easier recyclability and for more cost-efficient processes for the manufacture of the material [38]. This way, the carbon fibre would be used for the main structure of Aether to safe weight, meaning the fuselage, the wing or the empennage. However, CFRP is expensive in terms of recyclability due to the difficult processes. Since aluminium alloys are more easily recycled, for smaller structures that are highly intense loaded, that may wear out more easily and that require more maintenance, the Aluminium alloy Al-Li 2198 is used. This alloy is broadly used in the aerospace industry due to its extremely high strength levels and, thus, would be the best option for the structure that connects the rotors to the main structure [39].

11.3. Wing Loading and Structure

For the structural design of the wing, a wing box is placed to carry the specific loads produced during all flight phases. The preliminary design of the wing box, as observed in Figure 11.2 and Figure 11.3 is built of two spars located at $0.2\bar{c}$ and $0.6\bar{c}$ allowing for enough space in the leading edge for the electric systems of the proprotors and enough space for the ailerons in the trailing edge. These two spars are connected by the skin of the wing. This section will analyse the specific loads carried by the wing box during flight. This way, the most critical loads of flight can be identified and in a later stage of the design, size the spars, skin, and the reinforcement needed for the wing box.

---

[1] https://www.sonotec.com/en/material/carbon.html [Cited 26 January 2022]
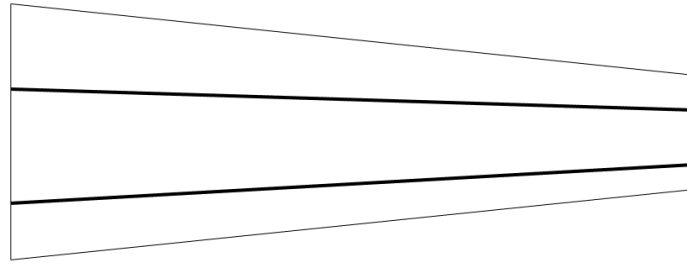
Figure 11.2: *Sketch of wingbox spar spanwise location in the wing.*
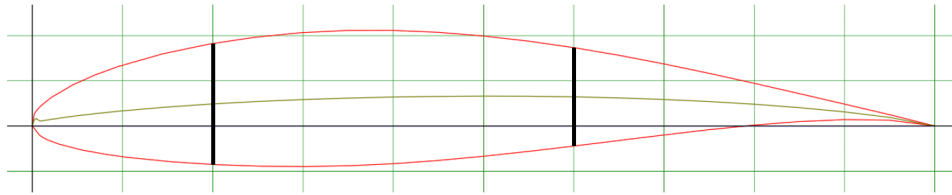
Figure 11.3: *Sketch of wingbox spar location in the selected NACA63(2)-615 airfoil.* [2]

A general Free Body Diagram (FBD) showing the thrust forces carried by the wing box of one wing can be depicted in Figure 11.4. For simplicity of the sketch, Lift, Drag, and Weight is not included in the FBD, since it is merely to show the reaction forces at the root of the wing (shown in green) where the wing is connected to the fuselage, as well as to show the thrust forces during cruise (depicted in red) and the thrust forces during hover (depicted in blue). For the analysis of the internal loading carried by this wing box, some assumptions were made. Firstly, during cruise, lift, drag, and weight of the wing is assumed to act through the center line of the wing box, as well as the thrust of the proprotors. This means there is no torque acting during cruise. This torque was estimated to be neglected and, thus, torque is only studied during hover. Additionally, the lift, drag, and wing weight are assumed to be uniformly distributed loads. Furthermore, the weight of the batteries, placed inside of the wing box, is not taken into account for the calculations. The placement of the battery is still undefined but it is known that it will be placed as close to the fuselage as possible. This means that the reaction moment created by the battery is expected to be small compared to the other loads acting on the wing box. Also, the weight of the battery will actually be advantageous for the stresses acting in the wing box as a result of the loads. The weight would create a counter moment compared to the lift created by the wing during cruise or the thrust by the rotors during hover. This means the wing box is actually being over-designed.

[2]http://airfoiltools.com/airfoil/details?airfoil=naca632615-il [Cited 20 January 2022]
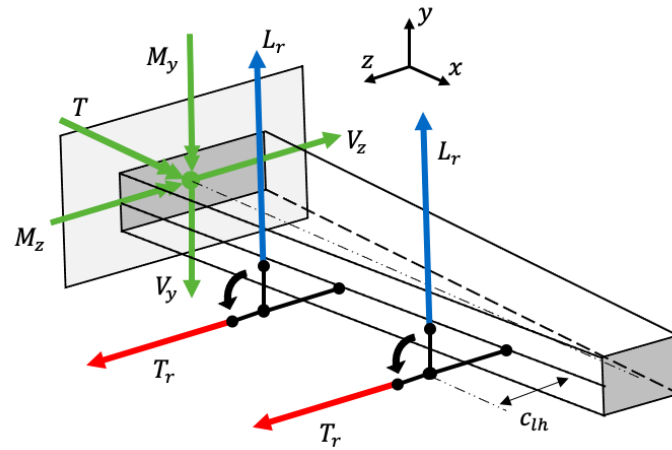
Figure 11.4: *FBD Wingbox*

11.3.1. Wing loading analysis during cruise

Firstly, the analysis of the loads during cruise was studied. The main loads acting during this phase can be observed in the FBDs in Figure 11.5 and Figure 11.6. Here, the wing box of on wing modelled as a beam is observed in both the XY and XZ plane, which are the frontal and top view respectively, with the wing root as origin.
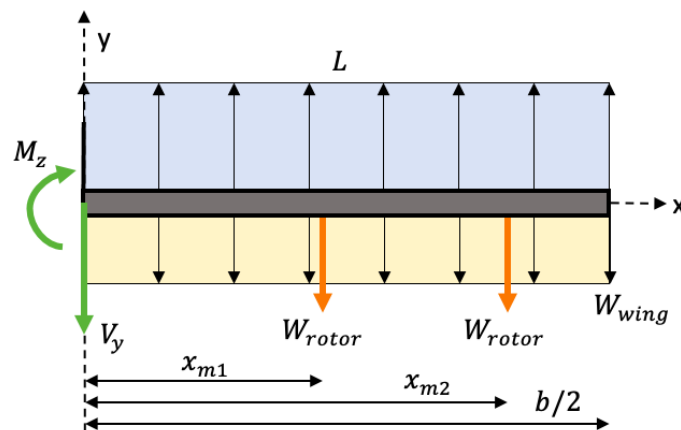
Figure 11.5: *Free Body Diagram of the loads acting in the wing box shown in the XY plane during cruise.*
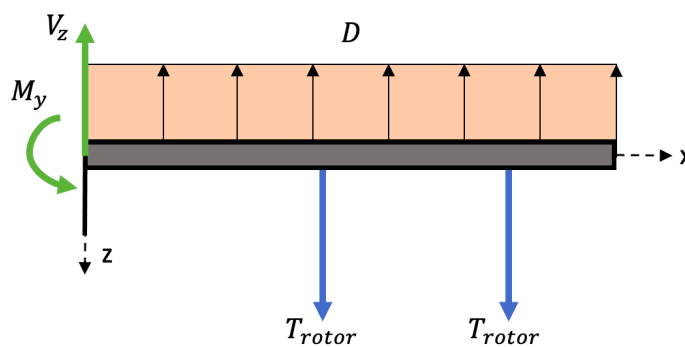
Figure 11.6: *Free Body Diagram of the loads acting in the wing box shown in the XZ plane during cruise.*

With these FBDs, the reaction forces at the root of the wing (shown in green) were calculated. These are shown in Equation 11.1 and Equation 11.2 for the XY plane, and in Equation 11.3 and Equation 11.4 for the XZ plane. These reaction forces were then used to find the internal shear force and moment along the wingspan. The internal loading diagrams are shown in Figure 11.7 and Figure 11.8 for the XY plane and Figure 11.9 and Figure 11.10 for the XZ plane.

$$V_{ycruise} = L\frac{b}{2} - W_w\frac{b}{2} - 2W_r \tag{11.1}$$

$$M_{zcruise} = (L - W_w)\frac{b}{2}\frac{b}{4} - W_r(x_{m1} + x_{m2}) \tag{11.2}$$

$$V_z = 2T_r - D\frac{b}{2} \tag{11.3}$$

$$M_y = T_r(x_{m1} + x_{m2}) - D\frac{b}{2}\frac{b}{4} \tag{11.4}$$

Figure 11.7: *Internal shear force diagram of one wing in spanwise direction in the XY plane during cruise starting on the wing root.*

Figure 11.8: *Internal moment diagram of one wing in spanwise direction in the XY plane during cruise starting on the wing root.*

Figure 11.9: *Internal shear force diagram of one wing in spanwise direction in the XZ plane during cruise starting on the wing root.*
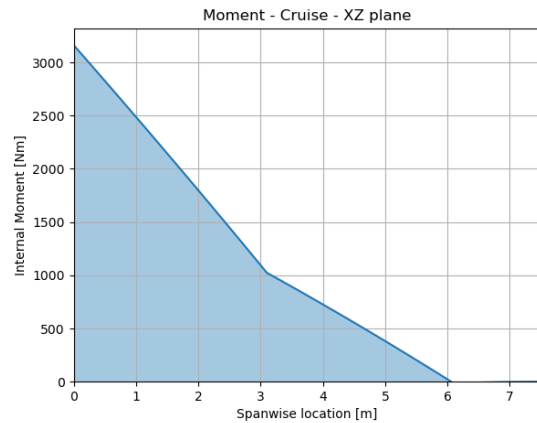
Figure 11.10: *Internal shear force diagram of one wing in spanwise direction in the XZ plane during cruise starting on the wing root.*

11.3.2. Wing loading analysis during hover

The same way as the previous sub-section, this sub-section studies the loading of the wing but during the hover phase of flight. The FBD for this phase can be observed in Figure 11.12. Similarly, the reaction forces were obtained and can be found in Equation 11.5, Equation 11.2, and Equation 11.7. It is important to note, the torque was found using the FBD shown in Figure 11.4 for a better visualization of the moment arm. This way, the internal loading was found and can be observed in Figure 11.12, Figure 11.13, and Figure 11.14 for shear force, internal moment, and internal torque, respectively.
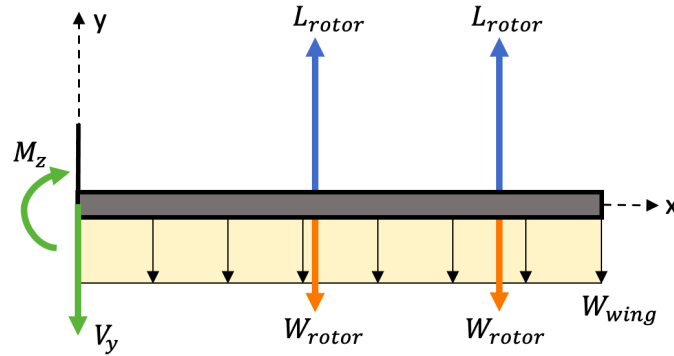
Figure 11.11: *Free Body Diagram of the loads acting in the wing box shown in the XY plane during hover.*

$$V_{yhover} = 2L_r - 2W_r - W_w \frac{b}{2} \tag{11.5}$$

$$M_{zhover} = (L_r - W_r)x_{m1} + (L_r - W_r)x_{m2} - W_w \frac{b}{2}\frac{b}{4} \tag{11.6}$$

$$T = (\frac{c_{r1}}{2} + cl_h)(L_r - W_r) + (\frac{c_{r2}}{2} + cl_h)(L_r - W_r) \tag{11.7}$$

Figure 11.12: *Internal shear force diagram of one wing in spanwise direction in the XY plane during hover starting on the wing root.*
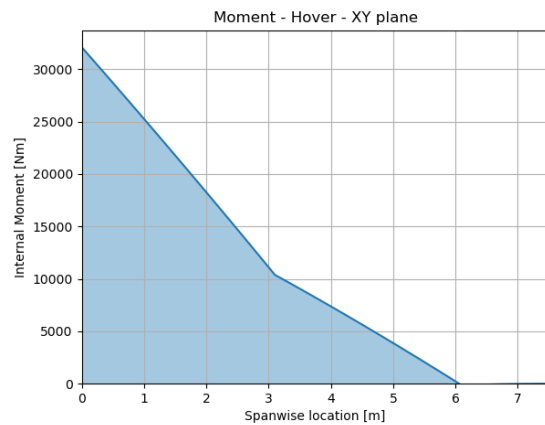
Figure 11.13: *Internal moment diagram of one wing in spanwise direction in the XY plane during hover starting on the wing root.*
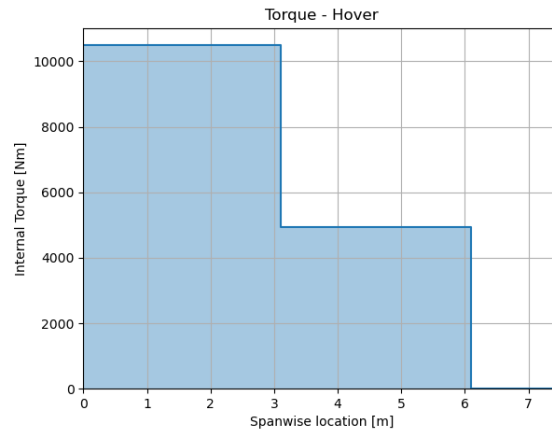
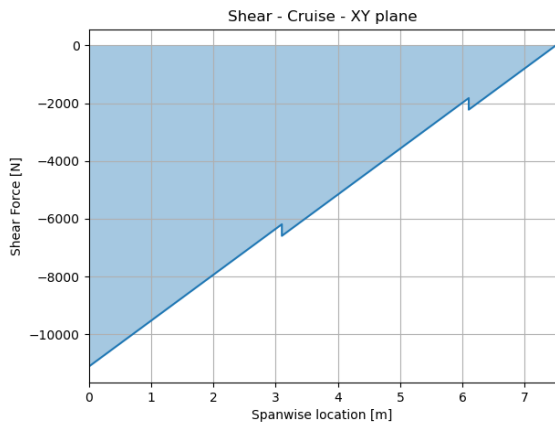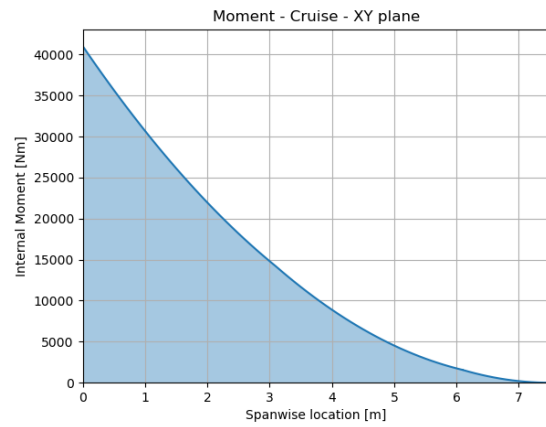**Figure 11.14:** *Internal torque diagram of one wing in spanwise direction in the XY plane during hover starting on the wing root.*

11.4. Rotor Shaft Loading and Structure

Another critical structure of Aether is the structure that hold and maintain in place the six different proprotors. For this, two different structures were designed: for the four wing mounted proprotors and for the two fuselage mounted proprotors. The latter can be observed in Figure 11.15, with the specific structure holding the proprotor shown in Figure 11.16. Simply by observation, it can be concluded that this structure is critical for safety, however, weight and aerodynamics play an important role for the design of this structure.

As observed, a hollow shaft structure was designed to be able to fit the turning mechanism as well as other electrical systems. It has a length of 1.985 [m] and it was given an aerodynamic shape with a bigger diameter in the horizontal plane than in the vertical plane. This gives a cross-section with a radius of 0.15 [m] in the horizontal plane, and a smaller radius of 0.13 [m] in the vertical plane.
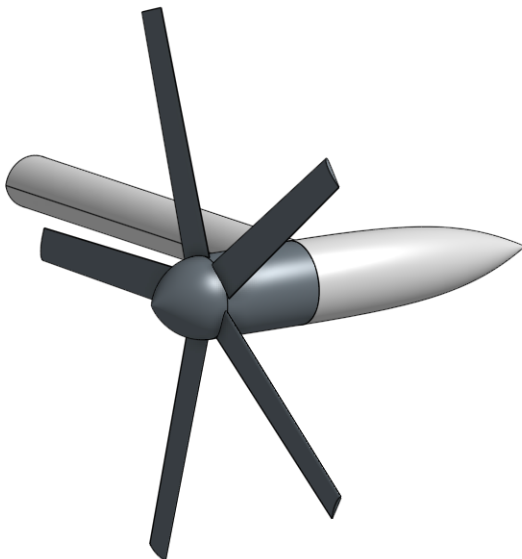
Figure 11.15: *Structure of fuselage-mounted rotor.*   **Figure 11.16:** *Shaft structure of fuselage-mounted rotor.*
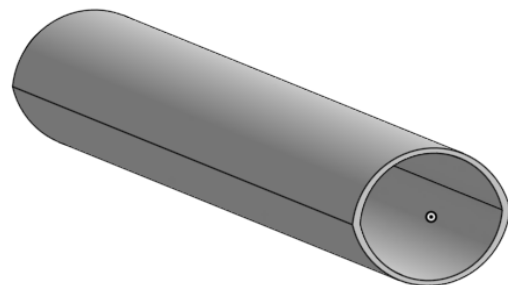
The thickness of the shaft was calculated using the moment Equation 11.8. For this, it was assumed

a circular hollow shaft of a radius of 0.13 [m] with the load analysis during hover with one rotor failure. This was chosen as the most critical phase for the rod due to the bending moment acting in the smaller diameter of the shaft and a bigger thrust needed for each of the five active rotors. Additionally the weight of the own shaft is neglected. These assumptions will mean the thickness of the shaft will be over-designed.

$$t_{min} = \frac{L \cdot W/5 \cdot SF \cdot n}{\pi \cdot R^2 \cdot \sigma_y} \tag{11.8}$$

With the determined safety factor, the maximum load during flight, and the determined maximum aluminium alloy's yield stress, a minimum thickness of 3.2 [mm] is needed for this structure.

For the wing mounted proprotors, a shaft structure is designed. This structure works as the rotating axis for the tilt-rotors during transition. This shaft connecting the rotor to the nacelle ensures it stays in place during its specific phase of the flight.

The structure is three point loaded and has a length of 0.2 [m] and the diameter was calculated using Equation 11.9. The most critical scenario is chosen for the diameter calculation, this being hover with one rotor failure. Again, with the determined safety factor, the maximum load during flight, and the determined maximum aluminium alloy's yield stress, a minimum diameter of 3.0 [cm] is needed.

$$D_{min} = \sqrt[3]{\frac{3 \cdot W/5 \cdot L \cdot SF \cdot n}{2 \cdot \sigma_y}} \tag{11.9}$$

11.5. Verification and Validation

Verification and validation procedures were implemented to ensure the correct implementation of the analytical model and to check for possible errors. One procedure to check the internal load diagrams that were performed for the wing box is checking the loads of the internal shear force diagrams. The internal shear force diagrams depicted in the diagrams for the different load cases should math the numerical calculations. This way, the shear force obtained at the distance of 0 [m] from the wing root, meaning at the origin should math the reaction force. Additionally the vertical jumps obtained throughout the wingspan direction of the diagrams are due to point loads acting on the wing box. By looking at the internal loading diagrams in Section 11.3 it is observed that the jumps coincide with the resultant point loads acting at that point. Furthermore, these diagrams were verified by using an external software to plot them. The software used is SkyCiv [3]. The internal shear force and internal moment for the cruise phase in the XY plane obtained with this software can be observed in Figure 11.17 and in Figure 11.18. By comparing these graphs to the ones obtained for the same phase and same plane, which are shown in Figure 11.7 and Figure 11.8 it can be concluded that the method used is correct. The graphs obtained are equal in terms of shape and magnitude.

---

[3] https://platform.skyciv.com/ [Cited 25 January 2021]
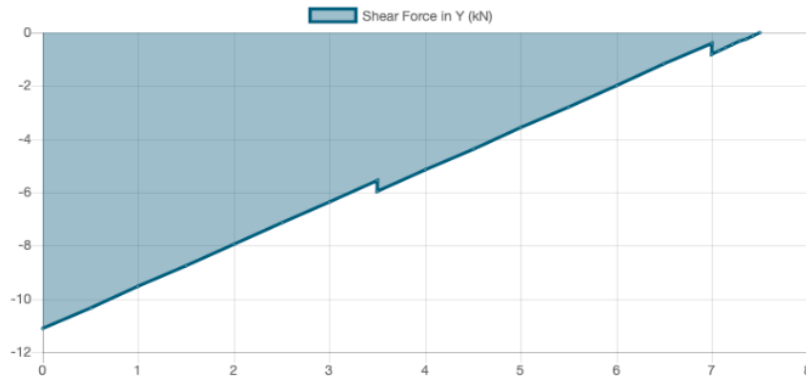
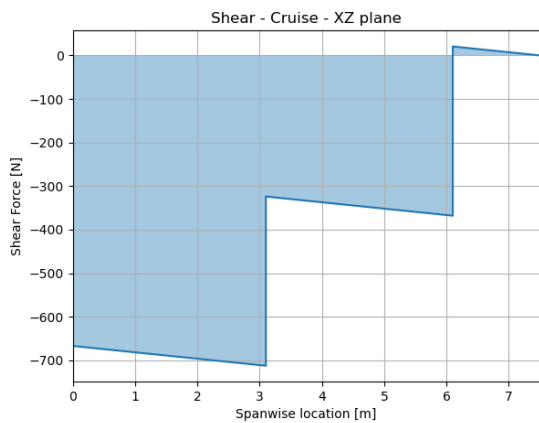**Figure 11.17:** *Internal shear force diagram of one wing in spanwise direction in the XY plane during cruise starting on the wing root obtained from external software SkyCiv.*
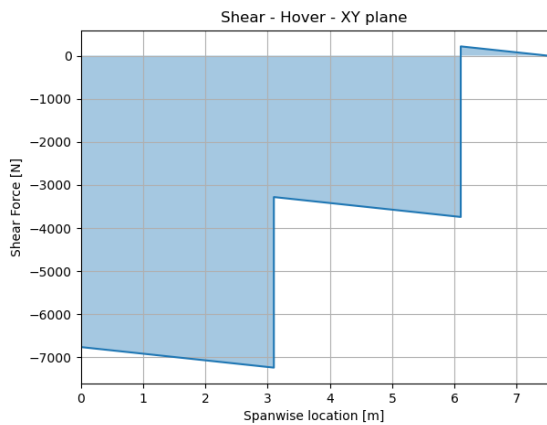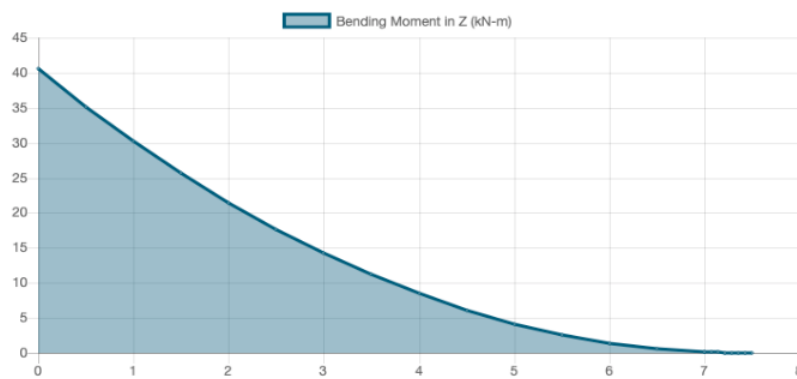

Figure 11.18: *Internal shear force diagram of one wing in spanwise direction in the XY plane during cruise starting on the wing root obtained from external software SkyCiv.*

For the verification of the shaft structure shown in Figure 11.16 a Finite Element Method (FEM) analysis was performed. This is shown in Figure 11.19 where the shaft is observed and the specific stresses are visualised. This model imitates reality: the origin which connects to the fuselage is fixed and the other end which connects to the rotor is where the thrust of the proprotor acts. It can be observed the connection to the fuselage is where the maximum stresses occur, with a maximum stress equal to the yield stress of the material used, this being the aluminium alloy Al-Li 2198 and thus, this model verifies the calculations of Section 11.4.
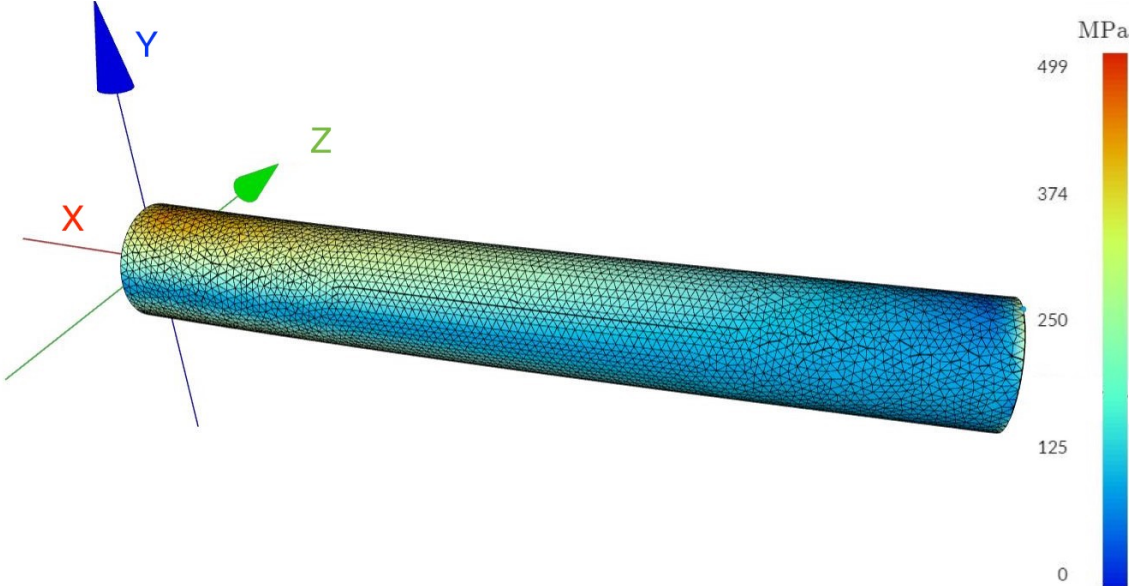
Figure 11.19: *FEM analysis of the back rotor beam in a pull up manoeuvre*

12
Stability and Control

Designing for stability and control is crucial to ensure the aircraft can remain airborne. This chapter explores the static stability, dynamic stability of the aircraft and propose a possible design of a controller.

12.1. General Framework

This section explains the general framework of designing the stability and control subsystem.

12.1.1. Reference frame

For the stability analysis, three different reference frames are used. These are listed below.

- **Vehicle-carried normal Earth reference frame**
  This reference frame has its origin at the aircraft's center of gravity. The Z_E axis is perpendicular to the Earth surface. The $X_E Y_E$ plane is tangent to the Earth surface.

- **Body fixed reference frame**
  This reference frame is right handed and is also fixed to the aircraft body. The origin is located at the aircraft's center of gravity. The X_b axis is in the symmetry plane of the aircraft and points forward. The Y_b axis points to the right and is perpendicular to the symmetry plane of the aircraft. The definition of X_b axis depends on the case to be studied, but X_s axis, which is parallel to the direction of motion of the center of gravity in the steady flight condition, is often used.

- **Aerodynamic (air-path) reference frame**
  This reference frame is coupled to the air path velocity and is right handed. The X_a axis is in the direction of the aerodynamic velocity and the Z_a is in the symmetry plane of the aircraft. The Y_a axis is perpendicular to the $X_b Z_b$ plane.

12.1.2. Control allocation

It is important to decide which control means are used for each type of aircraft maneuver. Table 12.1 shows the overview of the control means for the hover and cruise phase. During the hover phase, aircraft control is purely dependent on differentiating the rotational speed of the rotor. This is the most basic way of controlling a multicopter. In order to control all roll, pitch, and yaw motions in this method, the rotational direction must be distinguished in diagonal, also as shown in Figure 5.7. In the cruise phase, elevator and aileron comes into the control loop. Although it may be still possible to control the aircraft only by differentiating the rotational speed of rotor and tilt angle, control surfaces are considered as the better solution. The first reason is that it is inherently more reliable to physically counteract the aerodynamic forces or moments by other aerodynamic forces or moments. It requires less steps of quantization in the control loop, and thus there would be a lower risk for discrepancies from the desired output. Also, the technology to control the aircraft in this way is still at an early stage of its development, compared to other control surfaces.

During the transition phase, the aircraft is controlled by combining the method presented in the hover and cruise phase. A more detailed explanation about the transition phase will be given in Section 12.4.
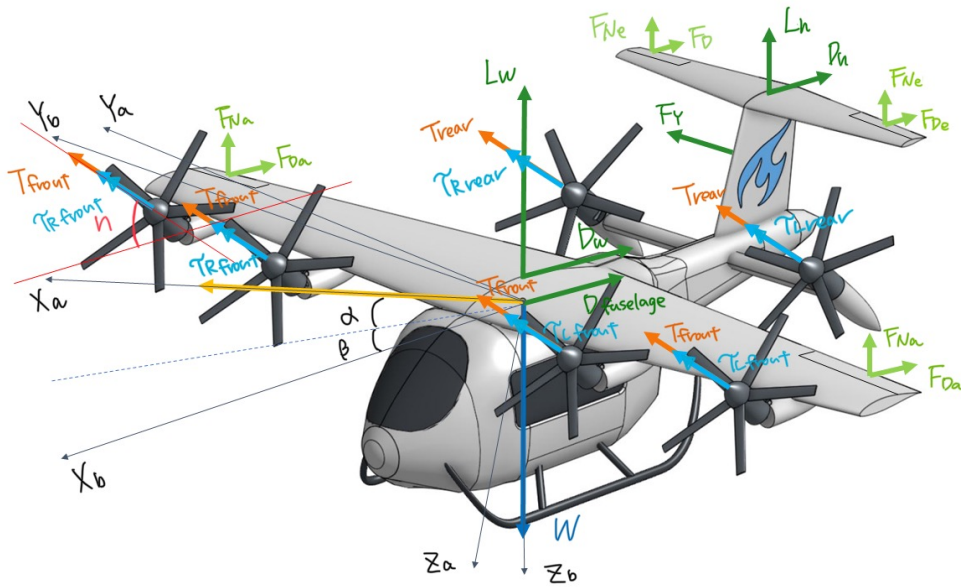
Figure 12.1: *Free body diagram in an arbitrary condition.*

Table 12.1: *Overview of control means for hover and cruise phase.*

	DOF	Symbol	Control means
Hover	Roll	ϕ	$\Delta\Omega$ of the left and right rotors
	Pitch	θ	$\Delta\Omega$ of the front and rear rotors
	Yaw	ψ	$\Delta\Omega$ of rotors with different rotational direction
	X	X	Tilting the rotor Δn
	Y	Y	-
	Z	Z	$\Delta\Omega$ of all rotors
Cruise	Roll	ϕ	Aileron deflection δ_a or $\Delta\Omega$ of rotors with different rotational direction
	Pitch	θ	Elevator deflection δ_e or changing tilt angle Δn
	Yaw	ψ	Rudder deflection δ_r or $\Delta\Omega$ of the left and right rotors
	X	X	$\Delta\Omega$ of all rotors
	Y	Y	Rudder deflection δ_r
	Z	Z	Elevator deflection δ_e, Δn, or $\Delta\Omega$
Transition			Combination of the ones listed above

12.1.3. Equations of motion

The very first step to analyze the aircraft's motion is to write the equations of motion. This subsection explains the assumptions made to simplify the equations, the calculation of the present forces, and the actual equations of motion of the aircraft.

To begin, the free body diagram of the aircraft in an arbitrary flight condition is shown in Figure 12.1.

Assumptions

In order to simplify the equations, the following assumptions are made:

- Earth is flat

- Earth is non-rotating

- Gravity field is constant

- The vehicle is a rigid body

- The vehicle is symmetrical about XZ-plane in body-fixed reference frame

- Drag force and thrust force act in the same line when the tilt angle n is at 0 degree (Cruise condition).

- The aerodynamics center is at the 25% of the MAC, and lift of the wing acts on this point.

- Distributed forces such as lift, drag and weight are considered as point forces.

- The length of the front tilt arm and rear tilt arm are the same.

- The main wing and horizontal tail is at the same height, in other words at the same coordinate in Z_b axis.

Simplified equations of motion

With the above-mentioned assumptions, the equation of motion in 3 degrees of freedom model can be written as shown in Equation 12.1 to Equation 12.3. In the analysis in longitudinal direction, roll and yaw is not taken into account, so an additional assumption $p = 0$ and $r = 0$ are made in Equation 12.3.

$$\Sigma F_X^b: \ m(\dot{u} + qw - rv) = 4T_{front}cos(n_{front}) + L_w sin(\alpha) - D_w cos(\alpha) - W sin(\theta)$$
$$- D_{fuselage}cos(\alpha) + 2T_{rear}cos(n_{rear}) + L_h sin(\alpha_h) - D_h cos(\alpha_h) \tag{12.1}$$

$$\Sigma F_Z^b: \ m(\dot{w} + pv - qu) = -4T_{front}sin(n_{front}) + L_w cos(\alpha) + D_w sin(\alpha) - W cos(\theta)$$
$$+ D_{fuselage}sin(\alpha) + 2T_{rear}sin(n_{rear}) + L_h cos(\alpha_h) + D_h sin(\alpha_h) \tag{12.2}$$

$$\Sigma M_{Y_{b\,cg}}: \ I_{yy}\dot{q} = (C_{m_{ac}} + C_{m_{\delta_e}}\delta_e)qS\bar{c} + L_w(x_{cg} - x_{ac}) + L_h(X_{ac_h} - X_{cg})$$
$$- (4T_{front}cos(n_{front}))(l_{tilt}sin(n_{front}))$$
$$+ (4T_{front}sin(n_{front}))((l_{tilt} + (X_{cg} - X_{T_{front}}))cos(n_{front}))$$
$$- (2T_{rear}cos(n_{rear}))(l_{tilt}sin(n_{rear})) - (2T_{rear}sin(n_{rear}))((X_{T_{rear}} - X_{cg}) - l_{tilt})cos(n_{rear}) \tag{12.3}$$

Thrust force

The thrust force is calculated by the Blade Element Theory in Equation 12.4, assuming the chord length is constant along the radius [40].

$$T = N \int_0^{R_e} C_l \frac{1}{2}\rho(\Omega r)^2 c dr$$
$$\approx \frac{N\rho c\Omega^2}{2} \int_0^{0.2R_e} C_{l0.2R}r^2 c dr + \int_{0.2Re}^{0.5R_e} C_{l0.5R}r^2 c dr + \int_{0.5Re}^{0.75R_e} C_{l0.75R}r^2 c dr + \int_{0.75Re}^{R_e} C_{lR}r^2 c dr \tag{12.4}$$

Where N is a number of the blades in one rotor, c is the chord length of the blade, C_l is the lift coefficient at the location stated in its subscript. R_e is effective radius, which is equal to $0.97R$.

Moment of inertia

The initial guess of the moment of inertia is made by scaling the existing aircraft. In this case, De Havilland Canada DHC-6 "Twin Otter" [1] aircraft is chosen for the comparison because the geometry of the aircraft is the closest to this aircraft among the ones that the data is available. The Twin Otter

---

[1] https://www.baesystems.com/en/heritage/de-havilland-canada-dhc-6-twin-otter

has I_{yy} of 29972 [kgm^2] with MTOW of 4150 [kg] and the longitudinal length of 15 [m] [2]. Since the calculation for the moment of inertia is "$I = mr^2$" with mass "m" and the radius "r", the moment of inertia can be scaled by the relationship in Equation 12.5. With this calculation, the moment of inertia of this aircraft was estimated to be 5478 [kgm^2].

$$I_{yy_1} = \frac{M_1}{M_2}\left(\frac{l_1}{l_2}\right)^2 I_{yy_2} \tag{12.5}$$

12.2. Static Stability

12.2.1. Center of gravity

To calculate the center of gravity position in the longitudinal direction of the aircraft, the different weight groups found in the class II weight estimation are used, together with the converging value of the empty operative weight both found in Chapter 8.

Firstly, the position of the center of gravity is found geometrically and then verified using the CATIA model of the aircraft. These initial values can be seen in Table 12.2 below.

Table 12.2: *Longitudinal center of gravity locations for main aircraft parameters.*

Parameter	Symbol	Location from the nose of the aircraft [m]
Wing	$X_{cg_{wing}}$	3.025
Rotors near wing root	$X_{cg_{rroot}}$	1.982
Rotors near wing tip	$X_{cg_{rtip}}$	2.482
Landing gear	$X_{cg_{lg}}$	3.505
Fuselage shell	X_{cg_f}	3.275
Horizontal tail	X_{cg_h}	8.1
Vertical tail	X_{cg_v}	7.9
Rotors at rear	$X_{cg_{rrear}}$	6.9
Battery	X_{cg_b}	2.75
Fixed equipment	$X_{cg_{feq}}$	0.85

To be able to find the operative empty weight CG location, all the above weights should be first grouped into two categories: fuselage group and wing group.

The fuselage group in this design, is defined as:

$$X_{cg_{FG}} = \frac{X_{cg_f} W_f + X_{cg_h} W_h + X_{cg_v} W_v + X_{cg_{rrear}} W_{rear} + X_{cg_b} W_b + X_{cg_{feq}} W_{feq}}{W_f + W_h + W_v + W_{rrear} + W_b + W_{feq}} \tag{12.6}$$

The wing group is then:

$$X_{cg_{WG}} = \frac{X_{cg_w} W_w + X_{cg_{rroot}} W_{rroot} + X_{cg_{rtip}} W_{rtip} + X_{cg_{lg}} W_{lg}}{W_w + W_{rroot} + W_{rtip} + W_{lg}} \tag{12.7}$$

Where the weight values for both groups can be found in Table 8.3.

Once this is done, the operative empty weight CG location, can be found by using the following equation:

$$X_{cg_{OE}} = \frac{X_{cg_{FG}} W_{FG} + X_{cg_{WG}} W_{WG}}{W_{FG} + W_{WG}} \tag{12.8}$$

---

[2]http://jsbsim.sourceforge.net/MassProps.html

Once this value is known, the leading edge position of the mean aerodynamic chord must be determined. This is done with the use of the following equation:

$$X_{LEMAC} = X_{cg_{FG}} - X_{cg_{OE}} + \frac{W_{WG}}{W_{FG}} \left(X_{cg_{FG}} - X_{cg_{OE}} \right) \tag{12.9}$$

Note that the value for $X_{cg_{OE}}$ is (in this case) considering a different reference frame as the value for $X_{cg_{FG}}$, namely the mean aerodynamic chord (MAC) as opposed to the fuselage nose.

Once the location of the X_{LEMAC} is known, the balancing of the aircraft can be performed. This is done with the use of a so-called potato diagram or CG range diagram in which the aircraft is loaded with cargo and passengers and the CG shift is measured. Typically this diagram also includes the fuel loading, but due to the aircraft being electric and thus not requiring fuel, the loading of the aircraft will be limited to passenger and cargo loading.

Using the cabin design parameters found in Chapter 7, the following CG locations can be found for the passengers and their baggage:

Table 12.3: *Longitudinal center of gravity locations for cargo and passengers.*

Parameter	Symbol	Location from the nose of the aircraft [m]
Front cargo	$X_{cg_{cfront}}$	1.4
Rear cargo	$X_{cg_{cback}}$	5.97
Pilot	$X_{cg_{pilot}}$	1.5
Front-left passenger	$X_{cg_{paxfl}}$	2.3
Front-right passenger	$X_{cg_{paxfr}}$	2.83
Rear-left passenger	$X_{cg_{paxrl}}$	3.6
Rear-right passenger	$X_{cg_{paxrr}}$	4.03

Using the values in Table 12.3, the CG range plot, or potato diagram can be produced. This is done by using the location of the empty operative weight center of gravity $X_{cg_{OE}}$ as a starting point. Then the aircraft is loaded first with the front cargo and then with the rear cargo, followed by the passengers from the front to the back of the aircraft. Then the same procedure is repeated starting from the rear of the aircraft. Please note that the front cargo refers to the carry-on luggage compartment in the front of the aircraft, while the rear cargo refers to the checked luggage compartment in the rear of the aircraft. All these cabin locations are depicted in Figure 7.4 and explained in further detail in Chapter 7.
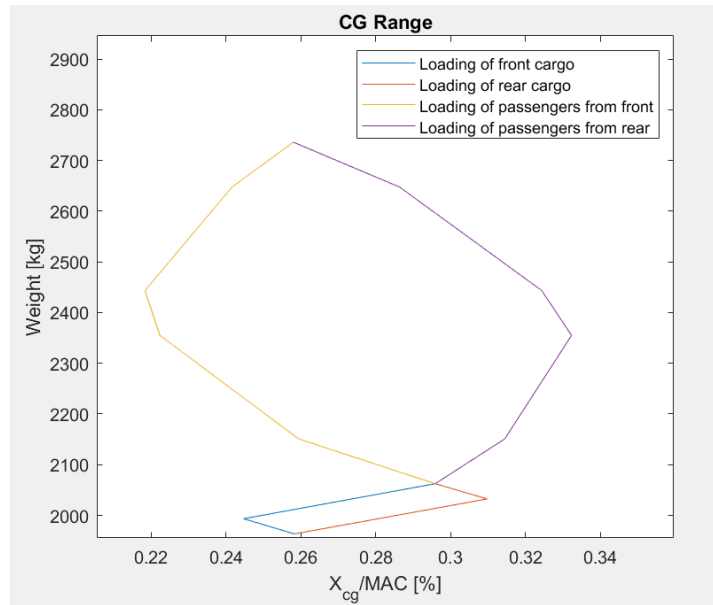
Figure 12.2: *Longitudinal CG range plot for the loading of passengers and baggage.*

Using Figure 12.2, the range of all possible center of gravity shifts during boarding of passengers and baggage are accounted for. It is also important to note that this plot is built using the CG positions as a percentage of the MAC, as can be seen in the x-axis of the plot above. These values can be found by subtracting each position by the initial X_{LEMAC} value found previously.

A safety margin of 2 [%] is added to this CG range to account for CG variations caused by passengers moving inside the aircraft.

Furthermore, as can be seen in the CG plot in Figure 12.2 , the center of gravity position when the aircraft is fully loaded remains close but does not move in front of the aerodynamic center, thus guaranteeing static stability during the flight.

12.2.2. Horizontal tail sizing

The size of the horizontal tail is a crucial factor for longitudinal static stability. The stability curve given in Equation 12.10. This ensures the aircraft is in statically stable condition, namely the the force acts in a way that the pitch of the aircraft is going back to equilibrium position when their is a disturbance. The stability margin of 0.05 is added to this equation. In addition, the aircraft has to be controllable. The controllability curve is given by Equation 12.11. These two equation creates a so-called "scissor plot" shown in Figure 12.3.

$$\frac{S_h}{S} = \frac{x_{cg} - x_{ac} - 0.05}{\frac{C_{L\alpha_h}}{C_{L\alpha_{A-h}}}\left(1 - \frac{d\epsilon}{d\alpha}\right)\frac{l_h}{\bar{c}}\left(\frac{V_h}{V}\right)^2} \quad (12.10)$$

$$\frac{S_h}{S} = \frac{x_{cg} - x_{ac} + \frac{C_{mac}}{C_{L_{A-h}}}}{\frac{C_{L_h}}{C_{L_{A-h}}}\frac{l_h}{\bar{c}}\left(\frac{V_h}{V}\right)^2} \quad (12.11)$$

Comparing the scissor plot with the center of gravity range given in Subsection 12.2.1, the minimum horizontal tail area and the optimized wing location can be obtained. The two yellow line shows the most forward and aft CG location as a function of X_{LEMAC} in fraction of the fuselage length l_{fg}. This value is shown in the right vertical axis. Adjusting the vertical location of these two graphs so that the two points of intersection is on the same vertical location, the optimum wing location is determined. The two intersection is connected by a black line at this condition. Therefore, from the value of the right vertical axis, it is concluded that the optimum X_{LEMAC} location is at 0.286 of the fuselage length.

In addition, the minimum horizontal tail area that ensures both controllability and stability can be obtained in the left vertical axis in the same graph. One can see that the minimum required area is $0.19S = 5.227[m^2]$.
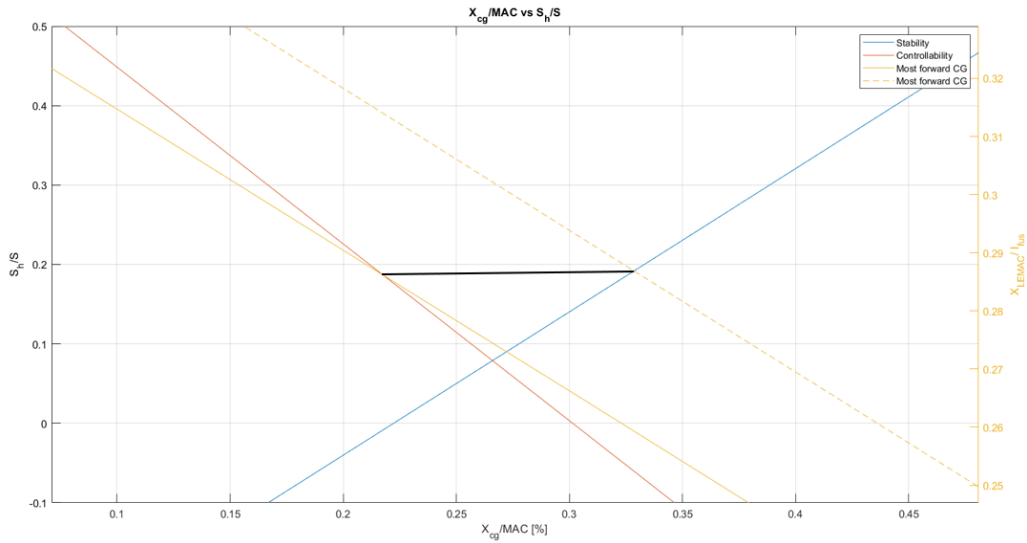
Figure 12.3: *Stability and controllability plot with most forward and aft CG location.*

12.2.3. Vertical tail sizing

The vertical tail has an important role for lateral stability. Here, an initial estimation of its size is made based on a statistical data. The vertical tail area is determined using Equation 12.12.

$$S_v = \frac{C_{VT} bS}{l_v} \tag{12.12}$$

where C_{VT} is a tail volume coefficient, which is 0.04 in this case [33]. l_v is a vertical tail length, which is estimated as 4.2 [m]. This leads to the vertical tail area of 4.43 $[m]^2$. The other parameters about geometry is discussed in Chapter 10.

12.2.4. Simulation result

After deciding the horizontal tail area, a simulation was run to check if the aircraft response is actually statically stable in the longitudinal direction. The simulation code was made based on the equation of motion presented in Subsection 12.1.3. Figure 12.4 shows the simulation result for the cruise phase starting from the trim condition.
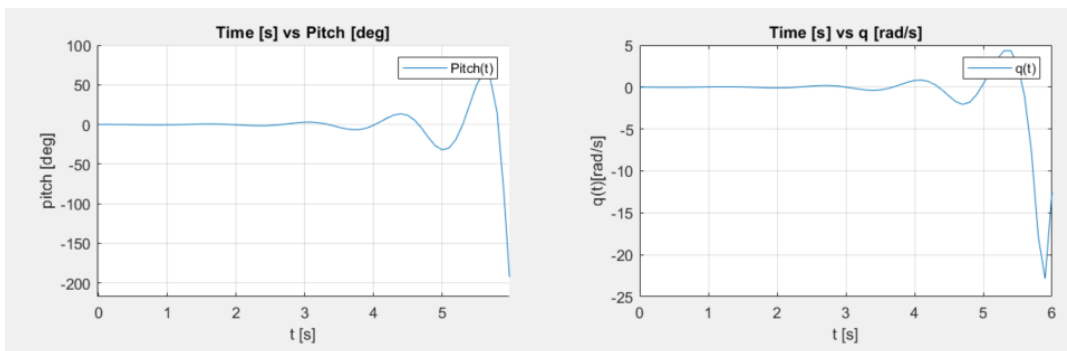
Figure 12.4: *Simulation result for cruise phase*

The simulation result showed that the aircraft is statically stable in the longitudinal direction, as the pitching moment is acting in a way that counteracts the change in pitching angle and angular velocity. The result over time is discussed in Section 12.3 and Section 12.5.

12.3. Dynamic Stability and Control

The next step of the stability analysis is calculating the dynamic stability. First, the dynamic stability for cruise phase is analyzed in Subsection 12.3.1. The results are presented as eigenvalues of the short period and Phugoid motion. Next, Subsection 12.3.2 informs on the dynamic stability for the hover phase and this controller's architecture.

12.3.1. Cruise

To begin with analyzing the dynamics stability, the equation of motion presented in Subsection 12.1.3 is linearized with respect to the relevant flight condition. This creates a linear system that can be inputted in a software like MATLAB. For the cruise phase, the most common flight condition is the steady, straight flight. This can be further categorized into two types, namely the symmetric flight and the asymmetric flight. This section explains the dynamic stability for steady, straight, and symmetric flight.

Linearized equation of motion for steady symmetric flight

Since the aircraft is assumed to be symmetric about $X_b Z_b$ plane as explained in Subsection 12.1.3, the steady, straight, symmetric flight condition has the following properties:

$$
\begin{array}{llll}
u \neq 0 & \dot{u} = 0 & p = 0 & \dot{p} = 0 \\
v = 0 & \dot{v} = 0 & q = 0 & \dot{q} = 0 \\
w \neq 0 & \dot{w} = 0 & r = 0 & \dot{r} = 0 \\
\Phi = 0 & \dot{\Phi} = 0 & X \neq 0 & \dot{X} = 0 \\
\theta = 0 & \dot{\theta} = 0 & Y = 0 & \dot{Y} = 0 \\
\psi = 0 & \dot{\psi} = 0 & Z \neq 0 & \dot{Z} = 0
\end{array}
$$

This means that there is no acceleration or change in bank, pitch and roll angle. Then the equation given in Subsection 12.1.3 can be linearized about the trim point. This is done by calculating the Taylor expansion about the trim point. After that, the second order or higher terms in the expansion are ignored.

Furthermore, the parameters are non-dimensionalised to make the analysis more handy. The non-dimensionalised parameters can be seen in the following:

$$
\hat{u} = \frac{u}{V} \qquad \alpha = \frac{w}{V} \qquad \theta = \theta \qquad \hat{q} = \frac{q\bar{c}}{V}
$$

The forces and moment are also non-dimensionalised by dividing them by $\frac{1}{2}\rho V^2 S$ and $\frac{1}{2}\rho V^2 S\bar{c}$ respectively. This leads to a non-dimensional linearized equation of motion for symmetric flight shown in Equation 12.13.

$$
\begin{bmatrix}
C_{X_u} - 2\mu_c D_c & C_{X_\alpha} & C_{Z_0} & C_{X_q} \\
C_{Z_u} & C_{Z_\alpha} + (C_{Z_{\dot{\alpha}}} - 2\mu_c)D_c & -C_{X_0} & C_{Z_q} + 2\mu_c \\
0 & 0 & -D_c & 1 \\
C_{m_u} & C_{m_{\dot{\alpha}}} D_c & 0 & C_{m_q} - 2\mu_c K_Y^2 D_c
\end{bmatrix}
\begin{bmatrix}
\hat{u} \\ \alpha \\ \theta \\ \frac{q\bar{c}}{V}
\end{bmatrix}
=
\begin{bmatrix}
-C_{X_{\delta_e}} & -C_{X_{\delta_t}} \\
-C_{Y_{\delta_e}} & -C_{Y_{\delta_t}}
\end{bmatrix}
\begin{bmatrix}
\delta_e \\ \delta_t
\end{bmatrix}
$$

$$(12.13)$$

Stability and control derivatives

Having the non-dimensionalised and linearised equation of motion ready, the next step is to calculate the stability and control derivatives. Using the stability reference frame, which defines the

initial angle of attack α_0 equals zero in the steady flight condition, θ_0 is the same as the initial flight path angle γ_0. In the cruise phase, the flight path angle is 0, so θ_0 is 0. Therefore:

$$C_{X_0} = \frac{W \sin\theta_0}{\frac{1}{2}\rho V^2 S} \qquad (12.14) \qquad\qquad C_{Z_0} = -\frac{W \cos\theta_0}{\frac{1}{2}\rho V^2 S} \qquad (12.15)$$

Other stability and control derivatives such as C_{X_u} are also calculated analytically by differentiating the corresponding force or moment.

Furthermore, control derivatives with respect to the elevator deflection, $C_{Z_{\delta_e}}$ and $C_{m_{\delta_e}}$, are calculated by using Equation 12.16 and Equation 12.17. Naturally both values are negative as the positive elevator deflection produces more lift (negative Z force) and pitch down moment (negative M_y moment). $C_{X_{\delta_e}}$ is set as zero because its contribution is small enough to be neglected.

$$C_{Z_{\delta_e}} = -C_{N_{h_\alpha}}\left(\frac{V_h}{V}\right)^2 \frac{S_h}{S} \qquad (12.16) \qquad\qquad C_{m_{\delta_e}} = -C_{N_{h_\alpha}}\left(\frac{V_h}{V}\right)^2 \frac{S_h l_h}{S \bar{c}} \qquad (12.17)$$

Lastly, the derivatives with respect to $\dot{\alpha}$ is computed by Equation 12.18 and Equation 12.19. These derivatives are required to consider the effect of "delay" after the change in angle of attack is actually reflected to the aircraft motion.

$$C_{Z_{\dot\alpha}} = -C_{N_{h_\alpha}}\left(\frac{V_h}{V}\right)^2 \frac{d\varepsilon}{d\alpha}\frac{l_h}{\bar{c}} \qquad (12.18) \qquad\qquad C_{m_{\dot\alpha}} = -C_{N_{h_\alpha}}\frac{d\varepsilon}{d\alpha}\left(\frac{V_h}{V}\right)^2 \frac{l_h^2}{\bar{c}^2} \qquad (12.19)$$

The overview of the stability and control derivatives are shown in Table 12.4.

Table 12.4: *Non-dimensionalized stability and control derivatives*

C_{X_0}	0	C_{Z_0}	-0.5392		
C_{X_u}	-0.7019	C_{Z_u}	-1.6	C_{m_u}	0.1211
C_{X_α}	0.2181	C_{Z_α}	-5.3159	C_{m_α}	-1.2547
$C_{X_{\dot\alpha}}$	0	$C_{Z_{\dot\alpha}}$	-0.7149	$C_{m_{\dot\alpha}}$	-2.6453
C_{X_q}	0	C_{Z_q}	-4.4574	C_{m_q}	-4.7993
$C_{X_{\delta_e}}$	0	$C_{Z_{\delta_e}}$	-1.1385	$C_{m_{\delta_e}}$	-2.2287
$C_{X_{\delta_{t\,front}}}$	1	$C_{Z_{\delta_{t\,front}}}$	0	$C_{m_{\delta_{t\,front}}}$	0
$C_{X_{\delta_{t\,rear}}}$	1	$C_{Z_{\delta_{t\,rear}}}$	0	$C_{m_{\delta_{t\,rear}}}$	0

State space model for steady symmetric flight

After establishing the equation of motion and knowing the derivatives, the next step is to transform the equation of motion into a state space form. The details of this transformation step is omitted in this report due to the page limitation, but one can find it in p.110 of the Flight Dynamics lecture notes [41].

The derived symmetric equation of motion in state space form is in Equation 12.20.

$$\begin{bmatrix} \dot{\hat{u}} \\ \dot{\alpha} \\ \dot{\theta} \\ \frac{\dot{q}\bar{c}}{V} \end{bmatrix} = \begin{bmatrix} x_u & x_\alpha & x_\theta & 0 \\ z_u & z_\alpha & z_\theta & z_q \\ 0 & 0 & 0 & \frac{V}{\bar{c}} \\ m_u & m_\alpha & m_\theta & m_q \end{bmatrix} \begin{bmatrix} \hat{u} \\ \alpha \\ \theta \\ \frac{q\bar{c}}{V} \end{bmatrix} + \begin{bmatrix} x_{\delta_e} & x_{\delta_t} \\ z_{\delta_e} & z_{\delta_t} \\ 0 & 0 \\ m_{\delta_e} & m_{\delta_t} \end{bmatrix} \begin{bmatrix} \delta_e \\ \delta_t \end{bmatrix} \qquad (12.20)$$

Analysis of eigenmotions

In a symmetric flight, two eigenmodes can be analyzed in the dynamic stability analysis: short period and phugoid. The short period motion is a response in a short period of time as the name suggests, and the phugoid motion is another periodic motion in a longer period. The eignevalues of these motions are shown in Table 12.5.

Table 12.5: *Eigen values of symmetric flight modes*

Eigenmode	Real component	Imaginary component
Short period	-0.0432	1.5327 i
Phugoid	-0.0049	0.0119 i

From the obtained eigenvalue, it can be concluded that both short period and phugoid motions are stable because the real components of the eigenvalues are both negative. This is common for the airplane configurations as it is normally designed to damp the oscillation, for example by the effect from the horizontal tail.

In addition, the time to damp to half amplitude can be calculated by Equation 12.21 [41].

$$T_{\frac{1}{2}} = -\frac{0.693}{\xi_c}\frac{\bar{c}}{V} \tag{12.21}$$

With ξ_c is the real component of the eigenvalue. The time to damp to half amplitude is 0.061 [s] for short period motion and 0.5371 [s] for phugoid motion.

12.3.2. Hover
For the hover phase, the aircraft control depends on differentiating rotational speed of the rotors. This section presents the controller architecture for the hover phase.
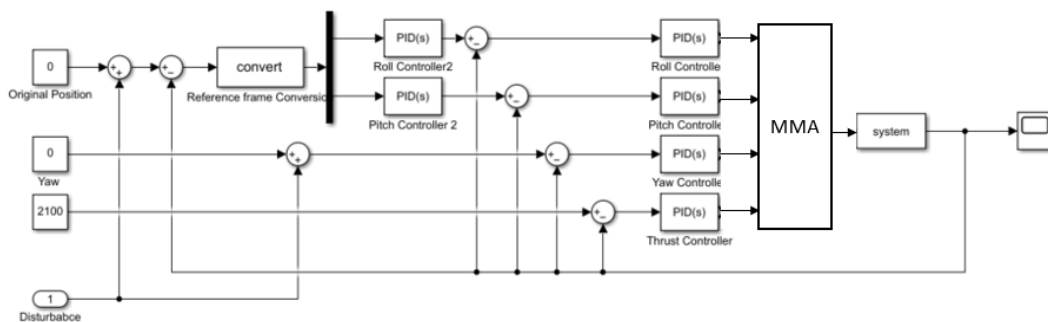
Figure 12.5: *Controller architecture for hover phase*

In the inner loop, there are three PID controllers to control pitch, roll, yaw and thrust separately. These signals are fed into Motor Mixing Algorithm (MMA), which calculates the appropriate rotational speed for each motor to perform the desired flight. The output of the MMA is reflected to the actual rotational speed, and then the outcome measured by the sensors are fedback to the feedforward signal.
In the outer loop, there are two additional PID controllers and the algorithm to convert from the earth reference frame to the body fixed reference frame. This is to ensure that the aircraft stays in the same position during hover even when there is a change in pitch or roll angle, or disturbance such as wind gust.

12.4. Transition Flight
The transition flight, namely the shift from the hover phase to cruise phase or vice versa, is the most difficult phase for the tilt rotor aircraft. Considering the shift from hover to the non-vertical climb, the aircraft has to switch from a helicopter configuration to an airplane configuration basically. There are mainly three things that happen in this phase: **1.** Tilt the rotor mechanism, **2.** Gain hor-

izontal velocity and lift from wing, **3.** Shift from helicopter control mode to airplane control mode. Possible ideas for 1 and 2 are presented in Subsection 5.2.2. Here, **3.** Shift from helicopter control mode to airplane control mode is considered further.

When the aircraft is shifting to the airplane phase, control surfaces should be added in the control loop presented in Figure 12.5. This would be at parallel to the MMA in the figure. Also, the MMA has to have an tilt angle as an input.

12.5. Verification and Validation

12.5.1. Verification of Cruise Analysis

For the verification of the dynamic stability analysis of the cruise phase, the obtained stability and control derivatives are compared with the values of Cessna Ce500 'Citation' aircraft. The first reason why this aircraft is chosen for the comparison is that the characteristics of the aircraft are similar in terms MTOW, cruise speed, and configuration of wing and fuselage. Even though this eVTOL is different in the sense it is a tilt rotor aircraft, it can be considered as an airplane during cruise phase because the proprotors are tilted in the way that the thrust force is parallel to the X_b axis. In addition, the Citation aircraft is one of the few aircraft whose stability and control derivatives are easily accessible. The basic characteristics of Cessna Ce500 and its derivative values are shown in Figure 12.6.

V	$=$	59.9 m/sec	m	$=$	4547.8 kg	$\bar{c}$	$=$	2.022 m
S	$=$	24.2 m^2	l_h	$=$	5.5 m	μ_c	$=$	102.7
K_Y^2	$=$	0.980	x_{cg}	$=$	0.30 $\bar{c}$			

C_{X_0}	$=$	0	C_{Z_0}	$=$	-1.1360			
C_{X_u}	$=$	-0.2199	C_{Z_u}	$=$	-2.2720	C_{m_u}	$=$	0
C_{X_α}	$=$	0.4653	C_{Z_α}	$=$	-5.1600	C_{m_α}	$=$	-0.4300
$C_{X_{\dot{\alpha}}}$	$=$	0	$C_{Z_{\dot{\alpha}}}$	$=$	-1.4300	$C_{m_{\dot{\alpha}}}$	$=$	-3.7000
C_{X_q}	$=$	0	C_{Z_q}	$=$	-3.8600	C_{m_q}	$=$	-7.0400
$C_{X_{\delta_e}}$	$=$	0	$C_{Z_{\delta_e}}$	$=$	-0.6238	$C_{m_{\delta_e}}$	$=$	-1.5530

Figure 12.6: *Stability and Control derivatives of Cessna Ce500 Citation aircraft [41]*

Comparing the values presented in Table 12.4 with Figure 12.6, one can notice several points. First, it can be seen that each derivative has the same sign. This makes sense because a certain change will affect in the same direction for both aircraft, as the basic configuration of the two aircraft is the same. The sign can be also checked analytically. For example, taking the derivatives of X, C_{X_u} is negative. This makes sense because if u, speed in X direction is increased, the drag force, which as the primary effect in C_{X_u} increase. This increases the negative force in the X-direction. Besides comparing the sign, their magnitudes can be compared. For example, looking at the C_m derivative, C_{m_q} has the largest magnitude for both aircraft. This matches with intuition and the design aim, because it can be easily imagined that the largest moment is required to be back to the original, stable position when the pitch angler velocity is increased.

III

OPERATIONS

13

Cost Analysis

The following chapter evaluates the cost of Aether by breaking down the life cycle cost and estimating the costs for each phase. Section 13.1 starts by explaining how the total system cost is broken down into separate phases and sectors. Then, Section 13.2 estimated the costs related to research and development, while Section 13.3 evaluates and compares the operational costs in the USA and Europe. Section 13.4 adresses the costs related to the disposal of an aircraft, while Section 13.5 analyses production costs. Finally, Section 13.6 discusses the possible ticket prices that a customer would have to pay for a trip.

13.1. Cost Breakdown Structure

For any large financial investments, it is paramount that the financing of all life cycle costs are budgeted and tracked. Planning this in advance can avoid the company getting bankrupt and helps foresee possible events that could also alter the production process. As a starting point, a cost breakdown structure is made such that the division of cost for a single Aether unit is known. Typical top level groups that sum up to the total costs for aircraft are research and development, production, operation, and disposal[33]. A visual representation of the cost breakdown structure with a more detailed breakdown can be seen in Figure 13.1.
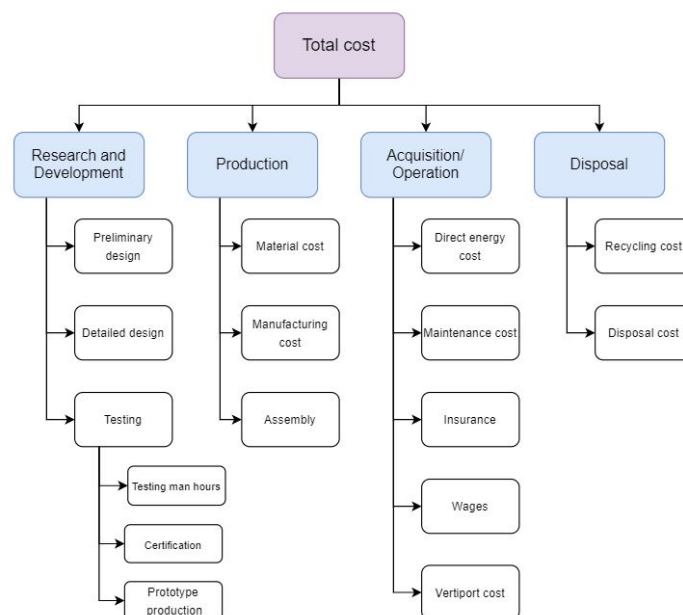
Figure 13.1: *Cost breakdown structure for a single Aether unit*

13.2. Research and Development Cost

Following the cost breakdown structure, the research and development costs of the project can be broken down into the preliminary design phase, detailed design phase, and the testing phase. For the preliminary design phase, a total of 7 students worked full time for a total of 10 weeks, amounting to a total of 2800 work hours. According to the Economic Research Institute, an average hourly

salary for a mechanical engineer in the Netherlands is 36.4 $/$h$, meaning that a total of 101,900 $ would be invested for the preliminary design phase.

For the detailed design phase, an considerably higher number of people are required and a first order estimate based on statistical data given by Raymer can be used, and follows Equation 13.1, where Q is the production quantity[33]. Substituting the appropriate values and using a production quantity of 100, the total man hours to complete the detailed design phase amount to 463,303 h, and with the same average salary as before, the cost totals 16,864,229 $.

$$H_{detailed} = 4.86 W_e^{0.777} V_{max}^{0.894} Q^{0.163} \tag{13.1}$$

For the testing costs, there is the man hour costs to perform the actual tests, the production of the prototypes, and the cost for certification. For the first factor, a similar approach can be taken again from Raymer, and follows Equation 13.2, with FTA being the total amount of flight tests made, and assumed to be 4[33]. Substituting the appropriate values gives a total testing phase cost of 3,359,693 $, which accounts for the man hours of engineers. For the production cost of the prototypes, it is assumed that three prototypes are made for the four tests; two for normal testing and one for ultimate destructive testing. It is also assumed that the production cost will be half the cost of the production cost of a first unit as the interior, varnishing, paint, and other equipment will not be necessary to perform the tests. Following the production cost for the 1st unit of 4,360,827 $, the total cost for producing the prototypes amounts to 6,541,240 $. Finally, for certification, the cost to certify a general aviation aircraft is around 25$ million[1], giving a total cost for testing of 34,900,933 $.

$$C_{testing} = 1243.03 W_e^{0.325} V_{max}^{0.822} FTA^{1.21} \tag{13.2}$$

A summary of the cost breakdown for the research and development phase of the life cycle cost is tabulated in Table 13.1.

Table 13.1: *Breakdown of the research and development costs for Aether.*

Research and Development Cost ($)	
Preliminary Design phase	101,900
Detailed design phase	16,864,229
Testing phase	34,900,933
Total	51,867,062

13.3. Operational Cost

The operational costs of Aether can be split into maintenance cost, direct energy cost, vertiport costs, wages, and insurance costs. The maintenance costs are fairly fixed throughout Aether's operational lifetime and according to the eVTOL company Uber Elevate are approximately 112 $/$h^2$. On the other hand, the direct energy costs will highly depend on the country of operation as the cost of energy can vastly differ. For example, the average cost of electricity for the transportation sector in the United States of America in October 2021 was 0.103 $/$kWh^3$, while in Europe the average

---

[1]https://www.plm.automation.siemens.com/global/pl/our-story/customers/tlg-aerospace/51461/#:~:text=Certification%20is%20estimated%20to%20cost,million%20for%20a%20commercial%20aircraft. [cited 24/01/2022]

[2]https://evtol.com/news/why-uber-thinks-evtol-air-taxis-will-be-affordable/ [cited 10/01/2022]

[3]https://www.cleanenergywire.org/factsheets/what-german-households-pay-power [cited 10/01/2022]

energy price for non household consumers in the first half of 2021 was 0.15 $/$kWh$[4],which is 50% more than in the USA. To have a better understanding of what the effects of this difference in energy cost has, the operational cost in both countries will be analysed and compared. The operational cost will be calculated using Equation 13.3, which sums the hourly maintenance and direct energy costs and multiplies that by the time to complete a trip.

$$C_{op} = \left(C_{maintenance} + C_{energy}\right) t \tag{13.3}$$

Assuming that the all trips require the maximum range and consequently a total energy consumption of 202.9 kWh, the direct energy cost in the USA for one trip would amount to 20.9 $, while in Europe the direct energy cost would be 30.4 $. Assuming that Aether will be operative from 8am to 10pm, the amount of trips per day can be calculated. Detailed more thoroughly in Chapter 14, the battery will be exchangeable, and thus the time between landing and next take off is limited by disembarking, pre flight checks, and embarking time. All these procedures are assumed to take 20 minutes, allowing 10 flights per day to take place per aircraft. For the cost of use of the vertiport, a general aviation cost of hangar use in 2016-2017 had monthly prices of multi hangar storage of 0.42 $/$ft^2$ [42], meaning that the vertiport cost for one aircraft amounts to 620 $ per month. For the wages, it is assumed that the pilot earns an average salary of 81,241 $[5], and the two ground crew earning an average salary of 28,803 $[6], making the cost of wages per year total to 138,847 $. It is assumed that other airport employees are payed by the airport or payed by government subsidies. Finally, the yearly insurance costs in the USA and Europe are 2145 $ and 2880 $ respectively, which amount to 1% of the operational cost which is consistent with the insurance costs of commercial aircraft [33]. Using these values, the operational costs in the USA and Europe are calculated for a single trip, 1 day, 1 year, and the lifetime of the aircraft of 20 years. Results are tabulated in Table 13.2.

Table 13.2: *Operational costs of Aether in the USA and Europe for 1 trip, 1 day, 1 year, and 20 years in operation.*

	Operational cost ($)	
	United States of America	Europe
1 trip	115	124
1 day	1147	1236
1 year	561,374	594,029
20 years	11,227,490	11,880,588

It is evident that over the course of the lifetime of an aircraft, the operational costs in Europe would be over half a million dollars more than in the USA. While over the course of 20 years this sum is not considerable, with the production of 500 units the company could save 250$ million over the lifetime of operation Aether. This is a crucial factor that will have to be taken into account when first starting the company as picking the USA as its launching location would mean cost savings in the millions of dollars. For this reason it is recommended that the first operational vehicles would be operated in the USA, and once the company has expanded its market share and accumulated more capital that it then would expand its service to Europe and other locations.

---

[4]https://ec.europa.eu/eurostat/statistics-explained/index.php?title=Electricity_price_statistics#Electricity_prices_for_non-household_consumers[cited 22/01/2022]

[5]https://www.comparably.com/salaries/salaries-for-helicopter-pilot [cited 25/01/2022]

[6]https://www.glassdoor.nl/Salaries/ground-crew-salary-SRCH_KO0,11.htm?countryRedirect=true [cited 25/01/2022]

13.4. Disposal Cost

The final phase of the cost breakdown structure relates to the disposal of the aircraft. The three main methods to accomplish this will be to either recycle materials, donate them, or dispose them in a landfill. Due to the sustainable nature of the company, as much of the material would be recycled as possible such that environmental effects would be minimised.

It is assumed that of the OEW without battery, 60% is carbon fiber, 20% is made of aluminium, and the final 20% are parts which cannot be recycled and must be disposed. The cost of recycling carbon fiber is estimated to be $5\$/kg$, meaning that the total cost to recycle 60% of the OEW would cost 4083 $ [43]. The other 20% of the OEW which is made of aluminium would be given to companies that accept scrap metals for free to then resell them. Thus, the cost for recycling the aluminium would be 0 $. The rest of the OEW which cannot be recycled will have to be disposed in a landfill. According to data from 2019-2020, the average cost of disposing waste in the USA was 53.72 $/$ton[7], meaning that the total cost of disposal for 20% of the OEW would be 20.1 $. Finally, it costs approximately $7\$/kWh$ to recycle lithium ion batteries, meaning that the cost to recycle the whole battery would amount to 1435 $[44]. A summary of the costs for the disposal phase of the aircraft can be found in Table 13.3.

Table 13.3: *Cost breakdown of the disposal phase of the aircraft.*

	Type of disposal	Cost ($)
Carbon fiber	Recycle	4083
Aluminium	Donation	0
Rest of OEW	Dispose	15
Battery	Recycle	1435
Total	-	5533

It is evident that the cost to recycle carbon fiber is the highest out of all the other parts, and this is due to the complex nature of the recycling process of carbon fiber. It would be significantly cheaper to dispose the whole aircraft as the cost for disposal is much lower than to recycle, but this would contradict the sustainable mission requirements of Aether, and thus as much waste as possible is recycled. Furthermore, there is the possibility of reusing the aircraft for another purpose, and Raymer estimates that this method provides a 10% positive return on the initial production cost[33]. However, at this moment there are no public proposals on how eVTOL's could be reused for different purposes, and to keep the financing on the conservative side, the disposal phase is assumed to make a monetary loss instead of profit.

13.5. Production Cost

The production costs relate to all the fixed costs that are expended for before the aircraft becomes operational. This includes manufacturing, material and assembly costs amongst other less cost demanding elements. Note that the costs to construct the vertiports is not taken into account as it is assumed that these will already be constructed by 2030. While empirical data is the most accurate method of estimating the production costs at this preliminary stage of the design, companies refrain from sharing extensive cost reports due to their confidentiality. Therefore, a closest estimate of the production cost is to take a percentage of the life cycle cost, which is the total cost of ownership of a vehicle from before it is produced until it is decommissioned or disposed. For the production cost, 25 % of the total life cycle cost is assumed. As all the other life cycle costs have been calculated, the

---

[7]https://www.statista.com/statistics/692063/cost-to-landfill-municipal-solid-waste-by-us-region/[cited 13/01/2021]

production cost can be straightforwardly computed. Assuming that the aircraft will be operated in the USA for 20 years, the production cost for one unit is estimated to be 4,360,827 $. With this, the total life cycle cost of a single unit amounts to 15,593,850 $ not including research and developments costs.

Incorporating the learning curve principle which theorises that as the production volume increases, the manufacturing cost decreases as workers become more skilled and consequently work more efficiently, ultimately reducing the production costs. Typical values for the learning curve factor range between 0.8 and 1.0[45]. As the concept of an eVTOL has already been proven in concept and flight tests, the manufacturability is feasible, and thus a learning curve factor of 0.8 is chosen. Using this, the theoretical production cost for the 100th unit totals 990,176 $. Table 13.4 summarises the production cost and total life cycle cost for the 1st and 100th unit in the USA.

Table 13.4: *Learning curve effect on production and life cycle cost for the 1st and 100th unit manufactured and operated in the USA.*

	Production cost ($)	Life cycle cost ($)
1st unit	4,360,827	15,593,850
100th unit	990,176	12,223,200

13.6. Ticket Price Estimation

To calculate the price of a ticket for a trip, a point in time where the company shall break even is chosen, and then the ticket prise can be calculated such that the total expenditure equals the total income at the chosen moment in time. Assuming that the break even point is set to 10 years, the total income made in these years must equal the production and operational costs expended until that point. Note that the following calculations are made with the assumption that the operational costs are based in the USA.

As mentioned in Section 13.3, 10 trips would be performed each day. With the aircraft operating 355 days a year (allowing 10 days per year for maintenance) and carrying 3 passengers, the total amount of passengers having travelled in 10 years amounts to 106,500. Dividing the 10 year life cycle cost for the 1st unit by this gives the ticket price of 146 $ per passenger. For the 100th unit, if the break even point would be kept the same the price per passenger would be 115 $. This gives a cost per mile for the 1st and 100th unit of 1.46 $ and 1.15 $, respectively. Compared to taxi fares which have a fare of 2.60 $ per mile[8], a trip with Aether would cost half as much as a taxi ride.

After the 10 year mark, the accumulated income of an Aether aircraft would surpass the expenses and turn into a profitable asset. If a unit has a total operational lifetime of 20 years, then the 1st unit would have a total profit of 16,472,377 $, while the 100th unit would have a total profit of 12,911,831 $. The first unit would make such a higher profit due to its higher ticket price, but it should be noted that the demand could be reduced if ticket prices would be viewed as too high. In that case, not all seats would be sold, and thus the income of the 1st aircraft would be lower than predicted. A summary of the ticket price for the 1st and 100th aircraft, along with the cost per mile and total profits are tabulated in Table 13.5. A break even analysis representation of how the costs vs income would look like for a break even point of 10 years can be seen in Figure 13.2.

---

[8]https://www.seattle.gov/your-rights-as-a-customer/file-a-complaint/taxi-for-hire-and-tnc-complaints/taxi-fares-how-much-does-a-ride-cost [cited 25/01/2022]

Table 13.5: *Ticket price for full range, cost per mile, lifetime profits and break even point for the 1st and 100th unit manufactured for a break even point of 10 years.*

	Full range ticket price ($)	Cost per mile ($)	Lifetime profits ($)	Break even point (yrs.)
1st unit	146	1.46	16,472,377	10
100th unit	115	1.15	12,911,831	10
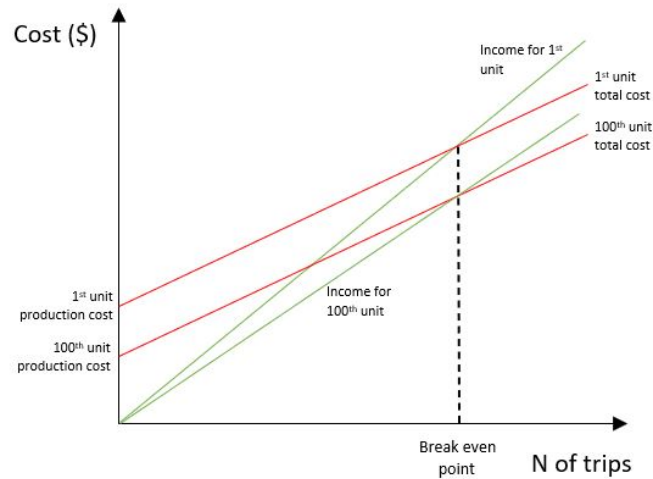
Figure 13.2: *Break even chart for 1st unit and 100th unit with constant break even point.*

In the case that the the ticket price of the first unit is kept for the 100th unit, the break even point would happen in advance and profits would increase. A visual representation of this can be seen in Figure 13.3, where due to the lower production cost with a fixed income would cause the break even point to happen with a lower amount of trips. Instead of 10 years, the break even point for the 100th aircraft would be 7.9 years, which translates to breaking even in the month of November of the 8th year, meaning that considerable higher profits can be made. Similar to before, a study would have to be conducted to check that prices per ticket are consistent with competitors and if the demand does not lower over time due to the high ticket prices. A summary of the lifetime profits and break even point for a price of 146 $ per ticket can be found in Table 13.6.

Table 13.6: *Ticket price for full range, cost per mile, lifetime profits and break even point for the 1st and 100th unit manufactured for a ticket price of 146 $*

	Full range ticket price ($)	Cost per mile ($)	Lifetime profits ($)	Break even point (yrs.)
1st unit	146	1.46	16,472,377	10
100th unit	146	1.46	19,843,028	7.9
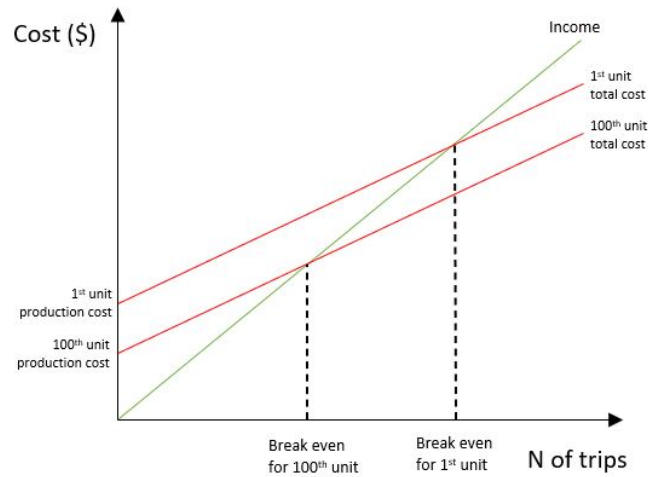
Figure 13.3: *Break even chart for 1st unit and 100th unit with fixed ticket price of 146$.*

13.7. Total Revenue and Return on Investment

The total revenue is the income a company makes in its total lifetime minus the total costs it has invested in. Unlike the profits calculated in the ticket price section, this also factors in the cost of the research and developments. Table 13.7 shows a summary of the total revenue the company would make if they would sell 100, 200, or 500 units in total. It is evident that in the case that 500 units are produced and sold, choosing to keep the 146 $ ticket price would provide the company with close to 2 $ billion more in revenue.

Table 13.7: *Total revenue with various amounts of units sold and ticket prices of* 146 $ *and* 115 $.

	Total revenue ($bn)		
Units sold	100	200	500
146 $ ticket price	1.60	3.24	8.18
115 $ ticket price	1.24	2.53	6.40

To calculate the return on investment (ROI), Equation 13.4 can be used. Substituting the values for a ticket price of 115$ for the 100th unit gives a total lifetime ROI of 105.6%. This shows a low return on investment over the course of 20 years, and is due to the high operational costs in comparison to all other costs. A possible strategy to increase the ROI would be to ask for subsidies from the government on the maintenance or direct energy costs as these are the most cost intensive of the operational costs. The total life cycle would drastically decrease and then the return on investment would increase. Another method to increase the return on investment would be to keep the ticket price of 146$ for all units produced, as this would result in a ROI of 162%.

$$ROI = \frac{Total\ income - Total\ cost}{Total\ cost} \cdot 100 \tag{13.4}$$

<div align="right">

14

</div>

Operations and Logistics

Along with the design of the aircraft, the operations and logistics around the vehicle must also be outlined. In order to realize this mission of this project, a general planning of the operations, including the use of facilities, operation flow and maintenance needs to be evaluated. This chapter introduces the operations procedures of the aircraft, consisting of descriptions of use cases, infrastructure, operations, maintenance and project logic diagrams.

14.1. Use Cases

There are multiple aspects that must be considered to investigate the use case of the vehicle in an area. The first aspect is the number and the location of the vertiports. The vertiports shall be equitably distributed among the service area. One of the objectives of this project is to serve people with reduced mobility that are currently underserved, so an assessment into the population of a local area should be conducted to decide on the location of the vertiports. This also includes consideration for accessibility to other modes of public transport, and its capacity of accommodating passengers with reduced mobility. Moreover, public acceptance of the vehicle operation is another issue to be assessed. It is necessary to thoroughly investigate the level of environmental impact of the operation (mostly noise and maintenance of landscape aesthetics).

Another aspect to be evaluated is the range of service in an area. The range of service may be driven by the needs in a particular location. On the other hand the range is also limited by aircraft capabilities, potential natural hazards of operation and concerns on environmental effect. As stated in Chapter 2, the maximum range of one flight is 100 miles (161 km), and therefore if multiple locations of expected needs are within this range, it may be included in the service area. However, natural terrain such as mountains may limit the route selection of flight by requiring the aircraft to detour and therefore increasing the total distance of flight. For example, the direct distance between Los Angeles International Airport and Victorville, CA is approximately 75 miles, but Mount San Antonio lies along this distance, with a maximum elevation of over 3000 meters . As the aircraft is not designed to operate over such altitude, the flight path must be detoured, taking a total distance of approximately 100 miles for the trip. For this reason, the vertiport location should be decided with a realistic assessment of the total flight distance instead of a simple direct distance. and frequency of natural disaster occurrence such as storms, wild fires or heavy snow fall may hinder the operation of the aircraft. Moreover, the aircraft shall not be operated in locations where operation would damage the aesthetics of the landscape. The service area shall be evaluated with the above points taken into consideration.

Finally, the expected number of service in the area shall be investigated upon planning. From a business perspective, it is required that a certain amount of flight is maintained to generate revenue. The expected number of service will influence the optimal size of fleet per service area, and therefore the scale of the central vertiport facility. It is necessary to investigate the demand of the service in different time frames, as initial service may be limited due to higher costs and general acceptance of the public on a novel vehicle.

14.2. Infrastructure

This section describes the necessary infrastructure for the operation of the air taxi.

14.2.1. Vertiport

The vertiports are the primary bases of the aircrafts, and they are the origin and the destination of flights. The minimum infrastructure of a vertiport consist of a landing pad, a charging point, storage system for battery exchange and a ground support office. The ground support office has multiple functions: accommodating passengers before flight for check in, conducting security checks and assisting boarding and disembarking process of the passengers. The vertiports are to be located in various locations of the operation area. This may be on open fields, rooftops of buildings, airports, hospital buildings or any other locations where there may be need and appropriate space for aircraft operation may be secured. For each operation area, at least one central vertiport is to be established, in which the central management of operations take place. This includes a maintenance service for the vehicles, an office to organize the operation of the fleet, and an office for the general logistics. Thus, the central vertiport consists of a hangar, a landing pad with a system to transport the vehicle into the hangar, and the offices for management. The central vertiport may be located in an airport in the local area. By doing so, human resources and expertise may be fluidly transferred from other airlines operating in the same airport.

Figure 14.1: *Artist impression of the boarding process at a vertiport.*

14.2.2. Air traffic management

Air traffic management for this aircraft mainly involves airspace in low altitudes. The cruise altitude of this aircraft is 2000 feet above ground level, and this is equivalent of an altitude for final approach for large commercial airliners. Since the current controlled airspace is established around heavy traffic areas, such low altitudes may not be within the bounds in which ATC services are provided. Therefore, with increased traffic with increased usage of AAM vehicles, it may become necessary to establish new controlled airspace especially around urban areas to control the flow of traffic for such vehicles. Moreover, the assessment of air traffic control for UAM by the MIT International Center for Air Transportation concluded that the current separation standards under IFR operations have not been scaled to the current standards of Communication, Navigation and Surveillance equipment [46]. Therefore, a more wide use of the VTOL aircrats for similar purpose may require these factors to be reevaluated.

14.2.3. Maintenance infrastructure

The maintenance infrastructure is to be constructed in the central vertiport of the service area. It will be mainly used to conduct routine checks of the aircraft, but also to accommodate aircraft in case of minor failure. Furthermore, a more serious failure shall be dealt at the location where the aircraft

last landed. Therefore, the vertiports shall have some capacity to accommodate these potential cases of maintenance.

14.3. Operations Procedures

In the following section the operation procedures are taken from the Midterm Report and explained more thoroughly based on modifications presented in this report[13].

14.3.1. Customer interface

To operate the aircraft for customers, a smartphone app or a website shall be the interface for reservation of the air taxi. Upon reservation, it is necessary to collect some documents such as a personal identification document and information on the passenger's extent of disability. Once all necessary information is collected, the reservation is complete, and the air taxi will arrive at the origin at the designated time of departure.

14.3.2. Pre-flight operations

The pre-flight operations begin by planning the flight plan to the destination. This flight plan shall consider the weather conditions along the flight path, wind directions, and possible terrains. The optimal flight path shall be constructed with these considerations taken into account. After this step, the pre-flight inspection of the aircraft shall be conducted to check for any damages or faulty, specially the four rotors and the control surfaces. After this is done, the boarding of the passenger may be started with the assistance of the crew.

14.3.3. In-flight operations

The in-flight phase begins as the aircraft door is closed. The crew shall first ensure that the seat belt and other safety device for the passenger is equipped. As the pre-start checklist is completed, the aircraft rotors may be started. Once the aircraft is ready for departure, the aircraft may takeoff as the ATC grants clearance. As described in Table 5.2, the aircraft will hover 10 seconds at an altitude in ground effect, vertically climb to AGL altitude of 100 feet, and hover again for 10 seconds at this altitude. Then, the air taxi has to transition from rotorcraft configuration to cruise configuration. For this, the aircraft will first accelerate to target climb speed without altitude change by tilting all four rotors to a preset optimal angle. As the aircraft gains enough lift from the wings, the rotors will fully tilt to be parallel with the longitudinal axis of the aircraft. The aircraft will continue its climb at the specified angle until it reaches the cruise altitude of 4000 feet ASL (2000 feet AGL). If possible, the passenger may unfasten their seat belt during cruise. The aircraft will start its descent to descend at a flight path angle of 4 degrees. At an altitude of 100 feet AGL, the aircraft will transfer back to the rotorcraft configuration and hover in more or less of a "reverse" process of the takeoff transition. As the aircraft completes its vertical descend and IGE hover, the aircraft will land at its destination. Once the rotors are stopped and parking breaks are applied, the crew shall open the door. In case of any emergencies during flight, such as rotor failure or extreme weather conditions, stated in **??**, the air taxi will be able to glide if at sufficient altitude due to the wing and the control surfaces present.

14.3.4. Post-flight operations

As the door is opened, the crew shall first set the wheel stoppers on the landing gear. After this is done, the passenger may disembark from the aircraft with the assist of the crew. After the disembarking, the crew shall connect the aircraft to a power source to charge its batteries. During this time, the crew shall conduct a post-flight inspection of the aircraft and clean the cabin, including some contact surfaces that may be an a hazard for infections. Once the charging is complete, the aircraft is ready for the next flight.

14.3.5. Emergency procedures and ditching

The emergency procedure for this aircraft needs special considerations for the capability of the passenger. In the case of a hard landing, the passenger should be able to take a brace position, in which the head should be placed on the surface that it is most likely to strike. In the case of an evacuation, the pilot should assist the evacuation process, and if possible, inform ground personnel for assistance. In the case of ditching, the passengers shall equip themselves with a life vest installed in the seats. If they are unable to do so, they shall seek help from other passengers or the crew whenever possible. After landing on water, the crew shall assist the evacuation of the passenger onto the flotation device deployed from the door. It is crucial that the pilot informs about the emergency situation to the ground either through the ATC or by releasing a distress signal. This will enable ground support to assist possible evacuation process.

14.4. Battery Recharging

The batteries of Aether is partially exchangeable, in which the battery stored in the undercarriage may be exchanged. The other part of the battery, stored in the root chord area of the wing are only chargeable directly. As the mass of the exchangeable battery is more than 300 kg, a transportation system for battery is required to transport it into the storage and charging space in the vertiport. The batteries are to be charged when the aircraft is on flight, so that once an aircraft arrives it is ready to depart with the minimal interval time.

14.5. Vehicle Maintenance

Some parts that are crucial for a safe flight are the turning mechanism of the aircraft and the motors on each proprotor. These parts must be checked before every flight. Moreover, it is also necessary to check for damages on fuselage or propellers and parts that could loosen such as screws, bolts and nuts. In addition, regular maintenance checks of the aircraft is necessary after a certain number or hours of flight. In these maintenances, a detailed check on significant elements such as proprotors, structures, electrical system, and control systems shall be conducted.

14.6. Project Logic Diagrams

A plan is formulated for the general procedures that would have to be carried out after the DSE for Aether to shape into reality. Firstly, a work breakdown structure is given in Figure 14.2 and outlines the hierarchical breakdown of the the top level phases including the estimated time required to complete them. Using this, a workflow diagram is made which organises the tasks from the work breakdown structure into chronological order. Finally, a project Gantt chart can be constructed, which schedules the tasks in a timeline. Furthermore, dependencies are clearly shown by the arrows, and this helps indicate what tasks will be affected in case of delays.
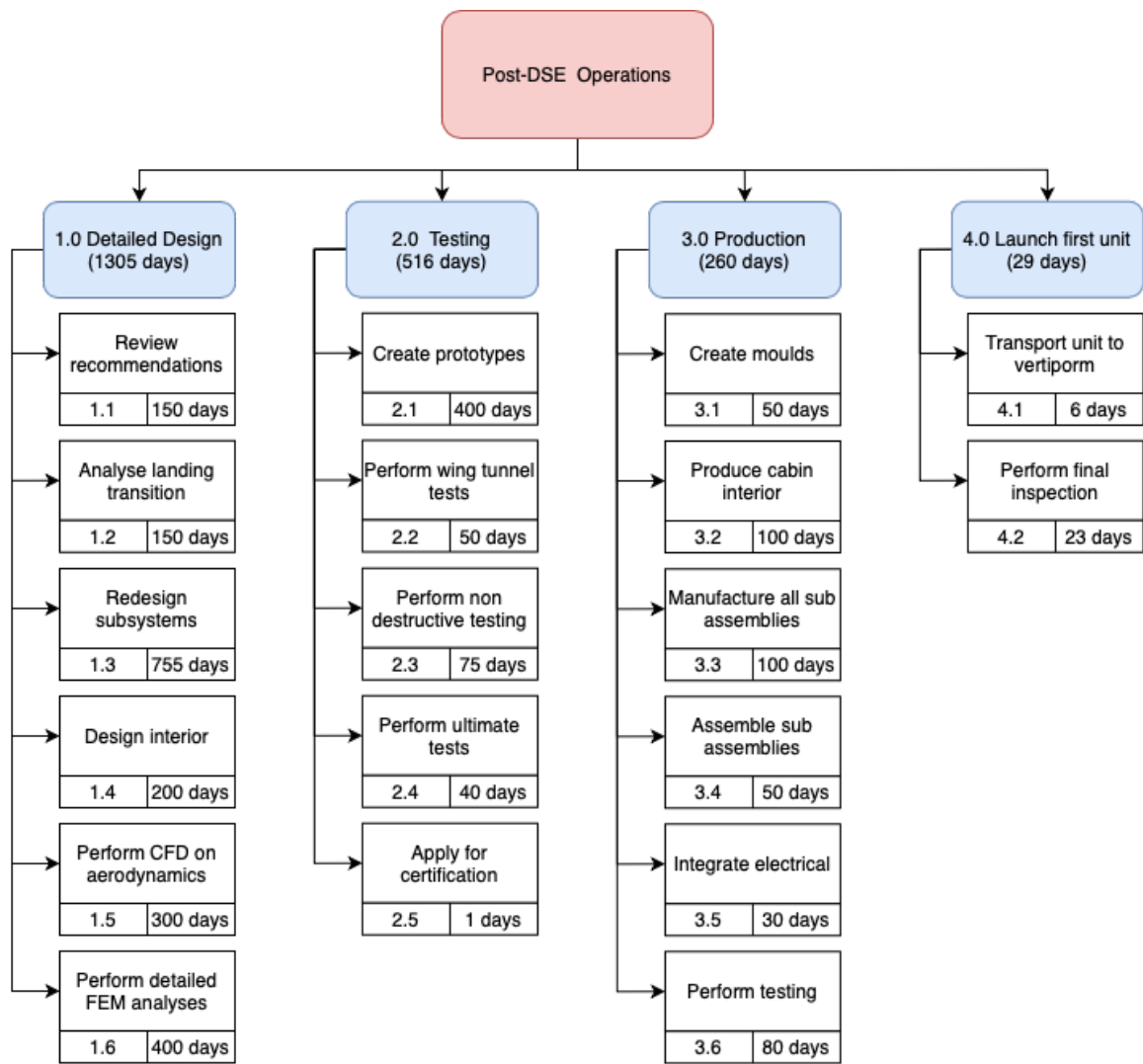
Figure 14.2: *Operations Breakdown Structure*

Work Flow Diagram for DSE Project: eVTOL Air Taxi for PRM, Post-DSE Operations

ID	Task Mode	Task Code	Task Name	Duration
1		1.0	**Detailed design**	**1305 days**
2		1.1	Review recommend	150 days
3		1.2	Analyse landing transition	150 days
4		1.3	Redesign subsyster	755 days
5		1.4	Design interior	200 days
6		1.5	Perform CFD on aerodynamics	300 days
7		1.6	Perform detailed FEM analyses	400 days
8		2.0	**Testing**	**516 days?**
9		2.1	Create prototypes	400 days
10		2.2	Perform wind tunnel tests	50 days
11		2.3	Perform non destructive testing	75 days
12		2.4	Perform ultimate tests	40 days
13		2.5	Apply for certification	1 day
14		3.0	**Production**	**260 days**
15		3.1	Create moulds	50 days
16		3.2	Produce cabin interior	100 days
17		3.3	Manufacture all sub assemblies	100 days
18		3.4	Assemble sub assemblies	50 days
19		3.5	Integrate electrical	30 days
20		3.6	Perform testing	80 days
21		4.0	**Launch first unit**	**29 days**
22		4.1	Transport unit to vertiport	6 days
23		4.2	Perform final inspection	23 days

15

Certification

The certification of the vehicle passes through the compliance of the design with the certification basis set up in [23], as a set of requirements to be followed. This chapter investigates the compliance with said requirements in Section 15.1 and the risk assessment related to technical and operational risk in Section 15.2

15.1. Compliance Matrix

The following compliance matrix verifies whether each requirements has been met or not. For the ones which are not met, an explanation of why it was not achieved is written down beside it. The following tables make up the compliance matrix. A summary of the code abbreviation meanings is tabulated in Table 15.1.

Table 15.1: *Code abbreviation definitions.*

Abbreviation	Definition	Abbreviation	Definition	Abbreviation	Definition
AE	Aerodynamics	CA	Cabin	CON	Constraint
COS	Cost	CRT	Certification	OP	Operation
PER	Performance	PP	Propulsion and power	STA	Stability
STR	Structure	SUS	Sustainability	TC	Technical
TL	Top level	VFS	Vertical Flight Society		

Table 15.2: *Compliance for top level requirements.*

Code	Requirement	Compliance	Notes
TL-CON-VFS-01	The aircraft propulsion system shall be all electric.	✓	
TL-CON-VFS-02	The aircraft shall be accessible to people with disabilities of all types.	✓	
TL-CON-VFS-03	The aircraft shall be controlled by one pilot.	✓	
TL-CON-VFS-04	The system shall be able to land vertically.	✓	
TL-CON-VFS-05	The system shall be able to take off vertically.	✓	
TL-CON-VFS-06	The aircraft shall have a range of 100 [$miles$] (161 [km]).	✓	
TL-TC-01	The aircraft shall be able to transport a maximum of 4 passengers.	✓	
TL-TC-02	The aircraft shall be controllable throughout its mission.		TBD
TL-TC-03	The aircraft shall be longitudinally stable (Cm-alpha negative).	✓	
TL-TC-04	The aircraft shall comply with all appropriate certification requirements.	✓	
TL-TC-05	The aircraft shall be designed to perform an emergency landing at any time.		Not able to land on water
TL-CON-CRT-01	The aircraft shall not have design features that experience has shown to be hazardous or unreliable.		Further analysis is required
TL-CON-CRT-02	The Maximum Take Off Weight (MTOW) of the aircraft shall not exceed 3175 [kg].	✓	
TL-CON-TIM-01	The aircraft shall be designed in 10 weeks.	✓	Still in conceptual phase
TL-CON-COS-01	The production cost of one aircraft shall be less than USD 3 million.	✓	

Table 15.3: *Compliance for operational requirements.*

Code	Requirement	Compliance	Notes
CON-VFS-OP-01	The aircraft shall be able to carry the baggage of all passengers.	✓	
CON-VFS-OP-02	Each passenger shall be able to have one piece of checked baggage having total linear dimension of 158 [cm] and weighing up to 23 [kg].	✓	
CON-VFS-OP-03	Each passenger shall be able to have one piece of carry on having dimensions 56x36x23 [cm] and weighing up to 10 [kg].	✓	
CON-VFS-OP-04	Each passenger shall be able to have one piece of personal item having dimensions 45x35x20 [cm] and weighing up to 5 [kg].	✓	
CON-VFS-OP-05	The aircraft shall be able to operate in urban environments.	✓	
CON-VFS-OP-06	The aircraft shall be able to operate in suburban environments.	✓	
CON-VFS-OP-07	The aircraft shall be able to operate in rural environments.	✓	
CON-CRT-OP-01	The aircraft shall be protected against lightning induced effects.		TBD
CON-CRT-OP-04	The system shall be designed to minimize the possibility of immediate injury in the event of ditching.		Has not been determined
CON-CRT-OP-05	The system shall be designed such that egress after ditching must be possible for all passengers.	✓	
CON-CRT-OP-06	Each crew and passenger area shall have means of rapid evacuation in case of a crash landing.		Requires further analysis
CON-CRT-OP-07	Each crew and passenger area shall have means of rapid evacuation in case of fire.		Requires further analysis
CON-CRT-OP-08	Passenger and crew doors which act also as emergency doors shall be accessible to all passengers and crew.	✓	
CON-CRT-OP-09	Complete evacuation of the aircraft shall be possible within 90 seconds.		Requires further analysis
CON-CRT-OP-10	The probability of the aircraft coming to rest on its side shall be essentially zero.		Requires further analysis
CON-CRT-OP-11	Each emergency exit shall have means to open the door from the outside.	✓	
CON-CRT-OP-12	Each emergency exit shall have means to open the door from the inside.	✓	
CON-CRT-OP-14	Each emergency exit shall be visible from a distance equal to the width of the cabin.		Requires further analysis
TC-OP-01	The aircraft shall house a flotation device used for water landings.		Requires further analysis
TC-OP-02	The aircraft shall be able to float in emergency situations and not sink during emergency water landing for at least 15 minutes.		Requires further analysis
TC-OP-03	Clear maintenance procedures shall be in place to help ensure the continued durability, integrity and functionality of the parts and systems.		In progress
TC-OP-04	The battery level shall be known to the pilot at all times.		In progress
TC-OP-05	The battery level of discharge shall be known to the pilot at all times.		In progress
TC-OP-06	The operational lifetime of the aircraft shall be at least 20 years.	✓	
TC-OP-07	The aircraft shall be able to conduct 15000 trips in its operational lifetime.	✓	
TC-OP-08	The aircraft shall have means of allowing passengers to enter and exit the aircraft.	✓	
TC-OP-09	The aircraft shall be able to communicate with Air Traffic Control.	✓	
TC-OP-10	The aircraft's safety features in response to propulsion system failure shall be determined.		In progress

Table 15.4: *Compliance for performance requirements.*

Code	Requirement	Compliance	Notes
CON-VFS-PER-01	The aircraft shall perform hover In Ground Effect (IGE) for 10 seconds.	✓	
CON-VFS-PER-02	The system shall be able to vertically climb to 30.48 [m] with Rate of Climb (ROC) of 0.8128 [m/s].	✓	
CON-VFS-PER-03	The system shall be able to hover Out of Ground Effect (OGE) at 30.48 [m] for 10 seconds	✓	
CON-VFS-PER-04	The system shall be able to perform steady climb to 609.6 [m] Above Ground Level (AGL) at a climb gradient of 1:6 (9.46 degree angle of climb).	✓	
CON-VFS-PER-05	The system shall be able to cruise at an altitude of 609.6 [m].	✓	
CON-VFS-PER-06	The system shall be able to conduct steady descent to 30.48 [m] AGL at an angle of descent of 4 degrees.	✓	
CON-VFS-PER-07	The system shall be able to perform a vertical descent to IGE with a rate of descent of <TBS> [m/s].	✓	
CON-VFS-PER-08	The aircraft shall be capable of continued flight following any single failure of the electrical distribution system.		Requires simulation/testing
CON-VFS-PER-09	The aircraft shall be capable of IGE hover following any single failure of the electrical distribution system.		Requires simulation/testing
CON-CRT-PER-01	The landing speeds shall guarantee minimum performance.	✓	
CON-CRT-PER-02	The aircraft shall be accelerated to Take-off Safety Speed (V_{toss}) while clearing any surface by 4.6 [m] (15 [ft]).		Location dependent
CON-CRT-PER-03	Starting at the point at which the aircraft reaches 200 [ft] above the take-off elevation, the aircraft shall be accelerated to the Final Take-off Speed (VFTO).	✓	
CON-CRT-PER-04	Starting at the point at which the aircraft reaches 200 [ft] above the take-off elevation, the aircraft shall then be capable of a directional trajectory change with at least 3 [deg/s].	✓	
CON-CRT-PER-05	Flying at V_{FTO} shall provide a manoeuvring capability of not less than 3 [deg/s] of turn rate.		Requires further analysis
CON-CRT-PER-06	The aircraft operational speed range shall be established.	✓	
CON-CRT-PER-07	The available power shall correspond to the power available by the batteries.	✓	
CON-CRT-PER-08	The steady rate of climb shall be determined with maximum continuous power on each rotor.	✓	
CON-CRT-PER-09	The steady rate of climb shall be determined with maximum weight.	✓	
CON-CRT-PER-10	The steady rate of descent shall be determined with maximum weight.	✓	
CON-CRT-PER-11	The steady rate of climb shall be determined with the critical engine inoperative.	✓	
CON-CRT-PER-12	The steady rate of descent shall be determined with the critical engine inoperative.	✓	
CON-CRT-PER-14	The aircraft shall be able to transition from one flight condition to another without exceeding the limit load factor in normal conditions.		Requires further analysis
CON-CRT-PER-15	The aircraft shall be able to transition from one flight condition to another without exceeding the limit load factor in one engine inoperative conditions.		Requires further analysis/testing
CON-CRT-PER-16	The aircraft shall be able to withstand load factors of -0.5 to +2.	✓	
CON-CRT-PER-17	The aircraft shall be able to withstand loads from a 30 [ft/s] gust for any flight condition.		Requires further analysis

Table 15.5: *Compliance for propulsion and power requirements.*

Code	Requirement	Compliance	Notes
CON-VFS-PP-01	The system shall perform the mission with an idealized battery with an energy density of 400 [Wh/kg].	✓	
CON-VFS-PP-02	No additional power sources shall be available during flight.	✓	
CON-VFS-PP-03	The battery reserve energy shall be equal to at least 20 minutes of continuous draw of the power level at cruise condition.	✓	
CON-CRT-PP-01	The aircraft shall have a power supply independent from the main lighting system to light the emergency exit signs.	✓	
CON-CRT-PP-02	The aircraft shall have a power supply independent from the main lighting system to provide enough general lighting in the cabin.	✓	
CON-CRT-PP-03	The emergency lighting shall provide the required level of illumination for at least 10 minutes after an emergency landing.		Requires further analysis
CON-CRT-PP-04	The load distribution for lift/thrust unit designs shall be determined.	✓	
CON-CRT-PP-05	Any single failure of an automatic power or thrust system shall not prevent continued safe flight and landing of the aircraft.	✓	Requires testing/simulation
TC-PP-01	The aircraft shall have a primary high voltage battery.	✓	
TC-PP-02	The aircraft shall have a secondary low voltage battery.	✓	
TC-PP-03	Battery mass shall not exceed 800 [kg].	✓	
TC-PP-04	The dimensions of the battery shall be determined.	✓	
TC-PP-05	Powertrain efficiency shall be at least 90-95 %.	✓	Requires further analysis
TC-PP-06	There shall be fire detection mechanisms in the powerplant compartment.	✓	
TC-PP-07	Detailed power requirements shall be determined for all critical flight conditions.	✓	

Table 15.6: *Compliance for structural requirements.*

Code	Requirement	Compliance	Notes
CON-VFS-STR-01	The aircraft length with rotors turning shall be no greater than 15.24 [m].	✓	
CON-VFS-STR-02	The aircraft width with rotors turning shall be no greater than 15.24 [m].	✓	
CON-CRT-STR-01	If outboard fins or winglets are included on the horizontal surfaces or wings of the aircraft, these surfaces shall be designed for their maximum load in combination with loads and moment exerted by the fins or winglets on the surfaces.	✓	
CON-CRT-STR-02	In the event of an emergency water landing, the total lift, assumed to act through the centre of gravity during water entry, shall not exceed two-thirds of the design maximum weight.	✓	
CON-CRT-STR-03	The propeller blades shall be at minimum 20 [cm] from any other structural part of the aircraft.	✓	
CON-CRT-STR-04	The center of gravity limits shall lie within the extremes within which the structure is proven.		Requires further analysis
CON-CRT-STR-05	The aircraft shall not have any excessive vibrations in any part or subsystem during operation.		Requires further analysis
CON-CRT-STR-06	The aircraft shall be able to sustain limit loads without permanent deformations.		Requires further analysis
CON-CRT-STR-07	The aircraft shall be able to sustain ultimate loads without failure.		Requires further analysis
CON-CRT-STR-08	Structures essential to a controlled landing shall be fireproof.		Requires further consideration
CON-CRT-STR-09	The design of the structure shall minimize the probability of fatigue failures.		Requires further analysis
CON-CRT-STR-10	The structural design loads from asymmetric thrust resulting from the failure of a powerplant unit shall be determined.		Requires further analysis
CON-CRT-STR-11	The aircraft shall be designed to minimize hazards to the aircraft due to structural damage by fragments from a rotating part failure.		Requires further analysis
CON-CRT-STR-12	A factor of safety for each critical design value for each part shall be determined.	✓	
CON-CRT-STR-13	The aircraft shall have a means of stopping with sufficient kinetic energy absorption for landing conditions.		Requires further analysis
CON-CRT-STR-14	The aircraft shall be designed to protect the pilot and flight controls from propellers.		Requires further analysis
CON-CRT-STR-15	The aircraft shall be designed to protect passengers from serious injury due to damage to windshields and windows.		Requires further analysis
CON-CRT-STR-16	Equipment containing high-energy rotors shall be designed or installed to protect the passengers and aircraft from uncontained fragments.		Requires further analysis
TC-STR-01	The aircraft shall have a landing system.	✓	
TC-STR-02	The loads which the landing system will have to support shall be determined.	✓	
TC-STR-03	The landing system shall prevent the aircraft from rolling over to its side.	✓	
TC-STR-04	The landing system shall prevent the aircraft from tipping over.	✓	
TC-STR-05	The landing system shall aid in providing a smooth deceleration during landing.	✓	
TC-STR-06	For the use of composite structures, failure due to fatigue loads shall be avoided throughout the operational life of the aircraft.	✓	
TC-STR-07	Motor compartments shall be designed to resist vibrational loads.	✓	
TC-STR-08	The landing gear shall be able to withstand the landing loads.	✓	

Table 15.7: *Compliance for cabin requirements.*

Code	Requirement	Compliance	Notes
CON-VFS-CA-01	The baseline configuration of the cabin interior shall be able to accommodate four adult passengers without disabilities.	✓	
CON-VFS-CA-02	The configuration of the cabin interior shall be able to accommodate no less than two adult passengers with disabilities.	✓	
CON-VFS-CA-03	The cabin shall have a baggage compartment for checked baggage.	✓	
CON-VFS-CA-04	For disabled passengers, the baggage compartment shall accommodate their required durable medical equipment in addition to their baggage.	✓	
CON-CRT-CA-01	Handrails shall allow persons with disabilities to grasp them from outside the vehicle while starting to board, and to continue to use them throughout the boarding process.	✓	
CON-CRT-CA-02	The handrail shall have a cross-sectional diameter between 11/4 inches and 11/2 inches or shall provide an equivalent grasping surface.	✓	
CON-CRT-CA-03	Handrails shall not interfere with wheelchair or mobility aid maneuverability when entering or leaving the vehicle.	✓	
CON-CRT-CA-04	The wheelchair securement system shall be placed as near to the accessible entrance as practicable and shall have a clear floor area of 30 inches by 48 inches.	✓	
CON-CRT-CA-05	For each wheelchair or mobility aid securement device provided, a passenger shoulder harness shall be provided.	✓	
CON-CRT-CA-06	For each wheelchair or mobility aid securement device provided, a passenger seat belt shall be provided.	✓	
CON-CRT-CA-07	All aisles, steps, floor areas where people walk and floors in securement locations shall have slip-resistant surfaces.		Requires further analysis
CON-CRT-CA-08	Doorways shall have at least 20 lumen of illumination measured on the lift or ramp, when deployed at the vehicle floor level.		Requires further analysis
CON-CRT-CA-09	The vehicle doorways shall have outside lights which, when the door is open, provide at least 10 lumen of illumination on the street surface for a distance of 3 feet.		Requires further analysis
CON-CRT-CA-10	The aircraft shall provide sufficient external view so that the pilot can perform their task of safely controlling the aircraft flight path.	✓	
CON-CRT-CA-11	Optical distortions in the windshield, especially in the prime viewing areas shall be avoided.	✓	
CON-CRT-CA-12	The aircraft shall have a precipitation removing device for the windshield.		Requires further consideration
CON-CRT-CA-13	The external field of view shall be sufficient in day/night, and not impaired by precipitation or snow conditions.		Requires further consideration
CON-CRT-CA-14	Windshields and windows shall be made of material that will not break into dangerous fragments.		Requires further consideration
CON-CRT-CA-15	Cockpit controls shall be located to provide convenient operation, unrestricted movement of each control and to prevent confusion and inadvertent operation.		Requires further consideration
CON-CRT-CA-16	Each external door shall be located to ensure that persons using the door will not be endangered by rotors, propellers, engine intakes, and exhaust when operating procedures are used.	✓	
CON-CRT-CA-17	The surroundings of all seats designated for occupancy during takeoff and landing shall be free of sharp edges.	✓	
CON-CRT-CA-18	The surroundings of all seats designated for occupancy during takeoff and landing shall be free of protuberances.	✓	
CON-CRT-CA-19	The surroundings of all seats designated for occupancy during takeoff and landing shall be free of hard surfaces.	✓	
CON-CRT-CA-20	Each occupant's seat shall have a combined safety belt and shoulder harness with a single-point release.	✓	
CON-CRT-CA-21	If seat backs do not have a firm handhold, aisles shall contain hand grips or rails to let the occupants steady themselves while using the aisle in moderately rough air.	✓	
CON-CRT-CA-22	Each non-PRM passenger seat and its supporting structure shall be designed for an occupant weight of at least 77 [kg].	✓	
CON-CRT-CA-23	The cabin air shall be free of any hazardous or harmful gases.	✓	
CON-CRT-CA-24	Emergency exit signs shall be placed above or next to emergency exits.	✓	
CON-CRT-CA-25	The emergency exit signs shall have a minimum luminescence of 0.56 lumen per [m^2].		Requires further consideration
CON-CRT-CA-26	Each occupant protection system shall not create a hazard that causes secondary injury to the passengers.		Requires further consideration
CON-CRT-CA-27	The cabin shall have readily located and easily accessible to emergency exits.	✓	
CON-CRT-CA-28	The pilot, while seated, shall be able to easily access the fire extinguishing means in the cabin.		Requires further consideration
TC-CA-01	Each PRM seat and its supporting structure shall be designed for an occupant weight of at least 90.72[kg] and a wheelchair weight of at least at least 113.4[kg].	✓	
TC-CA-02	The cabin seats shall be able to accommodate booster seats approved for aviation use.		Requires further analysis
TC-CA-03	The system shall be designed not to induce epilepsy.	✓	
TC-CA-04	The cabin shall accommodate animals which fit in kennels of sizes 44[cm] × 30[cm] × 19[cm].	✓	
TC-CA-05	The cabin shall have measures mitigating passenger infections from viruses.	✓	

117

Table 15.8: *Compliance for control and stability requirements*

Code	Requirement	Compliance	Notes
CON-CRT-STA-01	The aircraft shall be controllable during steady flight.	✓	
CON-CRT-STA-02	The aircraft shall be controllable during takeoff.	✓	
CON-CRT-STA-03	The aircraft shall be controllable during hover.	✓	
CON-CRT-STA-04	The aircraft shall be controllable during climb.	✓	
CON-CRT-STA-05	The aircraft shall be controllable during turning.	✓	
CON-CRT-STA-06	The aircraft shall be controllable during landing.	✓	
CON-CRT-STA-07	The controls shall prevent sudden motor operation when not commanded by the pilot.		Requires further analysis
CON-CRT-STA-08	The landing speeds shall guarantee minimum controllability.	✓	
CON-CRT-STA-09	The aircraft shall maintain longitudinal trim.	✓	
TC-STA-01	The centre of gravity range for safe operation shall be determined.	✓	

Table 15.9: *Compliance for aerodynamic requirements.*

Code	Requirement	Compliance	Notes
CON-VFS-AE	Tip speeds of propellers shall not exceed 600 $[ft/s]$.	✓	
CON-VFS-AE	The blade characteristics of propellers shall be determined.	✓	
CON-CRT-AE-01	The aircraft shall have controllable stall characteristics.	✓	
TC-AE	For any lifting surface that stalls within the operational envelope, the mitigation of these stall effects shall be determined.	✓	

15.2. Risk Assessment

Predicting and assessing the possible risks is essential for successful design and safe operation. In this section, all the possible risks in the design phase and the operational phase are assessed and their mitigation methods are presented. The result of the risk assessment is shown in the pre-mitigation and post-mitigation risk map.

15.2.1. Risk identification

To begin with, the possible risks are identified in four different categories, namely financial, technological, design, and operational risks. These risks are tagged with codes starting from "FI", "TE", "DE", and "OP" respectively. The Table 15.10 shows the all the identified risks together with their consequences.

Table 15.10: *Risk identification table with possible consequences*

ID	Department	Risk element	Worst consequences
FI-1	Financial	Parts/Component/Material price volatility	Selection of substitute supplier, A rise in aircraft price
FI-2		Market competition	Shift of demand to substitute products
FI-3		Investors/sponsors loss	Delayed schedule, reallocation of resource, Cancellation of project
FI-4		Stock market crash	Delayed schedule, reallocation of resource, Cancellation of project
FI-5		Budget miscalculation	Reallocation of resource
TE-1	Propulsion	Battery failure	Propulsion system inoperable, Fire during flight
TE-2		One blade failure	Fuselage damage, Loss of control
TE-3		One motor failure	Loss of control
TE-4		Gearbox failure	Loss of control
TE-5		Inverter failure	Loss of power
TE-6	Structure	Fatigue in Material	Separation of parts during flight, Crach
TE-7		Exceediing the maximum loading factor	Damage in the components
TE-8		Damaged door mechanism	Unable to evacuate/open door
TE-9	Electronics	Communication system failure	Unable to communicate with ATC
TE-10		Failure in Power Distribution Unit	Unable to adjust the power output, Loss of control
TE-11		Disconnection in electronic power circuit	Loss of power
TE-12		Sensors failure	Incorrect measurement, Wrong input for control
TE-13	Control & Stability	Tilt rotor mechanism inoperable	Uncontrollable hover and climb
TE-14		Control surface actuator failure	Unable to maneuver, Loss of control
TE-15		Controller hardware failure	Loss of control
DE-1	Design	Misdesign of controller	Unable to conduct certain maneuver, Loss of control
DE-2		Incorrect cabin sizing	Not comfortable for PRM/PRM do not fit
DE-3		Incorrect load calculations	Unable to carry design payload, Structural failure
DE-4		Incompatibility during design integration	Redesining, schedule delay
DE-5		Certification rejection	Redesigning, Additional expenses
OP-1	Operation	Extreme weather conditions	Operation difficulty, accidents
OP-2		Seismic/volcanic activities	Damaged aircraft, operation difficulty, Accidents
OP-3		Hijacking	Terrorist attacks
OP-4		Pilot error	Accidents
OP-5		Sudden passenger medical problem	Emergency landings
OP-6		Sudden crew medical problem	Accidents
OP-7		Bird strike	Damage to structure or propellers
OP-8		Conjection of air traffic	Prolonged flight time, Insufficient energy
OP-9		Insufficient maintenance	Emergency landing, Accidents

15.2.2. Risk assessment and mitigation

The next step is to assess the risk level of the identified risks. The risk level of each risk is defined as a product of its likelihood and its concequence. The likelihood and consequences scales are defined as shown in Table 15.11.

Table 15.11: *Likelihood and consequences scales*

Scale	Likelihood	Consequences
1	0.001%	Less than a week schedule delay/ Less than half a day delay of the service
2	0.01%	Less than a month of the schedule service/ More than half a day delay of the service
3	0.1%	Less than half a year of the schedule delay/ Light injury / Termination of the partial service
4	1%	More than half a year of the schedule delay/ Severe injury/ Temporaral termination of the entire service
5	10%	Permanant termination of the entire service/ Death

The percentages shown in Table 15.11 is the probabilities that the event occurs at any point during the development or production phase or during one operation, depending on the risk type. The risk level is assessed for each risk and the possible mitigation methods are considered. The mitigation method, as well as pre-mitigation and post-mitigation risk levels are presented in Table 15.12.

Table 15.12: *Risk assessment table with their mitigation methods*

ID	Pre-mitigation			Mitigation method	Post mitigation		
	Likeli-hood	Conse-quence	Risk level		Likeli-hood	Conse-quence	Risk level
FI-1	4	2	8	Allocation of extra budget margin	4	1	4
FI-2	3	4	12	Differentiation of product characteristics	3	3	9
FI-3	1	5	5	Thorough execution of risk mitigations to prevent problems and avoid major delays	1	4	4
FI-4	1	4	4	Make use of capital buffer	1	4	4
FI-5	4	2	8	Allocation of extra budget margin	4	1	4
TE-1	3	4	12	Replace battery regulary, Have a redundant battery system	3	3	9
TE-2	2	4	8	Design in fail-safe way	2	3	6
TE-3	2	5	10	Design in fail-safe way	2	4	8
TE-4	2	5	10	Regular maintenance	1	5	5
TE-5	2	4	8	regular maintenance	1	4	4
TE-6	2	5	10	Conduct regular maintainance and pre-flight checks	1	5	5
TE-7	1	5	5	Equip a flight manual aboiut possible maneuver, Equip warning system	1	4	4
TE-8	2	4	8	Arrange the evacuation procedure throught window	2	3	6
TE-9	2	5	10	Implement redundant system for primary flight instruments	2	4	8
TE-10	2	5	10	Design in fault tolerant way	2	4	8
TE-11	2	5	10	Have a redundant wire, Use normaly on switch	2	4	8
TE-12	2	4	8	Have redundant instruments where possible	2	3	6
TE-13	2	5	10	Ragular maintenance	1	5	5
TE-14	2	4	8	Regular maintenance	1	4	4
TE-15	1	5	5	Have a redundant system	1	4	4
DE-1	1	4	4	Validation, Test with prototype	1	4	4
DE-2	1	3	3	Validation, Test with prototype	1	3	3
DE-3	2	4	8	Validation, Test with prototype	1	4	4
DE-4	3	3	9	Regular meeting with in a team, Use N2 chart	2	3	6
DE-5	3	3	9	Thorough planning and considerations for certification requirements	2	3	6
OP-1	2	3	6	Establish standards for weather conditions in which operation shall be suspended	2	2	4
OP-2	2	4	8	Establish protocols for ensuring vertiport safety upon earthquakes	2	3	6
OP-3	1	5	5	Sufficient separation modes between passenger and pilot	1	4	4
OP-4	2	4	8	Conduct pilot's health check before flights	1	4	4
OP-5	4	2	8	Treatment available onboard, Planned access to closest vertiport	4	1	4
OP-6	1	5	5	Conduct pilot's health check before flights, Possibly include emergency auto landing system	1	4	4
OP-7	3	4	12	Equip bird detector at the vertiport or on the aircraft	2	4	8
OP-8	3	2	6	Equip reserve energy, Develop efficient Air traffic management system	3	1	3
OP-9	2	4	8	Set up manual for maintenance procedure, Regular training of mechanics	1	4	4

15.2.3. Risk map

Finally, the assessed risks are gathered in the risk maps. Figure 15.1 shows the pre-mitigation risks and Figure 15.2 shows the post-mitigation risks. The The color blue, green, yellow, orange, and red indicates that the risk level is "Negligible", "Low", "Moderate", "High", and "Extreme" respectively.

As a result, no risk is presented in the right bottom corner, meaning high and extreme risks are avoided after applying effective mitigation method.

		Consequence				
		1	2	3	4	5
Likelihood	1			DE-2	FI-4, DE-1, OP-4	FI-3, TE-7, OP-3, OP-6, TE-15
	2			OP-1	TE-2, TE-5, TE-8, DE-3, OP-2, OP-4, TE-12, TE-14, OP-9	TE-3, TE-4, TE-6, TE-9, TE-10, TE-11, TE-13
	3		OP-8	DE-4, DE-5	FI-2, TE-1, OP-7	
	4		FI-1, FI-5, OP-5			
	5					

Figure 15.1: *Pre-mitigation risk map*

		Consequence				
		1	2	3	4	5
Likelihood	1			DE-2	FI-3, FI-4, TE-5, TE-7, TE-14, TE-15, DE-1, DE-3, OP-3, OP-4, OP-6, OP-9	TE-4, TE-6, TE-14
	2		OP-1	TE-2, TE-8, TE-12, DE-4, DE-5, OP-2,	TE-3, TE-9, TE-10, TE-11, OP-7	
	3	OP-8		FI-2, TE-1		
	4	FI-1, FI-5, OP-5				
	5					

Figure 15.2: *Post-mitigation risk map*

<div align="right">

16

</div>

Sustainable Development Strategy

The following chapter relates to the sustainable approaches and methods that Aether adopts and can adopt during production and operation. At first the sustainable relation to the environment is explained, followed by an analysis of the economic opportunities Aether can bring to communities. Finally, the social sustainability advantages are discussed.

16.1. Environmental Sustainability

The environmental sustainability relates to the effect the project has on the environment. This starts already at the research and development phase of the project and has to be taken account for until and including the disposal of the aircraft. The first environmental factor to assess is the perceived noise from the aircraft. Not only is this important for the neighboring community, vertiports located in rural locations can have animals nearby which can be negatively affected by loud noises. The noise analysis conducted in Chapter 10 confirmed that the noise levels are manageable, even at close vicinity, and thus special vertiports with sound barriers will not have to be constructed. The effect of rotational noise at larger distances, however, has to be considered for determining the allowable distance between housing establishments and vertiports.

An important factor for maintaining a sustainable approach to the post operational phase of the aircraft is the method of disposal. As mentioned in Chapter 13, 60% of the aircraft is made of carbon fiber, 20% is aluminium, and the remaining 20% is made of non-recyclable material. Aluminium is one of the easiest metals to recycle, and thus has a sustainable outcome. Carbon fiber, although much harder to recycle than aluminium, has had recent developments of recycling methods. Although these are significantly expensive, it is much more sustainable than to dispose the material. Furthermore, it can be argued that the weight saving from using carbon fiber compensates for the recycling cost by reducing the overall weight of the aircraft, and ultimately reducing the power requirements and energy needs for a trip. Ideally, all the parts and materials will want to be reused for another purpose of recycled into scrap material. However, the parts which are not able to be recycled or reused will have to be disposed in a landfill. However, there is a high probability that by the time the first aircraft retires in 2050, that new methods of recycling could be developed or the parts are found another purpose in another industry.

A negative aspect of the design is the use of lithium-ion batteries which are harmful to the environment. It is important to carefully dispose the lithium-ion batteries once their lifetime ends. The energy sources from which the rechargeable battery takes power should also be renewable. If the power grid from which the charging station gets its energy is fueled by non-renewable sources, the design cannot be said to be more sustainable than combustion vehicles despite being electric. A solution for this would be to introduce solar panels to the vertiports in order to make the eVTOL system fully self-sufficient.

16.2. Economic Sustainability

For the economic sustainability, a major impact Aether aircraft will have will be its contribution to a sustainable city. Nowadays it is known that electric vehicles over extended periods of time are much more sustainable than combustion vehicles, and thus an aircraft that is electric is a strong unique selling point and will be supported by the public. Furthermore, when this service will be used more

frequent and will become the norm, road traffic will be heavily reduced, further reducing pollution and cost on road traffic management.

In terms of job creation and economic growth of the local community, an Aether aircraft during operation is estimated to open over 3 permanent jobs per aircraft. This includes the pilot and 2 ground crew to help the passengers and perform maintenance. Outside of operation, the headquarters and vertiport staff are estimated to hire thousands of employees for research and development purposes, marketing, financing, operations, etc. Workers will have to be trained, which further increases the jobs available in the area and allows people to advance their career and learn jobs in the tertiary sector.

The use of the airspace in urban areas could also ruin the landscape. This negatively affects the sustainability. From the economic perspective, it would make historic landmarks of the city uglier, having a negative impact on tourism. This is especially important for countries and cities that base most of their economy on tourism.

16.3. Social Sustainability

Social sustainability is the process of creating and maintaining places that promote wellbeing between communities and individuals alike. A more socially sustainable city or community overall has a higher happiness index, which has favourable effects on the work industries.

Aether especially aims to increase the opportunities and broaden the options for PRM. As travelling to locations further away from ones home becomes much easier, social activities and jobs which were not accessible before are now part of their circle of influence. Having more opportunities generally increases ones ambitions and ultimately with more options, the chance of finding a fulfilling workplace is much greater. Similarly, this principle can also be applied to children with reduced mobility, which would have a considerably easier and comfortable method of transportation for longer distances.

In terms of the reduction in road traffic, people will be overall less stressed as they would not waste time in their vehicle for extended periods of time. Studies show that traffic increases anxiety and stress in people, which ultimately decreases the happiness index of that community[1].

There is a risk that the eVTOL will not be accepted by the society. Even one accident during the beginning of operation in a large urban area could decrease public acceptance and eliminate the eVTOL from the market. This is especially significant in case there are deaths and injuries or there is damage to historical monuments. Another scenario in which the eVTOL would not be acceptd by the public anymore would be in case of terrorist attacks.

---

[1] https://pharmeasy.in/blog/stress-anxiety-pollution-effects-of-traffic-jam-on-health/#:~:text=Adrenaline%20Rush%20and%20Other%20Health%20Issues&text=Also%2C%20the%20ability%20to%20estimate,and%20judgment%20may%20be%20reduced. [cited 21 January 2022]

17
Conclusion

The Aether aircraft is designed to serve the mission need statement of "Transport passengers with reduced mobility from point A to point B through air sustainably and safely". Moreover, the following project objective statement was constructed to lead the project in a certain direction to kickstart the project: "Design an all-electric Vertical Take-Off and Landing aircraft capable of transporting no less than two passengers with reduced mobility over a range of 100 miles". The center of the design which was presented in the report focused on the inclusivity, safety, sustainability and affordability of the Aether aircraft. The project was delivered by 7 students in a limited time frame of 10 weeks. This Final Report presented the phases of design to prepare the project to initiate in real life. In order to provide a solution to the mission need and the project objective, the final project design for the vehicle and the operations are elaborated in this report.

The final design of the aircraft is centered around the needs of the passengers. Several personas of passengers with reduced mobility were constructed, and based on what those passengers need during the trip, the sizing of the cabin was performed. Considering all passenger needs found from the market analysis, a comforting and accessible cabin was designed, aiming for people with disabilities of all types to be able to use the aircraft safely. On the other hand, a more spacious cabin is found to be more favourable to cater to the PRM with claustrophobia and therefore it is recommended to be taken into account for the detailed design.

Concluding the analyses, considering that the mission range requirement of 161 km centers around the battery and its energy density, an Aether aircraft similar in the design of this report would only be feasible once batteries with an energy density of 400 $[Wh/kg]$. This would see the aircraft have a maximum takeoff weight (MTOW) close to 2667 $[kg]$, with a total payload capacity of 700 $[kg]$. Using a battery with today's capabilities would see a drastic decrease in range or payload weight, and thus the Aircraft is not recommended to be constructed until the battery technology improves.

In terms of the safety of Aether, the aircraft was designed to allow for any single failure of the motors or electrical system to have minimal consequences on the mission. A combination of contingency and reliability ensured the safety of the passengers and the pilot. Analyses showed that the aircraft was stable when on ground and in flight, with a controller architecture ensuring the pilot has complete control of the aircraft at all times. Due to time limitations, the controllability of the aircraft in transition was not able to be analysed, and thus there is the possibility that requirements are not met for this phase of flight.

In terms of the affordability, the Aether aircraft was found to be most affordable and convenient when used for intracity rather than intercity travel. As the ticket price for the 161 $[km]$ range totals 115$, taking a train presents an option three to four times cheaper, at the expense of approximately double the travel time. On the other hand, for intracity travel, taking Aether would be faster and cheaper. For example, taking the Gatwick airport to Heathrow airport transfer with Aether as opposed to a taxi would save approximately 30 minutes of travel time, and be half as expensive. Another application for the aircraft would be for inter-island travel. This would make use of the maximum range available, and additionally be much cheaper and faster than helicopter rides. It is therefore crucial to choose the right location of operation that has the maximum demand, such that the market gap is filled and profits are maximised.

Lastly, for the operational side of the aircraft, an important obstacle which will have to be thought about is the lack of air traffic control for low altitude and urban areas. The majority of air traffic control is for commercial and general aviation which have cruise altitudes much higher than the mission profile, and thus a new type of air traffic control will have to be created to safely operate the eVTOL aircraft.

All in all, the design of the aircraft would be feasible to construct in the case that some limitations are revised and taken into consideration. When constructed, it would provide an inclusive and fast service of transportation for people with reduced mobility, capable of transporting them between rural, suburban, and urban environments.

18

Recommendations

This chapter describes the future recommendations for the design of the aircraft divided per discipline.

Passenger Experience

Testing a Virtual Reality (VR) simulation of the interior design of the cabin would be beneficial to further consolidate the passenger experience for PRM in this design. In this manner some changes could be performed to verify said experience before investing on a real-scale model of the cabin. Also a more thorough inverstigation on cockpit controls would be beneficial to validate the final dimensions of the aircraft's cockpit.

Propulsion and Performance

One of the fundamental aspects of this aircraft is that the proprotors may be tilted depending on the phase of flight. In order to do so a tilting mechanism is required. There are multiple systems in which the tilting of the proprotors may be achieved. It is the recommendation of this report that the specific mechanism should be decided and evaluated in terms of tilting performance, power efficiency and safety.

To improve the performance of the aircraft, and improved analysis of the blades can be made using computational methods or CFD analysis. In this report the resultant thrust for the flight phases is taken to be in the middle of the rotor, but due to the advancing and retreating blades, a differential lift distribution along the disc is created and the thrust will have an offset from the middle of the propeller. As the post DSE analysis would be free from the VFS requirements, a non linear twist could also be incorporated in the blade such that each radial position maximises its thrust characteristics. A CFD analysis would also help analyse the wake of the propeller and its effect on other components of the aircraft. This would be especially crucial for the aircraft's hover condition as the wing mounted rotors have a portion of their area located directly above the wing, and the fuselage mounted rotors could have flow interference from the horizontal tail. A specific analysis of the taper is also recommended as the current taper is chosen only due to its common use in aircraft propellers. Having an improved taper ratio from testing would also further improve the performance and lift characteristics of the blades.

Powertrain

The main recommendation for the powertrain is to size the low voltage battery pack for volume and mass. This should be based on the power required for the five subsystems listed in the powertrain chapter. Another recommendation would be to establish the type of coolant and the temperature of the coolant for the cooling unit in the high voltage subsystem. Further optimizations can also be made to improve the efficiency of the tilt rotor power units. The battery can also be designed in more detail by evaluating the capacity and charging cycles in order to estimate the battery lifetime. In addition, the platform on which the exchangeable batteries will be placed in the undercarriage can be designed. It is important that this platform is user-friendly and minimizes the time required for exchanging the batteries. The last recommendation would be to make a more detailed design of the low voltage subsystem in order to have more improved grasp of the subsystem's components.

Structure and Materials

In terms of structural and material analysis, it is recommended to perform a specific manoeuvre diagram. The preliminary diagram presented in this report should be updated according to the specific manoeuvre loads. The maximum load obtained will be used for the analysis of all the structures of Aether. Furthermore, for the design of the wing loading, a more specific analysis of the loads should be performed. Then, the analysis of internal loads of the specific loads acting on the wing box should be studied. With these analysis the specific design of the wing box can be performed; this means, the sizing and placement of reinforcement structures such as stringers, stiffeners, or ribs. Then, the structures that support the proprotors should be studied and analysed more thoroughly. Analysis of the deflection, peak stresses, fatigue, or vibrations should be performed. Additionally, other structures such as the fuselage, the rotor hub, or the landing gear, which are essential to Aether's structural integrity, should be studied for their sizing.

Control and Stability

Another recommendation for further analysis in the field of control and stability would be to design an improved controller, which could enable the aircraft to have only 4 rotors. As explained in Chapter 5, the primary reason why a 6 rotor configuration is chosen, is to ensure the aircraft can continue hovering in case of one rotor failure. This is one of possible solutions, but there are other ways to tackle this problem. For example, using fault tolerant control could enable a quadcopter to continue hovering with one engine failure [47].

At the time of writing this report, this control system is only tested for UAV and the control for yawing motion is not yet established for it. Thus, it is not at the stage of implementing it for an air taxi mission. However, if this technology is established further in the future, this would reduce the mass of the aircraft and could enable a more efficient flight.

Another recommendation in this field is further research on the design of the vertical tail. The vertical tail size is given in Subsection 12.2.3 and is only based on a vertical tail coefficient derived from empirical data. Directional stability analysis would be required to determine if the size of the vertical tail calculated in this report is sufficient.

Finally, for the stability and control of the aircraft, it would be beneficial to update the current model to a six degrees of freedom model to be able to analyse stability and control in the lateral direction.

Cost

It is recommended for the cost analysis that for each cost breakdown phase a more detailed analysis is carried out. Since this is still the preliminary phase of design, the cost analysis is highly approximated and thus should only be taken as a reference. More detailed recommendations for each life cycle phase of Aether are given.

For the research and developments phase, the detailed design phase will be more clear once the full team of engineers and designers has been hired. Similarly, a more accurate estimation of the testing phase will be clear closer to the end of the design phase. For operation, the maintenance costs would have to revised and estimated based on a deeper breakdown of all the maintenance operations which have to be carried out pre- and post flight. Additionally, a more detailed cost analysis is possible for production by estimating the cost of each sub assembly and component.

For the total revenue, incorporating interest would see higher returns as a 30-40 year operation of Aether would have significant returns on interest given that the profit is kept in a bank. Furthermore, taking into account inflation would also see the ticket prices rise over the years. Accurate

models predicting these rates would be required and a cost contingency is recommended to ensure that the company meets its profit targets.

Lastly, it is known that a product or service has four distinct life cycles; introduction, growth, maturity, and decline. It is important that during the end of maturity a product extension is brought forth to maintain a consistent income. This can be achieved in many ways, including creating a second version of Aether, entering new markets, and possibly improving the technology such that it has an longer range or lower travel time.

Operations

An important section of the requirements which was not analysed in the report relates to ditching and emergency procedures of the aircraft. In the initial conceptual design brainstorm, an inflatable raft attached in the inside of the undercarriage was proposed to be incorporated into the design. However, due to a lack of time, this design option was not analysed and sized for, and thus it is recommended that an appropriate raft is chosen and that enough space is made in the undercarriage to accommodate the raft. For emergency landings, an extensive analysis would have to be made on the landing stability of the aircraft in the event that the aircraft must land on rocky or uneven terrain.

Bibliography

[1] *"2021-2022 Request for Proposal eVTOL Air Taxi for Passengers with Reduced Mobility (PRM)"*. Vertical Flight Society, 2021.

[2] Dr. M.D. Pavel. *"Project Guide Design Synthesis Exercise. eVTOL Air Taxi for passengers with reduced mobility"*. TU Delft, 2021.

[3] M. Hader, S. Baur, S. Kopera, T. Schönberg, J.P. Hasenberg. *"Urban air mobility"*. Roland Berger, Nov. 2020.

[4] D. Wiegand, A. McIntosh, Y. Yemsi, D. Gebser, G. Richardson, A. Asseily. *Lilium Analyst Presentation*. 2021. URL: https://lilium.com/files/redaktion/refresh_feb2021/invest ors/20210615_Lilium_Analyst%5C%20Presentation.pdf.

[5] *Commercializing Aerial Ridesharing*. 2021.

[6] C. Al .Haddad, E. Chaniotakis, A. Straubinger, K. Plötner, C. Antoniou. "Factors affecting the adoption and use of urban air mobility". In: *Transportation Research Part A: Policy and Practice* 132 (2020), pp. 696–712. ISSN: 0965-8564. DOI: https://doi.org/10.1016/j.tra.2019 .12.020. URL: https://www.sciencedirect.com/science/article/pii/S09658564193 03830.

[7] M. McKay, R. Niemiec, F. Gandhi. *"Control Reconfiguration for a Hexacopter Experiencing Single Rotor Failure"*. Rensselaer Polytechnic Institute, 2016.

[8] W. Fu-Hsuan, H. Fu-Yuen, S. Jaw-Kuen. *"Analysis and Management of Motor Failures of Hexacopter in Hover"*. Tamkang University, 2021.

[9] Dr. Eberhard Gill. *"Verification and Validation for the Attitude and Orbit Control System"*. *AE3211-I*. TU Delft slides.

[10] B. Goldstein, A. Shulman. *"Accessibility requirements for public procurement of ICT products and services in Europe"*. European Telecommunications Standards Institute, France, Feb. 2013.

[11] P. Noorlander. *Innovation in wheelchair tiedown and occupant restraint systems*. TU Delft, 2010.

[12] M. Wilson. *Wheelchairs aren't welcome on airplanes. This invention removes any excuse*. https://www.fastcompany.com/90689196/wheelchairs-arent-welcome-on-airplanes-t his-invention-removes-any-excuse. Fast Company. 2021.

[13] A. Garcia Bulder, L. Domenech Garrido, N. Hashimoto, V. Zygouris, J. Tegisher, K. Iwamida, Y. Curgul. *"eVTOL - Air Taxi Midterm Report"*. TU Delft, 2021.

[14] Dr. M.D. Pavel. *"Helicopter performance stability control"*. *AE4314-21*. TU Delft slides.

[15] R. W. Prouty. *Helicopter Performance, Stability and Control*. Krieger Publishing Company, USA, 1986.

[16] Th. van Holten. *"Helicopter Performance, Stability and Control"*. Faculty of Aerospace Engineering Delft University of Technology Novembe,r 2002.

[17] J. Roskam. *Airplane Design Part V: Component Weight Estimation*. ISBN-10 1884885500. Design, Analysis and Research Corporation (DARcorporation), 1999.

[18] J. A. Crabtree. *Weight Estimation for Helicopter Design Analysis*. Society of Aeronautical Weight Engineers, 1958.

[19] H. Sampson. *Will a passenger weight check be part of the pre-flight experience?* https://www .washingtonpost.com/travel/2021/06/17/airline-weight-passenger-faa/.

[20] J. Gordon Leishman. *Principles of Helicopter Aerodynamics*. Cambridge University, USA, 2006.

[21]   Toray Advanced Composites. *Toray BT250E-6 Product Sheet*. Toray. CA, USA, 2021.

[22]   H. Löbberding, S. Wessel, C. Offermanns, M. Kehrer, J. Rother, H. Heimes, A. Kampker. *"From Cell to Battery System in BEVs: Analysis of System Packing Efficiency and Cell Types"*. World Electric Vehicle Journal, 2020.

[23]   A. Garcia Bulder, L. Domenech Garrido, N. Hashimoto, V. Zygouris, J. Tegischer, K. Iwamida, Y. Curgul. *"Final Baseline Report"*. TU Delft, 2021.

[24]   D. Fertis. *New Airfoil Design Concept with Improved Aerodynamic Characteristics*. 1994.

[25]   B. Cantwell. *The NACA Airfoil Series*. https://web.stanford.edu/~cantwell/AA200_Course_Material/The%20NACA%20airfoil%20series.pdf.

[26]   M.H. Sadraey. *Aircraft Design: A Systems Engineering Approach*. Wiley, New Jersey, 2013.

[27]   L. Young, M. Derby. *Rotor/Wing Interaction in Hover*. NASA, 2002.

[28]   J. Anderson. *Introduction to Aerodynamics*. McGraw Hill Education, New York, 2017.

[29]   B. Chandrasekaran. *Method for the Prediction of the Installation Aerodynamics of a Propfan at Subsonic Speeds*. Langley Research Centre, 1985.

[30]   A. Wendorff, A. Variyar, C. Ilario, E. Botero, F. Capristan, J. Smart, J. Alonso, L. Kulik, M. Clarke, M. Colonno, M. Kruger, J.M. Vegh, P. Goncalves, R. Erhard, R. Fenrich, T. Orra, T. St. Francis, T. MacDonald, T. Momose, T. Economon, T. Lukaczyk, W. Maier. *SUAVE: An Aerospace Vehicle Environment for Designing Future Aircraft*. Version 2.1. 2020. URL: https://github.com/suavecode/SUAVE.

[31]   P.D. Sharpe. *AeroSandbox: A Differentiable Framework for Aircraft Design Optimization*. Massachusetts Institute of Technology, 2021.

[32]   P. Barua, T. Sousa, D. Scholz. *Empennage Statistics and Sizing Methods for Dorsal Fins*. Hamburg University of Applied Sciences, 2013.

[33]   D. Raymer. *Aircraft design - A conceptual approach*. American Institute of Aeronautics and Astronautics, USA, 2018.

[34]   Dr. J. Roskam, Dr. C.T. Edward Lan. *Airplane Aerodynamics and Performance*. ISBN 1-884885-44-6. Design,Analysis and Research Corporation, USA, 1997. Chap. Airplane Drag.

[35]   *Wetted Area Calculations*. http://aerodesign.stanford.edu/aircraftdesign/drag/wettedarea.html.

[36]   A. Brown. *"A Vehicle Design and Optimization Model for On-Demand Aviation"*. Massachusetts Institute of Technology, 2018.

[37]   M. V. Lowson, J. B. Ollerhead. *A theoretical study of helicopter rotor noise*. Wyle Laboratories, 1968.

[38]   G. Schinner, J. Brandt, H. Richter. *"Recycling Carbon-Fibre-Reinforced-Thermoplastic Composites"*. Daimler Benz AG, Forschung und Technik., 1996. DOI: https://doi.org/10.1177/089270579600900302.

[39]   N.D. Alexopoulos, E. Migklis, A. Stylianos, D.P. Myriounis. *"Fatigue behavior of the aeronautical Al–Li (2198) aluminum alloy under constant amplitude loading"*. International Journal of Fatigue., Nov. 2013. DOI: DOI:10.1016/j.ijfatigue.2013.07.009.

[40]   Th. van Holten. *AE4314 Helicopter Performance, Stability and Control*. 2002.

[41]   J.A. Mulder, W.H.J.J. van Staveren, J.C. van der Vaart, E. de Weerdt, C.C. de Visser, A.C. in 't Veld, E. Mooij. *AE3202 Flight Dynamics Lecture Note*. 2013.

[42]   Unknown. *LEE COUNTY PORT AUTHORITY RATES FEES FISCAL YEAR 2016-2017*. LEE COUNTY PORT AUTHORITY, 2017.

[43]   S.J. Pickering F. Meng J. McKechnie. *"An assessment of financial viability of recycled carbon fibre in automotive applications"*. University of Nottingham, 2018.

[44]   M.A. Rajaeifar L. Lander T. Cleaver. *"Financial viability of electric vehicle lithium-ion battery recycling"*. iScience, 2021.

[45]   K. Willcox. *16.885 Aircraft Systems Engineering - Cost Analysis.* URL: https://ocw.mit.edu /courses/aeronautics-and-astronautics/16-885j-aircraft-systems-engineerin g-fall-2004/lecture-notes/pres_willcox.pdf.

[46]   R. John Hansman Parker D. Vascik Hamsa Balakrishnan. *"Assessment OF Air Traffic Control for Urban Air Mobility and Unmanned Systems"*. MIT International Center for Air Transportation, 2018.

[47]   S. Sun, G. Cioffi, C. de Visser, D. Scaramuzza. ""Autonomous Quadrotor Flight Despite Rotor Failure With Onboard Vision Sensors: Frames vs. Events"". In: *IEEE Robotics and Automation Letters* 6.2 (2021), pp. 580–587. DOI: 10.1109/LRA.2020.3048875.

A

Task Distribution

Table A.1: *Distribution of the workload*

	Task	Student Name(s)
	Preface	Vasileios
	Executive Summary	Keiya, Antonio, Vasileios, Jonathan, Nanami
Chapter 1	Introduction	Antonio
Chapter 2	Project Overview	Jonathan
Chapter 3	Market Analysis	Nanami, Yaren
Chapter 4	Concept Trade Off	Jonathan
Chapter 5	Vehicle Specifications	Keiya, Jonathan, Antonio, Vasileios
Chapter 6	Design Methodology	Jonathan
Chapter 7	Passenger Experience	Laura, Antonio, Yaren
Chapter 8	Propulsion and Performance	Keiya, Yaren, Laura, Jonathan
Chapter 9	Powertrain	Keiya, Yaren
Chapter 10	Aerodynamics	Vasileios, Laura
Chapter 11	Structures and Materials	Antonio, Vasileios
Chapter 12	Stability and Control	Nanami, Laura
Chapter 13	Cost Analysis	Jonathan
Chapter 14	Operations and Logistics	Keiya, Antonio
Chapter 15	Certification	Vasileios, Nanami
Chapter 16	Sustainable Development Strategy	Yaren, Jonathan
Chapter 17	Conclusion	Keiya, Jonathan, Vasileios, Laura
Chapter 18	Recommendations	Everyone
	Editors	Antonio, Laura